SORPTION AND DEGRADATION STUDIES OF ENVIRONMENTAL ORGANIC CONTAMINANTS BY COMPOUND-SPECIFIC STABLE ISOTOPE ANALYSIS

Dissertation

der Mathematisch-Naturwissenschaftlichen Fakultät

der Eberhard Karls Universität Tübingen

zur Erlangung des Grades eines

Doktors der Naturwissenschaften

(Dr. rer. nat.)

vorgelegt von

M.Sc. Heide Katharina Viola Schürner, geb. Bensch

aus Starnberg

Tübingen

2015

Gedruckt mit Genehmigung der Mathematisch-Naturwissenschaftlichen Fakultät der Eberhard Karls Universität Tübingen.

Tag der mündlichen Qualifikation:	25.09.2015
Dekan:	Prof. Dr. Wolfgang Rosenstiel
1. Berichterstatter:	PD Dr. Martin Elsner
2. Berichterstatter:	Prof. Dr. Peter Grathwohl

Es ist schwierig die Gefühle in Worte zu fassen, die mir in diesem Moment, in dem ich meiner Doktorarbeit die letzten Zeilen hinzufüge, durch den Kopf gehen. Es ist eine Mischung aus Freude, Erleichterung, aber auch Wehmut, die ich mit dem Ende dieser dreieinhalbjährigen Lebensphase verbinde. Ich möchte hiermit den Menschen danken, die mich in allen Belangen dabei unterstützt haben, diese Phase erfolgreich zu meistern.

Zuallererst gilt mein herzlichster Dank meinem Doktorvater PD Dr. Martin Elsner für seine hervorragende Betreuung, die interessante Themenstellung sowie die angenehme Atmosphäre innerhalb der Arbeitsgruppe. Sein Engagement und Optimismus, das von ihm geschaffene Forschungsumfeld und die ausgezeichnete Laborausstattung trugen wesentlich zum Gelingen dieser Arbeit bei.

Ich bedanke mich außerdem herzlich bei Prof. Dr. Peter Grathwohl (Eberhard Karls Universität Tübingen) und bei Prof. Dr. Oliver Trapp (Ruprecht-Karls-Universität Heidelberg) für die externe Betreuung und ihre hilfreichen Kommentare innerhalb des Thesis Committees.

Weiterer Dank gilt:

Unseren Ingenieuren und Technikern Ramona Brejcha, Martina Höche und Harald Lowag für ihre tatkräftige Hilfe bei technischen Problemen und ihre umfassende Unterstützung bei der täglichen Laborarbeit.

Meinen Kollegen aus der Arbeitsgruppe Umweltisotopenchemie, besonders Armin, Benni, Kathrin, Michl und Stefan, für die stets gute und freundschaftliche Zusammenarbeit. Außerdem Doreen, Janina, Katrin, Kerstin, Roland und Tina für regelmäßige Kaffeekränzchen und Cocktailabende sowie ungezählte Kilometer, zurückgelegt bei Firmen-, Frauen- und Stadtläufen. Für unterhaltsame Mittagspausen sorgten überdies Gabi, Günter und Ramona.

Sincere thanks to Prof. Dr. Larry Wackett, Prof. Dr. Agnieszka Dybala-Defratyka, Dr. Jennifer Seffernick, and Anna Grzybkowska for our inspiring and fruitful collaboration.

Prof. Dr. Olaf Cirpka, PD Dr. Christine Stumpp und Dr. Dominik Eckert für ihre Unterstützung bei der Datenmodellierung und -interpretation sowie Constanze Neumann für ihre Mithilfe im Rahmen ihrer Bachelorarbeit.

Dr. Stefan Cretnik und Dr. Kai Schüler von der Firma CTC Analytics für die Bereitstellung von Spezial-Vials und Autosampler-Equipment.

Große Dankbarkeit gilt außerdem meinem Mann Daniel für seine Liebe, seinen Zuspruch und seine Geduld, meiner Familie für ihren moralischen Beistand sowie Conny, Debora, Izi, Jenny, Karla, Lisa und Nadine für ihre langjährige Freundschaft und ihre Unterstützung in allen Lebenslagen.

We keep moving forward, opening new doors, and doing new things,
because we are curious and curiosity keeps leading us down new paths.

(Walt Disney)

Table of Contents

Summary

In view of the increasing worldwide importance of groundwater as drinking water resource, the investigation of organic micropollutants and their behavior in the environment is of great societal interest. A prime of environmental sciences is, therefore, to obtain a process understanding of the biological and physical behavior of these substances, which is essential for risk assessments regarding the environment and human health. However, evaluating these processes is often difficult, since, for instance, the degradation of a pollutant may be overestimated, if only concentrations are determined and dilution is not taken into account. In recent years, Compound-specific Stable Isotope Analysis (CSIA) has developed into an important tool, particularly in the assessment of biological pollutant degradation by microorganisms. This method analyzes the change in the naturally occurring isotopic ratio (*e.g.*, $^{13}C/^{12}C$) during a (bio)chemical reaction and, therefore, offers the ability to assess degradation independent of concentration measurements. To this end, the influence of physical processes such as sorption and diffusion on observable isotope fractionation is typically neglected.

In the first part of this work, CSIA was used to investigate the degradation mechanism of the herbicides atrazine and ametryn by the enzyme *s*-triazine hydrolase (TrzN), an enzyme which plays a central role in important microorganisms responsible for natural *s*-triazine degradation. Previous studies with *Arthrobacter aurescens* TC1 showed an inverse nitrogen isotope effects in atrazine degradation that delivered highly characteristic $^{13}C/^{12}C$ and $^{15}N/^{14}N$ fractionation trends for pathway identification and suggested that an *s*-triazine ring nitrogen atom was protonated in the enzyme TrzN. Additionally, TrzN crystal structure and mutagenesis indicated proton transfer from the residue E241. This study tested the general validity of these conclusions for atrazine and ametryn with purified TrzN and a site-directed mutant (TrzN-E241Q). The degradation of both herbicides by TrzN revealed a normal carbon and an inverse nitrogen isotope effect. TrzN-E241Q lacked activity with ametryn, whereas degradation of atrazine showed again a normal carbon and an inverse nitrogen isotope effect. Surprisingly, mutant TrzN-E241Q was – despite its loss of the acidic function – still capable of activating the substrates by protonation implicating another proton donor besides E241. Additionally, analysis of the sulfur isotope ratios of ametryn revealed that bond cleavage between ametryn and the

CH_3S^- leaving group in enzymatic catalysis with TrzN was rate-determining, while this is not the case for ametryn hydrolysis at pH 1.75. Furthermore, the measured normal sulfur isotope effect provided an explanation why TrzN-E241Q is able to convert atrazine, but not ametryn. Overall, the results emphasize a robust inverse $^{15}N/^{14}N$ fractionation pattern for identifying microbial *s*-triazine hydrolysis in the environment caused by multiple protonation options in TrzN. The results of this study were published in *Environmental Science and Technology*.

A second part of this work took a step towards natural systems and investigated isotope fractionation of pesticides and pharmaceuticals in a mesoscale aquifer model. Due to the mostly polar chemical structure including additional heteroatoms and their low concentrations in the environment, method development for typical micropollutant structures presents a challenge, especially for isotope analysis. These aspects highlight the need to enhance the understanding of how reliable (multi-element) CSIA can be used to study degradation of micropollutants in a near-natural setting. In the present study, a pulse of 2,6-dichlorobenzamide (BAM), bentazone, diclofenac, and ibuprofen was released into a mesoscale model aquifer with quasi-two-dimensional flow mimicking conditions in the saturated zone of sand filters or during artificial groundwater recharge. A comparison of their concentration breakthrough curves with that of the conservative tracer D_2O demonstrated that BAM and ibuprofen showed neither degradation nor sorption, while bentazone was transformed, but did not sorb significantly. Diclofenac, in contrast, showed both degradation and sorption. Carbon and nitrogen CSIA could be accomplished in similar concentrations as for "traditional" priority pollutants (low µg/L range), however, at the cost of measurement precision (uncertainties of ± 0.4-0.5‰ (carbon), ± 1‰ (nitrogen)). Nontheless, invariant carbon and nitrogen isotope values confirmed the results for BAM (no degradation, no sorption), while significant enrichment of ^{13}C and in particular ^{15}N compared to input values corroborated transformation of diclofenac and bentazone. Retardation of diclofenac was reflected in ^{15}N sorption isotope effects, whereas isotope fractionation of transverse dispersion could not be identified. These results provide a benchmark on the performance of CSIA to monitor the reactivity of micropollutants in aquifers and may guide future effort to accomplish CSIA at even lower concentrations (ng/L range).

A third part of this work focused on isotope fractionation caused by physical processes, in particular by sorption. The aim of this project was to provide a basic understanding of the processes associated with the sorption of contaminants to soil components. Thereby, the

isotope effects that occur during sorption of a substance between water and organic soil matrix were investigated by separate consideration of water-air and organic phase-air partitioning, respectively. This methodological approach is based (i) on the fact that in air no interactions between molecules occur and (ii) on the assumption that hydrogen bonds (normal isotope effect) and van-der-Waals forces (inverse isotope effect) represent the most important intermolecular interactions. To test these hypotheses, the equilibrium isotope effects of carbon (benzene, triethylamine, and trichloromethane) and hydrogen (trichloromethane) were determined for water-air partitioning with a modified headspace vial. For organic phase-air partitioning, some restrictions arose and the isotope analysis in this system is therefore pending. Nevertheless, the calculation of the expected sorption isotope effect using the measured water-air partitioning effect and a literature value (Rayleigh distillation of the pure substance) for benzene demonstrated good consistency with the isotope effect obtained in a study that investigated sorption of benzene to humic substances. Thus, for the first time sorption isotope effects could be explained by the underlying interactions between the solute and its surrounding solvent providing fundamental process understanding of sorption in different condensed phases.

Zusammenfassung

Im Hinblick auf die weltweit steigende Bedeutung von Grundwasser als Trinkwasserquelle ist die Untersuchung von organischen Spurenschadstoffen und deren Verhalten in der Umwelt von großem gesellschaftlichem Interesse. Hierbei steht vor allem das Prozessverständnis des biologischen und physikalischen Verhaltens dieser Substanzen im Mittelpunkt der Umweltwissenschaften, was für eine Risikoabschätzung der Gefahren für Mensch und Umwelt unerlässlich ist. Die Beurteilung dieser Prozesse ist jedoch oft schwierig, da durch Konzentrationsbestimmungen allein beispielsweise der Abbau eines Schadstoffes überschätzt würde, wenn Verdünnung nicht berücksichtigt wird. Substanz-spezifische Stabilisotopenanalytik (CSIA) hat sich in den letzten Jahren, insbesondere bei der Bewertung des biologischen Schadstoffabbaus durch Mikroorganismen, zu einem wichtigen Instrument entwickelt und bietet durch die Analyse der während einer (bio)chemischen Reaktion auftretenden Änderung des natürlichen Isotopenverhältnisses (z.B. $^{13}C/^{12}C$) die Möglichkeit, Abbau unabhängig von Konzentrationsbestimmung zu beurteilen. Dabei wird der Einfluss, den physikalische Prozesse wie Sorption und Diffusion auf die zu beobachtende Isotopenfraktionierung haben, typischerweise vernachlässigt.

Im ersten Teil der vorliegenden Arbeit wurde CSIA zur Aufklärung des Abbaumechanismus der Herbizide Atrazin und Ametryn durch das Enzym *s*-Triazinhydrolase (TrzN) verwendet. Dieses Enzym spielt eine zentrale Rolle in wichtigen Mikroorganismen, die für den Atrazinabbau in der Umwelt verantwortlich sind. Erste Studien mit *Arthrobacter aurescens* TC1 zeigten einen inversen Stickstoffisotopeneffekt beim Abbau von Atrazin, der charakteristische $^{13}C/^{12}C$ und $^{15}N/^{14}N$ Fraktionierung zur Identifizierung des Abbauweges lieferte und vermuten ließ, dass eines der Stickstoffatome des aromatischen *s*-Triazinringes durch das Enzym TrzN protoniert wird, wobei die Kristallstruktur und eine Mutagenese des Enzymes auf eine Protonenübertragung durch die Aminosäure Glutaminsäure E241 hindeuteten. Die generelle Gültigkeit dieser Schlussfolgerungen wurde in der vorliegenden Arbeit für Atrazin und Ametryn mit gereinigtem TrzN und einem spezifischen Mutanten (TrzN-E241Q) getestet. Der Abbau beider Herbizide mit TrzN ergab einen normalen Kohlenstoff- und einen inversen Stickstoffisotopeneffekt. Eine Umsetzung von Ametryn

mit TrzN-E241Q war nicht möglich, wohingegen der Abbau von Atrazin erneut einen normalen Kohlenstoff- und einen inversen Stickstoffisotopeneffekt zeigte. Mutant TrzN-E241Q war somit trotz Verlustes der Säurefunktion überraschenderweise in der Lage die Substrate durch Protonierung eines Stickstoffatomes zu aktivieren, was neben Glutaminsäure E241 auf einen weiteren Protonendonor innerhalb des katalytisch aktiven Zentrums hindeutet. Die Analyse der Schwefelisotopenverhältnisse von Ametryn ergab zudem, dass in der enzymatischen Katalyse mit TrzN der Bindungsbruch zwischen Ametrynmolekül und Abgangsgruppe CH_3S^- geschwindigkeitsbestimmend ist, während dies auf die chemische Hydrolyse bei pH 1.75 nicht zutrifft. Des Weiteren lieferte der gemessene normale Schwefelisotopeneffekt eine Erklärung dafür, dass TrzN-E241Q zwar Atrazin, jedoch nicht Ametryn umwandelt. Insgesamt betonen die Ergebnisse der Studie das Vorhandensein einer charakteristischen, inversen Fraktionierung von $^{15}N/^{14}N$ durch mehrfache Protonierungsmöglichkeiten in TrzN, die zur Identifizierung mikrobiologischer Hydrolyse von *s*-Triazinen in der Umwelt dienen kann. Die Ergebnisse dieser Studie wurden in *Environmental Science and Technology* veröffentlicht.

Ein weiteres Kapitel dieser Arbeit machte einen Schritt in Richtung natürlicher Systeme und befasste sich mit der Isotopenfraktionierung von Pestiziden und Pharmazeutika in einem mesoskaligen Modell eines Grundwasserleiters. Aufgrund ihrer meist polaren chemischen Struktur, einschließlich zusätzlicher Heteroatome, und ihrer niedrigen Konzentrationen in der Umwelt stellt die Methodenentwicklung für typische Spurenschadstoffe, besonders in der Isotopenanalytik, eine Herausforderung dar. Dies zeigt die Notwendigkeit eines besseren Verständnisses darüber, wie zuverlässig Isotopenanalytik (auch von mehreren Elementen) verwendet werden kann, um den Abbau von Spurenschadstoffen in einer naturnahen Situation zu untersuchen. In der vorliegenden Arbeit wurde ein Puls, vergleichbar mit Bedingungen in der gesättigten Zone eines Sandfilters oder während künstlicher Grundwasseranreicherung, bestehend aus 2,6-Dichlorbenzamid (BAM), Bentazon, Diclofenac und Ibuprofen in einen mesoskaligen Modellaquifer mit quasi-zweidimensionalem Fluss eingeleitet. Ein Vergleich der Konzentrationsdurchbruchskurven mit der des konservativen Tracers D_2O zeigte dabei für BAM und Ibuprofen weder Abbau, noch Sorption, während Bentazon umgewandelt wurde, aber nicht wesentlich sorbierte. Diclofenac zeigte hingegen sowohl Abbau, als auch Sorption. Die Kohlenstoff- und Stickstoffisotopenanalyse konnte in ähnlichen Konzentrationen (niedriger µg/L-Bereich) durchgeführt werden, wie die Isotopenanalyse „traditioneller“ Schadstoffe, allerdings auf Kosten der analytischen

Präzision mit Messunsicherheiten von ± 0.4-0.5‰ für Kohlenstoff und von ± 1‰ für Stickstoff. Dennoch bestätigten fehlende Kohlenstoff- und Stickstoff-isotopenfraktionierung die Ergebnisse für BAM (kein Abbau, keine Sorption), während deutliche Anreicherung von ^{13}C und besonders ^{15}N gegenüber dem Ausgangswert die Umsetzung von Diclofenac und Bentazon untermauerte. Die Retardation von Diclofenac spiegelte sich in den ^{15}N-Sorptionsisotopeneffekten wieder, während eine Isotopenfraktionierung durch transversale Dispersion nicht beobachtet werden konnte. Die Ergebnisse bieten einen Maßstab für die Leistungsfähigkeit von substanz-spezifischer Stabilisotopenanalytik bei der Überwachung von Spurenschadstoffen in Grundwasserleitern und können weitere Bemühungen motivieren, CSIA bei noch niedrigeren Konzentrationen (ng/L-Bereich) durchzuführen.

Der letzte Teil dieser Arbeit befasste sich mit der Isotopenfraktionierung, die durch physikalische Prozesse hervorgerufen wird, wobei besonders die Sorption im Vordergrund stand. Ziel des Projektes war es dabei, ein grundlegendes Verständnis für die Prozesse zu schaffen, die mit der Sorption von Kontaminanten an Bodenbestandteile zusammenhängen. Die Isotopeneffekte, die bei der Sorption einer Substanz zwischen Wasser und organischer Bodenmatrix auftreten, wurden dabei durch getrennte Betrachtung der Substanzverteilung zwischen Wasser-Luft und organischer Phase-Luft aufgeschlüsselt. Dieser methodische Ansatz beruht darauf, dass (i) in Luft keinerlei Wechselwirkung zwischen Molekülen stattfindet und (ii) Wasserstoffbrückenbindungen (normaler Isotopeneffekt) und van-der-Waals Kräfte (inverser Isotopeneffekt) die wichtigsten intermolekularen Wechselwirkungen darstellen. Mit dem entwickelten Modellsystem (ein speziell angefertigtes Headspace-Vial) konnte die Isotopen-fraktionierung von Kohlenstoff (Benzol, Triethylamin und Trichlormethan) und Wasserstoff (Trichlormethan) im Gleichgewicht zwischen Wasser und Luft bestimmt werden. Für die Verteilung zwischen organischer Phase und Luft ergaben sich Einschränkungen in dem oben genannten System, daher steht die Isotopenanalytik in diesem System noch aus. Dennoch zeigte die Berechnung des erwarteten Sorptionsisotopeneffektes mittels des gemessenen Wasser-Luft- und eines Literaturwertes (Rayleigh-Destillation der reinen Substanz) für Benzol eine gute Übereinstimmung mit einer Studie, die die Sorption von Benzol an Huminstoffe untersuchte. Damit konnten Sorptionsisotopeneffekte zum ersten Mal mit den Wechselwirkungen zwischen gelöstem Stoff und dem ihn umgebenden Lösungsmittel erklärt werden, was ein grundlegendes Prozessverständnis für Sorption in verschiedenen kondensierten Phasen liefert.

1

General Introduction

1.1 Groundwater Contamination by Organic Chemicals

Groundwater is a major drinking water resource and the increasing pollution of this freshwater system is a growing problem worldwide.[1,2] Among the most important contaminants are organic substances that enter the environment either as point sources at contaminated sites by accidental spills or mishandling (*e.g.*, chlorinated solvents, petrochemicals), or as micropollutants by omnipresent use (*e.g.*, pesticides, pharmaceuticals, or consumer care products).[2,3] Especially micropollutants are, although in low concentrations (ng/L to low µg/L), detected ubiquitously in drinking water and their effect on human and ecosystem health is largely unknown.[2,4] It is therefore of great interest to monitor the fate of organic contaminants in order to develop appropriate remediation techniques ensuring clean drinking water resources for future generations.

1.2 Environmental Behavior of Organic Contaminants

Once organic substances have been introduced to the environment, they are subjected to several processes depending on compound-specific properties such as water solubility and polarity on the one hand, and on environmental conditions (seasonal changes in temperature and humidity, pH, soil composition, *in situ* microbial composition) on the other hand.[5] Both aspects have an impact on the behavior of organic contaminants in the environment and may result in (i) (bio)chemical transformation (*i.e.*, biotic and abiotic degradation), (ii) sorption, and/or (iii) transport (*e.g.*, by leaching or run off). Among these processes, (bio)chemical transformation is the most important one, because it converts the contaminants to harmless substances. However, quantification of degradation is challenging, since mass balances cannot be closed easily. Transformation may be overestimated, for instance, by preferential sorption of contaminants to the soil matrix, while subsequent transformation of metabolites to potentially unknown products would lead to underestimation. In addition, degradation can take place simultaneously *via* competing pathways further hampering the assessment of degradation.[6] Hence, an alternative strategy to improve qualitative and quantitative evaluation of contaminants' fate in the environment is needed.

1.3 Compound-specific Stable Isotope Analysis (CSIA)

1.3.1 Fundamentals

An important approach to assess the fate of organic contaminants in groundwater is Compound-specific Stable Isotope Analysis (CSIA). In recent years, it has become a promising tool to distinguish contamination sources[7,8] and competing transformation pathways.[6,8,9] Additionally, it can be used to detect and even quantify (bio)degradation as well as to elucidate chemical or biological reaction mechanisms.[6,8,9] CSIA measures the isotopic composition of a substance at natural abundance that is given as ratio $^{h}E/^{l}E$ of the heavier isotope to the lighter isotope of the particular element *E* (*e.g.*, $^{13}C/^{12}C$, $^{2}H/^{1}H$, $^{15}N/^{14}N$, $^{18}O/^{16}O$). These ratios are expressed in the δ-notation (eq. 1.1) in per mil (‰) relative to an international reference material (*e.g.*, Vienna PeeDee Belemnite for carbon).

$$\delta\,{}^{h}E = \frac{\left[\left({}^{h}E/\,{}^{l}E\right)_{\text{sample}} - \left({}^{h}E/\,{}^{l}E\right)_{\text{reference}}\right]}{\left({}^{h}E/\,{}^{l}E\right)_{\text{reference}}} \qquad \text{eq. 1.1}$$

Different activation energies caused by the mass difference of the nuclides and the resulting difference in zero-point energies (ZPEs)[10,11] are the main reason for the kinetic isotope effect (KIE) that is given as

$$\text{KIE} = \frac{{}^{l}k}{{}^{h}k} \qquad \text{eq. 1.2}$$

with ${}^{l}k$ and ${}^{h}k$ as the reaction rate constants of the light and the heavy isotope, respectively. KIEs are mainly based on changes in the vibrational energies of molecular bonds between ground state and transition state. Due to the somewhat weaker bonds that are formed by the light isotopes (slightly higher ZPE), molecules containing light isotopes in the reactive position tend to react slightly faster during a chemical reaction, *i.e.*, they reach the transition state earlier due to the lower activation energy, than molecules containing the heavier isotope.[12] As a consequence, the heavier isotopologues become enriched in the remaining substrate, whereas the reaction product is enriched in light isotopologues (so-called normal kinetic isotope effect). Thereby, isotopic fractionation is mainly induced by bond cleavage and formation of new bonds in (bio)chemical transformation reactions, *e.g.*, in microbial biodegradation,[8,11] whereas

physical processes like sorption, dispersion, or volatilization are assumed to have negligible impact on isotopic fractionation (Figure 1.1).[11,13,14]

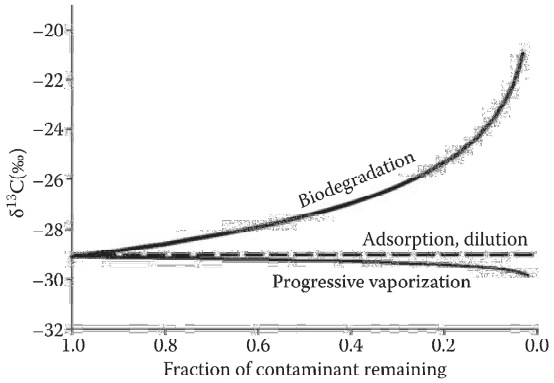

Figure 1.1: Potential of CSIA to distinguish between biodegradation and physical processes.[11]

Since isotope analysis by Gas Chromatography coupled to Isotope Ratio Mass Spectrometry (GC-IRMS, see 1.3.2) determines the isotopic ratios as compound average over all positions, KIEs can be directly associated with the fractionation factor α (eq. 1.3).

$$\frac{1}{\mathrm{KIE}_{bulk}} - 1 = \alpha - 1 = \varepsilon \qquad \text{eq. 1.3}$$

α is commonly expressed as enrichment factor ε which can be determined from batch experiments with microbial cultures[15-17] as the slope of the linear regression according to the logarithmic form of the Rayleigh equation (eq. 1.4 where R_t and R_0 are the measured isotope ratios at time t and at the beginning of the reaction, and f is the fraction of contaminant remaining at time t).[12,18] This equation describes the exponential increase of the isotope value during the course of degradation (Figure 1.1).

$$\ln \frac{R_t}{R_0} = \varepsilon \times \ln f \qquad \text{eq. 1.4}$$

Due to the fact that KIEs depend strongly on the type of bond being broken and, consequently, also on the kind of reaction that occurs,[19] different transformation pathways, *e.g.*, aerobic *vs.* anaerobic biodegradation, can be distinguished by a characteristic divergence in enrichment factors ε.[16,19,20] For large organic molecules,

however, the position-specific KIEs – mainly that of carbon and hydrogen – are "diluted" by isotope effects occurring in the non-reactive positions when analyzing the isotopic composition as molecular average. To obtain KIEs in reactive positions, a correction for the number of atoms in reactive positions *x* in relation to the total number of atoms *n* is required.[19] The Rayleigh equation (eq. 1.4) then becomes

$$\ln\frac{R_{reactive\ position}}{R_0} = \ln\frac{R_0 + n/x\ (R_t - R_0)}{R_0} = \varepsilon_{reactive\ position} \times \ln f \qquad \text{eq. 1.5}$$

with enrichment factor ε as:

$$\varepsilon_{reactive\ position} \approx \frac{n}{x} \times \varepsilon_{bulk} \qquad \text{eq. 1.6}$$

For those cases in which several atoms *z* of the same element are present in the reactive position (*i.e.*, intramolecular competition, *e.g.*, between the three hydrogen atoms in a -CH_3 group) an additional correction is needed.[19] The conversion of enrichment factors ε_{bulk} into position-specific apparent kinetic isotope effects (AKIEs, eq. 1.7) offers the chance to compare isotopic fractionation for the same kind of reaction in different contaminants.

$$\text{AKIE} = \frac{1}{z \times \varepsilon_{reactive\ position} + 1} = \frac{1}{z \times \frac{n}{x} \times \varepsilon_{bulk} + 1} \approx \frac{1}{n \times \varepsilon_{bulk} + 1} \qquad \text{eq. 1.7}$$

On the other hand, it needs to be considered that the information gained from isotope analysis can be biased, because only the rate-determining step of the overall process is observed. Besides the chemical reaction, other steps such as transport though cell membranes or formation of the enzyme-substrate complex are involved in the overall process and may be rate-determining. This "commitment to catalysis"[21] can lead to a decrease in the apparent kinetic isotope effect and can, therefore, make the identification of transformation mechanisms difficult. A relevant approach to handle the masking effects is provided when plotting the isotopic signatures of two elements against each other (*e.g.*, $\delta^{13}C$ and $\delta^{15}N$) in so-called two-dimensional isotope plots. Since both elements are affected by the same masking effects, resulting isotope data can be considered relative to each other.[19] This enables an even more robust interpretation of different transformation mechanisms in environmental systems by comparison with laboratory studies.[22,23]

1.3.2 Instrumentation

The most common analytical technique of CSIA is Gas Chromatography coupled to Isotope Ratio Mass Spectrometry (GC-IRMS) that is well described by W. A. Brand.[24] In short, after gas chromatographic separation, the target compound peaks are combusted online into the gas to be measured (*e.g.*, CO_2) and are then transferred to the IRMS (Figure 1.2).

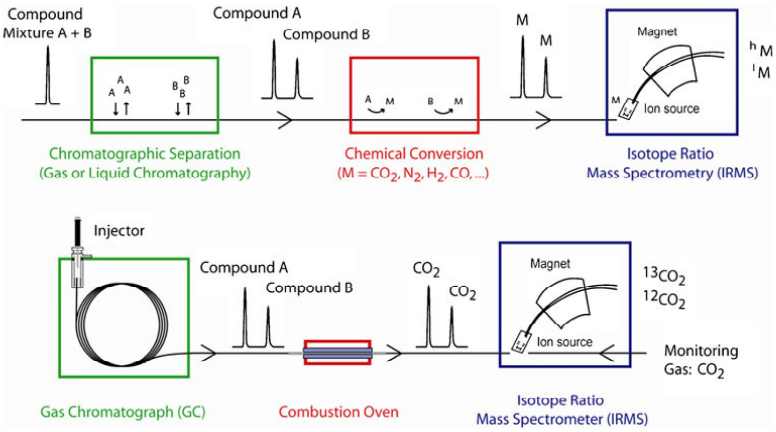

Figure 1.2: Principle of CSIA by GC-IRMS (upper panel) and instrumentation for carbon isotope analysis (lower panel).[25]

The analysis of other elements than carbon requires certain modifications on the system shown in Figure 1.2. For instance, an additional oven for the reduction of nitrogen oxides (NO_x) to nitrogen (N_2), as well as a possibility to trap carbon monoxide, which otherwise would interfere with the measurement of mass M = 28 ($^{14}N^{14}N$ and $^{12}C^{16}O$), is needed for the analysis of nitrogen isotopes. Depending on the analytical requirements, the GC-IRMS instrumentation can be used with the same preconcentration methods as conventional GC-MS, *e.g.*, Purge and Trap (P&T) for volatile analytes. Polar compounds need to be derivatized before analysis or Liquid Chromatography (LC) has to be coupled to the IRMS. A detailed overview on the state-of-the-art is given by Elsner *et al.*[25]

1.3.3 Research Gaps

In recent years, isotope analysis particularly focused on the assessment of organic priority pollutants such as aromatic hydrocarbons or chlorinated solvents at contaminated sites[26-28] and numerous field studies confirmed the applicability of CSIA for environmental monitoring.[8,29] Today, several aspects, especially for isotope analysis of micropollutants, warrant further investigation. (i) Degradation mechanisms of several pesticides and pharmaceuticals were already examined in various studies,[23,30,31] but due to the huge variety of competing biological and chemical pathways there is still a need to investigate underlying reaction mechanisms. Thereby, studies on the isotopic fractionation of different compounds of the same substance class may help to better understand the dominating processes that take place in the environment. (ii) Compared to the "traditional" volatile and non-polar priority pollutants, the different physicochemical properties of micropollutants (complex chemical structures, presence of heteroatoms, higher polarity) make CSIA challenging. Method development, for instance, often requires a derivatization step which leads to additional measurement uncertainties. Hence, investigation of micropollutants in environmentally relevant concentrations (ng/L to low µg/L range) in (near-)natural systems is a crucial point that requires further investigation. (iii) Although it is commonly assumed that physical processes such as sorption are influencing the fate of contaminants only marginally, recent studies using isotope analysis have demonstrated that these processes may have important impact on environmental systems.[32-34] Nonetheless, the underlying factors behind these isotope effects, *i.e.*, the changes in molecular vibrations that occur when a substance undergoes interactions with soil matrix, have not been studied in detail yet.

1.4 Objectives

This thesis aimed to further develop Compound-specific Stable Isotope Analysis in order to enhance the understanding of natural attenuation processes with respect to the following aspects.

The work presented in Chapter 2 focused on the elucidation of the reaction mechanism of atrazine and ametryn (*s*-triazine herbicides) hydrolysis on the enzymatic level by determination of carbon, nitrogen, and sulfur isotope fractionation. Additionally, it was investigated whether the inverse $^{15}N/^{14}N$ fractionation pattern of atrazine degradation by

Arthrobacter aurescens TC1 is also valid for other *s*-triazine herbicides and, thus, may serves as an indicator for their degradation in the environment.

Chapter 3 dealt with isotope effects of a pulse consisting of the micropollutants 2,6-dichlorobenzamide (BAM), bentazone, diclofenac, and ibuprofen in a mesoscale aquifer model mimicking field conditions. Here, the main focus was on the possibility to use (multi-element) CSIA to monitor the fate of micropollutants in a (near-)natural setup at environmentally relevant concentrations.

In Chapter 4, the drivers behind sorption isotope effects were investigated by water-air and hexadecane-air partitioning of benzene, triethylamine, and trichloromethane. In this study, air served as reference phase in which no intermolecular interactions occur, so that the direction and magnitude of the substances' isotope effects could be considered separately in correlation to the underlying type of molecular interaction (hydrogen bonding *vs.* van-der-Waals forces).

2

Characteristic Isotope Fractionation Patterns in *s*-Triazine Degradation Have Their Origin in Multiple Protonation Options in the *s*-Triazine Hydrolase TrzN

Heide K. V. Schürner, Jennifer L. Seffernick, Anna Gryzbkowska, Agnieszka Dybala-Defratyka, Lawrence P. Wackett, Martin Elsner, *Environ. Sci. Technol.* **2015**, *49*, 3490-3498

2.1 Introduction

Tracing pesticide degradation in the environment presents many challenges. Identification of the pertinent metabolic pathways is often incomplete. Even when metabolites are known, estimates of degradation that are based on parent compound/metabolite ratios can be biased: on the one hand, metabolites can be further transformed and, on the other hand, both parent compounds and metabolites may sorb to soil. Compound-specific Stable Isotope Analysis (CSIA) is an alternative, complementary tool to investigate contaminant degradation. The approach relies on the phenomenon that naturally occurring isotope ratios (*e.g.*, $^{13}C/^{12}C$, $^{15}N/^{14}N$) change within the parent compound during transformation reactions and it, therefore, does not depend on metabolite detection.[25,35] The changes in isotope ratios are induced by a kinetic isotope effect in the reactive bond and can be linked to the progress of degradation by the enrichment factor ε as described below.

ε-Values are negative if the isotope effect is normal (*i.e.*, light isotopologues are preferred and react faster), whereas ε-values are positive if the isotope effect is inverse (*i.e.*, heavy isotopologues are preferentially converted).

Furthermore, applications of CSIA can even be extended to investigate underlying transformation mechanisms of organic contaminants and to infer associated biodegradation pathways.[35] The combination of the isotopic signatures of two elements (*e.g.*, $\delta^{13}C$ and $\delta^{15}N$) in a two-dimensional isotope plot makes such studies possible. The resulting slope $\Delta = \delta^{15}N/\delta^{13}C = \varepsilon_{carbon}/\varepsilon_{nitrogen}$, typically differentiates between distinct reaction mechanisms because different bonds are involved and isotope effects of the participating elements change. This has been used to determine the difference between degradation pathways.[25,35,36] Because of this dependence on (bio)chemical reaction mechanisms – no matter whether the underlying transformation occurs with a purified enzyme or in natural ecosystems – these plots offer a unique opportunity to bridge the gap from the lab to the field and to identify which mechanisms of *s*-triazine degradation predominate in the environment.

s-Triazine herbicides like atrazine and ametryn have been used for over 50 years to control broadleaf and specific weeds,[37] and contamination of surface and groundwater has been observed.[38,39] The ability to monitor biotic and abiotic degradation mechanisms for *s*-triazine herbicides provides key knowledge fostering better environmental stewardship for agricultural chemicals. Specifically, the use of CSIA in studying atrazine

degradation has provided data on carbon and nitrogen isotope fractionation to distinguish atrazine degradation by different mechanisms: photolysis,[40] chemical hydrolysis,[23,41] and enzymatic breakdown.[23,31] Furthermore, distinct dual element isotope slopes were observed for different (bio)chemical transformation mechanisms. Most prominently, a characteristic inverse nitrogen isotope effect was observed for degradation by the bacterial strain *Arthrobacter aurescens* TC1[23] in which a hydrolytic dechlorination reaction occurred and a distinctly different pattern was observed for oxidative dealkylation by *Rhodococcus* sp. strain NI86/21.[31,42] The inverse nature of the nitrogen isotope effect with *Arthrobacter aurescens* TC1 provided evidence that bonding at the *N*-atom was stiffer in the transition state, suggesting that the atrazine molecule was protonated during enzymatic hydrolysis.[23] The significance of this observation was put into perspective by a subsequent study targeting the underlying enzyme TrzN.[43] The crystal structure of TrzN was solved, and the wild type TrzN was studied along with its site-directed mutant TrzN-E241Q for the ability to degrade atrazine and ametryn. Glutamic acid E241 was inferred to play a crucial role in wild type (which degraded both atrazine and ametryn) because ametryn hydrolysis stalled completely in the E241Q mutant where the glutamic acid (E241) had been replaced by glutamine (Q241) so that the ability of proton transfer from this side chain had been lost. In light of the evidence given by the inverse nitrogen isotope effect (which indicated that the *s*-triazine ring received a proton prior to hydrolysis) and with an interatomic distance of 3.3 Å between the *delta*-oxygen of E241 and the *s*-triazine ring nitrogen (which indicated that the distance was small enough to allow proton transfer from E241 to the *s*-triazine ring in the wild type) the glutamic acid residue was suggested to be the catalyst which protonates the *s*-triazine ring in the wild type and, thereby initializes the *s*-triazine degradation in TrzN. This interpretation was consistent with the pH-profile of the enzyme catalysis.[43]

Surprisingly, the same study found that the same mutant TrzN-E241Q (which did not degrade ametryn) was still able to effectuate hydrolysis of atrazine (albeit 11 times slower than wild type).[43] This raises the crucial question whether protonation of the *s*-triazine ring still takes place in the mutant and, therefore, whether such protonation is a common, or an exceptional feature of enzymatic *s*-triazine hydrolysis. If protonation of the *s*-triazine was a common feature, the inverse nitrogen isotope fractionation observed in Meyer *et al.*[23] would be a robust indicator of hydrolytic *s*-triazine biodegradation in nature. If not, isotope trends would be less consistent.

Potentially, the reaction of atrazine with the mutant TrzN-E241Q could be explained if atrazine was generally transformed faster than ametryn. This, however, is in contradiction with the observation that the wild type degraded atrazine four times *slower* than ametryn. These findings raise the following questions: (i) can the pattern of inverse nitrogen isotope fractionation that was previously observed in atrazine biodegradation[23] be reproduced for ametryn as well? (ii) Can this inverse isotope effect give evidence for the presence or absence of *s*-triazine protonation in TrzN-E241Q? (iii) If so, who is the proton donor? (iv) What is the mechanistic difference between atrazine and ametryn hydrolysis that makes ametryn hydrolysis faster in the wild type TrzN and stalls ametryn hydrolysis in the mutant? (v) Can protonation of the thiomethanolate (CH_3-S^-) leaving group facilitate ametryn hydrolysis, and can this role be pinpointed by sulfur isotope fractionation measurements?

The objective of this study was to investigate whether the inverse nitrogen isotope fractionation pattern is a general feature of *s*-triazine hydrolysis, through a better understanding of the underlying mechanistic details of enzymatic atrazine and ametryn degradation. To this end, compound-specific carbon, nitrogen and sulfur isotope effects were measured. Transformation of atrazine by purified TrzN was conducted to test whether isotope fractionation mirrors that of whole cell experiments with *Arthrobacter aurescens* TC1. The same experiment was conducted with TrzN-E241Q, to investigate if *s*-triazine ring protonation occurs even in the absence of E241, or if a distinctly different isotope fractionation pattern is observed. Subsequently, transformation of ametryn by TrzN was studied to investigate whether also for this substrate inverse nitrogen isotope effects are observed which would give evidence of *s*-triazine ring protonation. Sulfur isotope fractionation in the thiomethanolate leaving group was further measured to probe for a concerted *versus* stepwise nature in ametryn hydrolysis.[44] Finally, acidic hydrolysis of ametryn was performed as a reference experiment, and experiments were interpreted in comparison with complementary computational calculations.

2.2 Experimental Section

2.2.1 Chemicals

Ametryn (2-ethylamino-4-*iso*-propylamino-6-methylthio-1,3,5-triazine, CAS: 834-12-8, 98.5%), atrazine (2-chloro-4-ethylamino-6-*iso*-propylamino-1,3,5-triazine, CAS: 1912-24-9, 97.4%) and 2-hydroxyatrazine (CAS: 2163-68-0, 96.0%) were purchased from Fluka, supplied by Sigma-Aldrich (Seelze, Germany, https://www.sigmaaldrich.com). KH_2PO_4 was purchased from Alfa Aesar (Karlsruhe, Germany, https://www.alfa.com), K_2HPO_4 was from Merck (Darmstadt, Germany, http://www.merck.de), and H_3PO_4 (85%) and NaOH were from Sigma-Aldrich (Steinheim, Gernamy). Glycerol for molecular biology (≥ 99%) was purchased from Sigma-Aldrich (Steinheim, Germany). Milli-Q water was generated by a Milli-Q Advantage $A10_{system}$ (Millipore, Schwalbach, Germany, http://www.merckmillipore.com). Acetonitrile and ethyl acetate were from Fluka, supplied by Sigma Aldrich (Taufkirchen, Germany), dichloromethane and methanol were from Carl Roth (Karlsruhe, Germany, http://www.carlroth.com). All organic solvents were of LC-MS grade (purity > 0.99).

2.2.2 Enzymatic Hydrolysis of Atrazine and Ametryn

Purified enzymes TrzN and TrzN-E241Q were prepared as specified in Seffernick *et al*.[43] Degradation experiments were carried out in phosphate buffer (100 mM, pH 7, 10% glycerol). Experiments of atrazine contained 120 mL of 20 mg/L atrazine (111 mmol in total) with either 104 µg TrzN (specific activity: 1.7 µmol min^{-1} mg^{-1}) or 380 µg TrzN-E241Q (specific activity: 0.16 µmol min^{-1} mg^{-1}). Experiments of ametryn contained 400 mL of 100 mg/L ametryn (176 mmol in total) with 113 µg TrzN (specific activity: 6.8 µmol min^{-1} mg^{-1}). All experiments were performed in triplicates at 30 °C. A solution of each respective herbicide in phosphate buffer without enzyme was used as control.

2.2.3 Abiotic Hydrolysis of Ametryn

Triplicate experiments were conducted in acidic phosphate buffer (2 L, 100 mM, pH 1.75) with an initial ametryn concentration of ~100 mg/L. To increase the reaction rate, the experiment was performed at 60 °C.

2.2.4 Sampling

Samples were analyzed for substrate and product concentrations, and for isotope composition. Sample volumes for isotope analysis were between 2.5 mL (at the beginning of the reaction) and 35 mL (at the end of the reaction when less compound was left) for atrazine as well as between 10-90 mL for ametryn. For concentration analysis 2 mL for atrazine and ametryn were taken. All samples were immediately extracted with dichloromethane (2 × 1 mL for quantification, 2 × 10 mL for isotope analysis) to stop the enzymatic reaction and dried at room temperature under the fume hood. For concentration analysis, dried extracts were redissolved in methanol. For isotope analysis, samples were redissolved in ethyl acetate to a final concentration of ~50 mg/L (atrazine). In the case of abiotic hydrolysis, 2-4 mL were taken for quantification, adjusted to pH 7 using NaOH (92 mM), and measured without extraction. For isotope analysis, 15-570 mL were taken, adjusted to pH 7 with NaOH (92 mM), and extracted with dichloromethane (5 × 20 mL) which was evaporated at room temperature under the fume hood. Dried ametryn samples were split and used for sulfur isotope analysis by EA-IRMS (0.28-2.1 mg) as well as carbon and nitrogen isotope analysis by GC-IRMS (redissolved in ethyl acetate to a final concentration of ~100 mg/L).

2.2.5 Quantification with HPLC

Concentrations of atrazine, ametryn and 2-hydroxyatrazine were measured using a LC-A10 series HPLC system and quantified with CLASS VP V6.10 software (both Shimadzu, Kyōto, Japan, http://www.shimadzu.com). The column used was an Allure C18 (5 µm, 150 × 4.6 mm, Restek, Bad Homburg, Germany, http://www.restek.com). For detailed information on the method see Appendix A.1.1.

2.2.6 Compound-specific Stable Isotope Analysis

Carbon and nitrogen isotope analysis of atrazine and ametryn was performed on a GC-IRMS system consisting of a TRACE GC Ultra gas chromatograph (Thermo Fisher Scientific, Milan, Italy, http://www.thermofisher.com) equipped with a DB-5 analytical column (30 m, 0.25 mm ID, 1.0 µm film, Agilent Technologies, Böblingen, Germany, http://www.agilent.com), which was coupled to a Finnigan MAT 253 isotope ratio mass spectrometer *via* a Finnigan GC Combustion III interface (both Thermo Fisher Scientific,

Bremen, Germany). The initial GC oven temperature was 100 °C (hold 5 min), ramped 15 °C/min to 220°C, ramped 8 °C/min to 250 °C, and ramped 35 °C/min to 280 °C (hold 1 min). The standard deviation of atrazine measurements was ± 0.3‰ for both carbon and nitrogen, and ± 0.4‰ for carbon and ± 0.9‰ for nitrogen in ametryn measurements. Detailed information on the method is described in Appendix A.1.1.

$\delta^{13}C$ and $\delta^{15}N$ values are expressed in per mil relative to Vienna PeeDee Belemnite (V-PDB) and air, respectively:

$$\delta^{13}C = \frac{\left[\left({}^{13}C/{}^{12}C\right)_{sample} - \left({}^{13}C/{}^{12}C\right)_{standard}\right]}{\left({}^{13}C/{}^{12}C\right)_{standard}} \qquad \text{eq. 2.1}$$

$$\delta^{15}N = \frac{\left[\left({}^{15}N/{}^{14}N\right)_{sample} - \left({}^{15}N/{}^{14}N\right)_{standard}\right]}{\left({}^{15}N/{}^{14}N\right)_{standard}} \qquad \text{eq. 2.2}$$

Sulfur isotope analysis of ametryn was conducted on an EA-IRMS system consisting of an EuroEA elemental analyzer (EuroVector, Milan, Italy) coupled to a Finnigan MAT 253 IRMS by a FinniganConFlow III interface (both Thermo Fisher Scientific, Bremen, Germany). For detailed information on the method see Appendix A.1.1.

$\delta^{34}S$ values are expressed in per mil relative to Vienna Canyon Diablo Troilite (V-CDT):

$$\delta^{34}S = \frac{\left[\left({}^{34}S/{}^{32}S\right)_{sample} - \left({}^{34}S/{}^{32}S\right)_{standard}\right]}{\left({}^{34}S/{}^{32}S\right)_{standard}} \qquad \text{eq. 2.3}$$

Enrichment factors ε can be determined as the slope of the linear regression according to the Rayleigh equation

$$\ln\frac{R_t}{R_0} = \ln\left(\frac{\delta\,{}^{h}E_t + 1}{\delta\,{}^{h}E_0 + 1}\right) = \varepsilon \times \ln\left(\frac{c_t}{c_0}\right) \qquad \text{eq. 2.4}$$

where R_t and R_0 are the compound-specific isotope ratios of heavy and light isotopes (*e.g.*, $^{13}C/^{12}C$) at time *t* and at the beginning of the reaction, respectively. $\delta^{h}E_t$ and $\delta^{h}E_0$ are the corresponding isotopic signatures of the particular element *E*, and c_t/c_0 is the fraction of the remaining substrate. The enrichment factor ε reflects the average isotopic enrichment over all positions in the compound. For enzyme reactions, ε is related to the apparent kinetic isotope effect AKIE as follows (for the case of carbon), where v_{max} is the

Michaelis-Menten maximum rate, K is the Michaelis-Menten constant, and n is the number of carbon atoms in the substance. The equation is exact for $n = 1$; if $n \neq 1$, AKIEs tend to be underestimated in comparison to studies with labelled substrate (see the Supporting Information of Elsner *et al.*[19]).

$$\mathrm{AKIE}_{carbon} = \frac{^{12}(v_{max}/K)}{^{13}(v_{max}/K)} \approx \frac{1}{n \times \varepsilon_{carbon} + 1} \qquad \text{eq. 2.5}$$

2.3 Computational Calculations

The gas phase geometries of all molecular species were fully optimized at the density functional (DFT) level using the MPW1K[45] and M05-2X[46] functionals. They were combined with the 6-31+G(d,p)[47] and LANL2DZ[48] basis sets, respectively. To confirm located stationary points either as minima or transition state structures, vibrational analyses were carried out using harmonic oscillator and rigid-rotor approximations. All calculations were performed using the Gaussian 09 package.[49] Full details of free energy surfaces and all KIE calculations are provided in Appendix A.1.1.

2.4 Results and Discussion

2.4.1 Carbon and Nitrogen Isotope Fractionation during Enzymatic Hydrolysis of Atrazine

Wild type TrzN and TrzN-E241Q showed atrazine degradation (Appendix Figure A.1-1), whereas no degradation took place in control experiments lacking enzyme (Appendix Figure A.1-2). During transformation with TrzN, ^{13}C became enriched relative to ^{12}C in the remaining atrazine ($\varepsilon_{carbon} = -5.0‰ \pm 0.2‰$), corresponding to a normal carbon isotope effect, and ^{15}N became depleted relative to ^{14}N ($\varepsilon_{nitrogen} = 2.5‰ \pm 0.1‰$) representing an inverse nitrogen isotope effect (Figure 2.1). Similar observations were previously made for degradation of atrazine with the TrzN-containing bacterial strain *Arthrobacter aurescens* TC1[23] (Table 2.1). Together, these results confirm the conclusion of our previous study that atrazine degradation starts with protonation of a nitrogen atom of the *s*-triazine ring prior to nucleophilic aromatic substitution.[23,43]

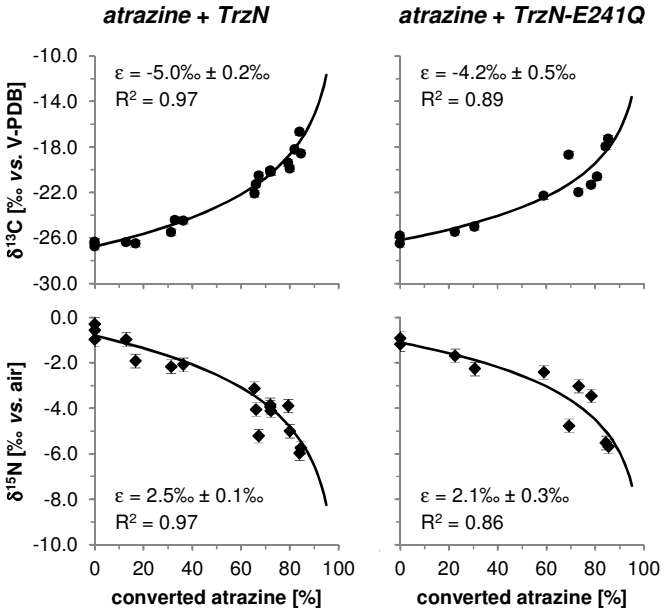

Figure 2.1: Changes in carbon and nitrogen isotope values during enzymatic hydrolysis of atrazine with TrzN (left) and the mutant TrzN-E241Q (right). Error bars represent total uncertainty of carbon (± 0.3‰) and nitrogen (± 0.3‰) isotope analysis.

A subsequent experiment investigated whether isotope fractionation trends differed in TrzN-E241Q, where the ability of proton transfer had been lost in Q241 so that protonation would not be expected by this residue. Surprisingly, Figure 2.1 shows almost identical trends ($\varepsilon_{nitrogen}$ = 2.1‰ ± 0.3‰, see Table 2.1) indicating that a nitrogen atom of atrazine was still protonated prior to hydrolysis. This raises the question of possible mechanistic explanations.

Table 2.1: Enrichment factors ε for carbon, nitrogen, and sulfur isotope effects determined according to the Rayleigh equation (eq. 2.4) and position-specific carbon and sulfur kinetic isotope effects (AKIEs), and average nitrogen isotope effects calculated at 60 °C for the mechanistic pathways of ametryn acidic hydrolysis (Figure 2.4).

	ε_{carbon} [‰]	$\varepsilon_{nitrogen}$ [‰]	$\Delta = \delta^{15}N/\delta^{13}C = \varepsilon_{carbon}/\varepsilon_{nitrogen}$	ε_{sulfur} [‰]	$AKIE_{carbon}$ [ ]	$AKIE_{nitrogen}$ [ ]	$AKIE_{sulfur}$ [ ]
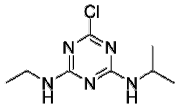							
atrazine with *A. aurescens* TC1[a]	-5.4 ± 0.6[a]	3.3 ± 0.4[a]	-0.61 ± 0.02[a]	-	1.045 ± 0.005[a]	0.974 ± 0.003[a]	-
atrazine with TrzN	-5.0 ± 0.2	2.5 ± 0.1	-0.54 ± 0.02	-	1.041 ± 0.002[d]	0.988 ± 0.001[d]	-
atrazine with TrzN-E241Q	-4.2 ± 0.5	2.1 ± 0.3	-0.50 ± 0.03	-	1.035 ± 0.004[d]	0.989 ± 0.001[d]	-
atrazine acidic hydrolysis (abiotic)[a]	-4.8 ± 0.4[a]	2.5 ± 0.2[a]	-0.52 ± 0.04[a]	-	1.040 ± 0.003[a]	0.988 ± 0.001[a]	-
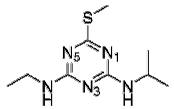							
ametryn with TrzN	-1.9 ± 0.2	4.3 ± 0.4	-1.91 ± 0.27	-14.7 ± 1.0	1.017 ± 0.002[d]	0.979 ± 0.002[d]	1.015 ± 0.001[d]
ametryn acidic hydrolysis							
measured	-2.4 ± 0.3	3.6 ± 0.4	-1.48 ± 0.20	-0.19 ± 0.04	1.022 ± 0.003[d]	0.982 ± 0.002[d]	1.0002 ± 0.00004[d]
theoretical prediction (protonated N_3)[b]	-3.77[c]	1.86[c]	*n.d.*	-0.30[c]	1.0351[e]	0.991[e]	1.0003
theoretical prediction (protonated S)[b]	-4.60[c]	-0.50[c]	*n.d.*	-2.89[c]	1.0432	1.0025	1.0029

[a] Data taken from ref. [23]. [b] N_3 and *S* indicate different protonation sites of the substrate molecule ametryn. [c] ε-Values are calculated from the sum of theoretically predicted position-specific KIEs for the rate determining steps of the studied pathways of ametryn hydrolysis (RC → TS1 and RC → TS for N_3 and *S* protonated mechanistic scenarios, respectively, Appendix Table A.1-1) according to eq. 2.5. [d] AKIEs are calculated from measured ε-values according to eq. 2.5. [e] Sum of the carbon and nitrogen position-specific kinetic isotope effects (Appendix Table A.1-1).

Figure 2.2 presents a possible mechanism how protonation of the *s*-triazine ring may be effectuated in TrzN (Protein Database ID: 3LS9) and TrzN-E241Q (Protein Database ID: 3LSB) based on a careful analysis of the enzyme X-ray crystal structures of both enzymes. Two water molecules in the enzymatic pocket are bound *via* hydrogen bonds to the zinc ion and threonine T325, respectively. For the wild type enzyme TrzN, we propose a mechanism in which the water molecule coordinated at the zinc ion shuttles a proton to glutamate E241 (*via* H274; Figure 2.2, first structure in middle panel) which becomes glutamic acid and protonates the atrazine, while the zinc-bound hydroxide ion functions as a nucleophile. In the mutated enzyme TrzN-E241Q, in contrast, we suggest that it is the second water molecule which protonates the atrazine as an alternate proton donor because its interatomic distance to the atrazine ring nitrogen atom is only 2.83 Å (Figure 2.2, lower panel – for comparison, the interatomic distance between E241 and the *s*-triazine ring in the wild type is 3.3 Å.[43] Additional distances are given in Appendix A.1.2).

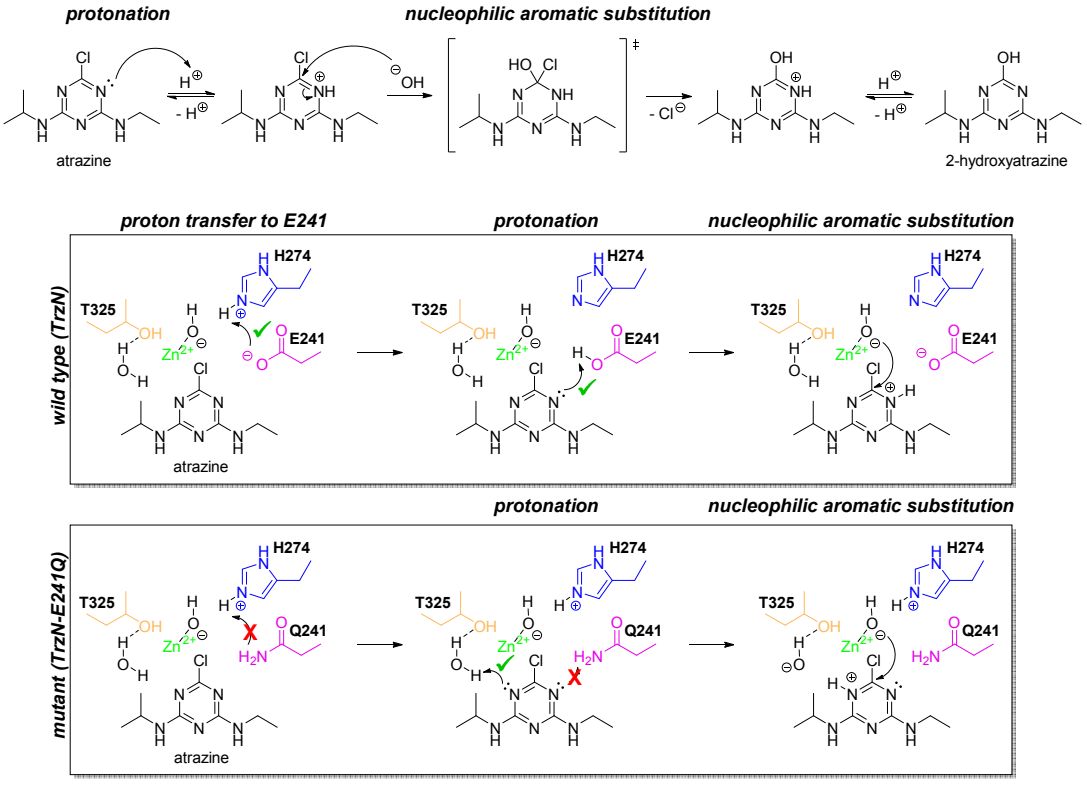

Figure 2.2: Proposed mechanism for the degradation of atrazine by wild type enzyme TrzN (middle panel) and mutated enzyme TrzN-E241Q (lower panel).

We, therefore, postulate (i) that whereas atrazine is protonated by E241 in the wild type TrzN, it is protonated by the non-nucleophilic water molecule in the mutant TrzN-E241Q, as shown in Figure 2.2 so that in both cases an inverse nitrogen isotope effect is observed leading to a consistent pattern of isotope fractionation;[43] (ii) that, consequently, the activation of the degradation process (substrate protonation) is less effective in the mutant.[43]

2.4.2 Carbon and Nitrogen Isotope Fractionation during Biotic and Abiotic Hydrolysis of Ametryn

In our experiments, ametryn was transformed both in enzymatic TrzN hydrolysis as well as in abiotic acidic hydrolysis at pH 1.75, as demonstrated by decreasing substrate and increasing product concentrations (Appendix Figure A.1-1), whereas no measurable degradation had previously been observed with TrzN-E241Q.[43] Control experiments (no enzyme, pH 7) showed no herbicide degradation (Appendix Figure A.1-2). Again, normal carbon (ε_{carbon} = -1.9‰ ± 0.2‰) and inverse nitrogen ($\varepsilon_{nitrogen}$ = 4.3‰ ± 0.4‰) isotope effects were observed suggesting that also in ametryn, an *s*-triazine nitrogen atom was protonated prior to hydrolysis (Figure 2.3). We also predicted position-specific carbon and nitrogen kinetic isotope effects (Appendix Table A.1-1) taking into account two mechanistic scenarios (Figure 2.4). The pathway in which the N_3 position in the *s*-triazine ring is protonated turned out to be a two-step reaction with the first step comprising the Meisenheimer-intermediate formation (Figure 2.4a, INT structure) and the second step describing thiomethyl group elimination. In the alternative mechanism sulfur protonation was considered which led to one-step reaction (Figure 2.4b). The comparison of theoretically predicted AKIEs with the experimental values presented in Table 2.1 clearly favors the nitrogen-protonation mechanism even though small discrepancies are observed between calculated and measured values. These differences are most likely due to the fact that in the theoretical prediction of apparent KIEs all position-specific effects, even those in positions that are distant from the reactive bond were taken into account which resulted in very small numbers most likely carrying larger errors. Deriving AKIEs from ε-values, on the other hand, assumes that the contribution of all these secondary positions will be the same which is never a case. Therefore, the obtained good qualitative agreement between theory and experiment in this study seemed satisfactory to us and sufficient for interpretation purposes. Figure 2.3 and Table 2.1 also show that carbon and nitrogen

isotope effects in chemical acidic hydrolysis and TrzN hydrolysis of ametryn were essentially identical. Together, these results suggest that protonation of *s*-triazine nitrogen atoms does not only occur in atrazine but also in ametryn and that it is, therefore, a recurring feature in TrzN catalysis.[43] It, however, fails to address why TrzN-E241Q does not degrade ametryn. A possible explanation is that – besides protonation of an *s*-triazine nitrogen atom – ametryn hydrolysis would in addition necessitate protonation of the CH_3-S^- leaving group (which would be missing in the mutant). To address this hypothesis, sulfur isotope effects were measured.

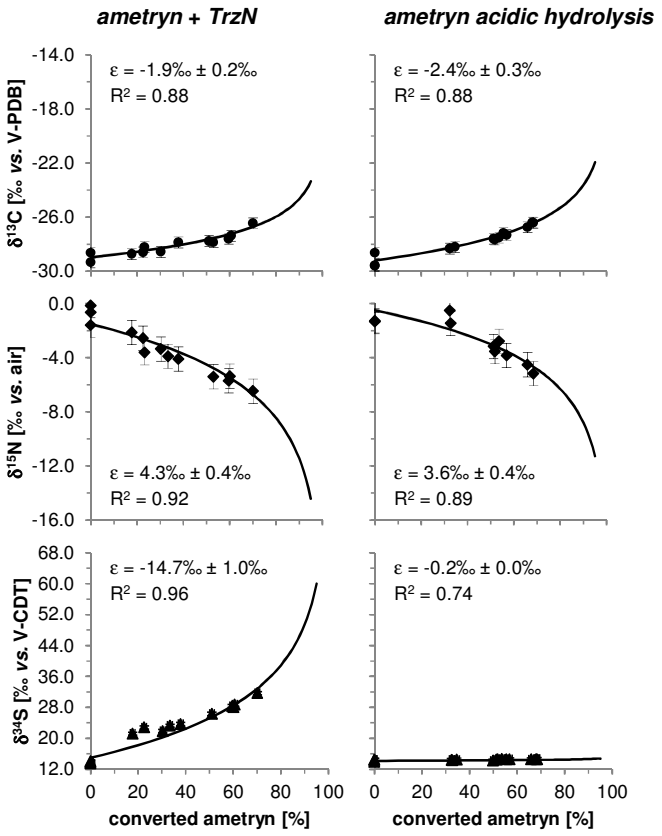

Figure 2.3: Changes in carbon, nitrogen, and sulfur isotope values during enzymatic ametryn hydrolysis with TrzN (left) and abiotic acidic ametryn hydrolysis at pH 1.75 (right). Error bars indicate total uncertainty of carbon (± 0.4‰), nitrogen (± 0.9‰), and sulfur (± 0.4‰) isotope analysis.

2.4.3 Sulfur Isotope Fractionation during Biotic and Abiotic Hydrolysis of Ametryn

In contrast to carbon and nitrogen isotope effects, sulfur isotope effects differed greatly between abiotic and TrzN-catalyzed hydrolysis of ametryn (Figure 2.3). A pronounced sulfur isotope effect as we observed in enzymatic hydrolysis ($AKIE_{sulfur} = 1.015 \pm 0.001$) is expected if cleavage of the *C-S* bond is rate-determining and $CH_3\text{-}S^-$ is released without previous protonation.[50] This result, therefore, indicates that the sulfur atom was *not* protonated prior to the nucleophilic substitution. In contrast, the small isotope effect ($AKIE_{sulfur} = 1.0002 \pm 0.00004$) observed in the abiotic hydrolysis can be explained by two potential hypotheses: (i) a small *apparent* isotope effect could arise – even despite a large intrinsic isotope effect - if *C-S* bond cleavage is not rate-determining or occurs after a first irreversible step; (ii) a small *intrinsic* isotope effect could be the net result of an *inverse* isotope effect due to *S*-protonation and a *normal* isotope effect during subsequent *C-S* bond cleavage to release thiomethanol ($CH_3\text{-}SH$). To further distinguish the two possibilities, computational calculations were performed.

For acidic ametryn hydrolysis our computational calculations predicted that protonation of the *S*-atom prior to hydrolysis would give a net *normal* isotope effect of $KIE_{sulfur} = 1.0029$ on the transition from RC to TS (Figure 2.4b). Such a normal leaving group isotope effect has recently been calculated, and experimentally demonstrated, for chlorine isotopes from atrazine by Grzybkowska *et al.*[44] In contrast, a negligible isotope effect was predicted for protonation of the *N*-atom prior to hydrolysis ($KIE_{sulfur} = 1.0003$ on the transition from RC to TS1, Figure 2.4a). This number more accurately reproduces our experimental value of $AKIE_{sulfur} = 1.0002 \pm 0.00004$ (Table 2.1). The calculations therefore confirm our second hypothesis: that the $AKIE_{sulfur}$ of unity arose because *C-S* bond cleavage is not rate-determining in acidic ametryn hydrolysis. As illustrated in Figure 2.4a, the formation of the Meisenheimer-like complex is predicted to be rate-determining – a reaction step in which no or negligible sulfur isotope effects are expected – so that a more pronounced sulfur isotope effect in subsequent *C-S* bond cleavage does not become visible in the substrate.

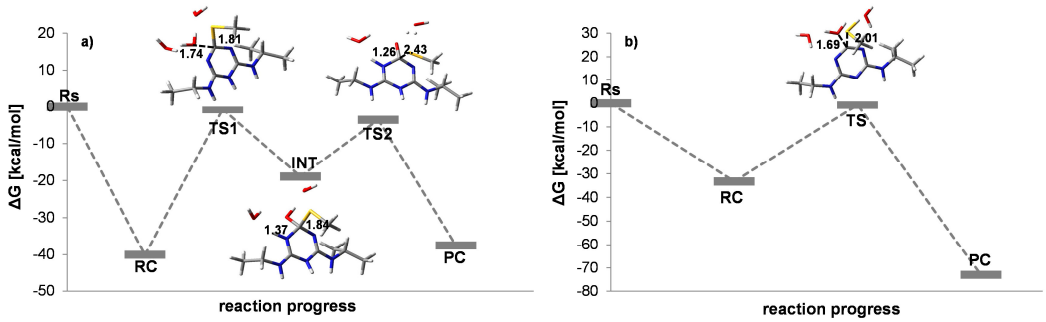

Figure 2.4: Free energy profiles for (a) the uncatalyzed acidic hydrolysis of ametryn with protonated N_3 position and (b) the uncatalyzed acidic hydrolysis of ametryn with protonated sulfur atom, respectively, obtained at the SMD_{water}/MPW1K/6-311+G(2df,2p)//MPW1K/6-31+G(d,p) level of calculations. Rs = reactants (ametryn and three water molecules treated separately), RC = reactants complex (ametryn and three water molecules treated as a supermolecule), TS = transition state, INT = intermediate (Meisenheimer-like complex) and PC = products complex. All energy values are related to the sum of energies of Rs. Key distances are given in angstroms.

In contrast, the strong normal sulfur isotope effect (*i.e.*, leaving group effect; $AKIE_{sulfur} = 1.015 \pm 0.001$) in enzymatic hydrolysis gives evidence that *C-S* bond cleavage was largely rate-determining and that it occurred before the first irreversible step. In particular, the pronounced sulfur leaving group isotope effect indicates that the enzyme accelerated the first step of the nucleophilic substitution (addition of nucleophile) relative to the *C-S* bond cleavage so that leaving group abstraction became rate-determining. Our preliminary computational data of ametryn hydrolysis in the wild type TrzN active site can contribute to this observation in the following way. Meisenheimer-like intermediate (EI) formation seems to be slightly exothermic if not neutral in the enzymatic environment (Figure 2.5b) in contrast to the large energetic cost of this step in aqueous solution (Figure 2.4a). If the first step of the enzymatic hydrolysis was also accompanied by significant energetic barrier, then $AKIE_{sulfur}$ would be much diminished either due to masking or complexity of reaction (two reaction steps contributing almost equally to the overall isotopic fractionation) in much the same way as in solution. In the enzymatic environment, however, the predicted, increased thermodynamic feasibility of the first step (*i.e.*, the small, almost negligible barrier for the Meisenheimer-complex formation) together with the pronounced energetic cost for the *C-S* bond cleavage indicates that it should not be the case and that the second step (*i.e.*, *C-S* bond cleavage) should be rate-limiting, consistent with our observed sulfur isotope effects.

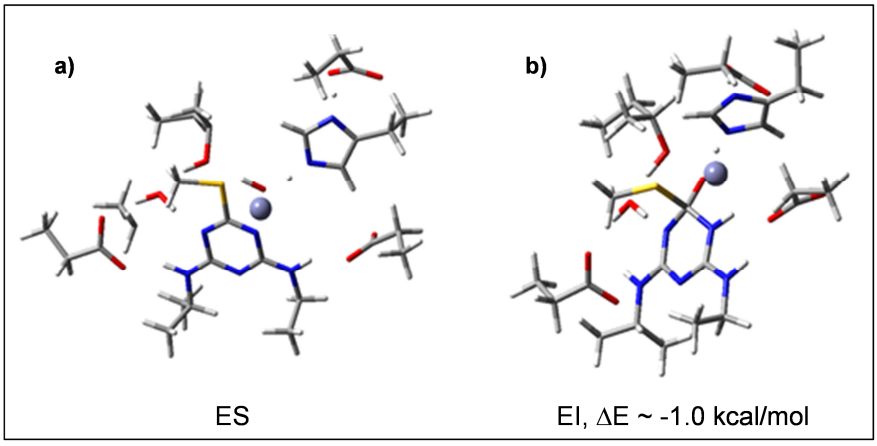

Figure 2.5: Optimized structure of enzyme-substrate (ES) and enzyme-intermediate (EI) complexes using the truncated models of the wild type enzyme TrzN and the SMD/MPW1K/6-311+G(2df,2p)//M05-2X/LANL2DZ level of theory. Zinc ion coordination sphere has been omitted for clarity. For the full model, see Appendix Figure A.1-4.

The observation of a large normal sulfur isotope effect ($AKIE_{sulfur} = 1.015 \pm 0.001$) also appears to rule out leaving group protonation which contrasts with the fact that ametryn hydrolysis activity does not occur in TrzN-E241Q even though atrazine hydrolysis continues. To reconcile both observations, we propose the following mechanism. First, we hypothesize that the CH_3S^- group is not protonated *before* but *after* leaving the ametryn molecule. We postulate that after *C*-*S* bond cleavage, protonation of CH_3S^- is necessary to avoid the back reaction (formation of ametryn out of 2-hydroxyatrazine) and that such post cleavage leaving group protonation is not necessary with atrazine because chloride is too weak a nucleophile to effectuate the back reaction from 2-hydroxyatrazine to atrazine. Furthermore, we hypothesize that such protonation of the leaving group is not possible in TrzN-E241Q according to the mechanism shown in Figure 2.6. In the wild type enzyme, the water bound by T325 can protonate the leaving group after *C*-*S* bond cleavage in a stepwise mechanism. In the mutated enzyme, however, protonation of the substrate may be taken over by the non-nucleophilic water molecule. Therefore, the proton of this water molecule would no longer be available to protonate the leaving thiomethanolate group in TrzN-E241Q so that ametryn degradation is prevented.

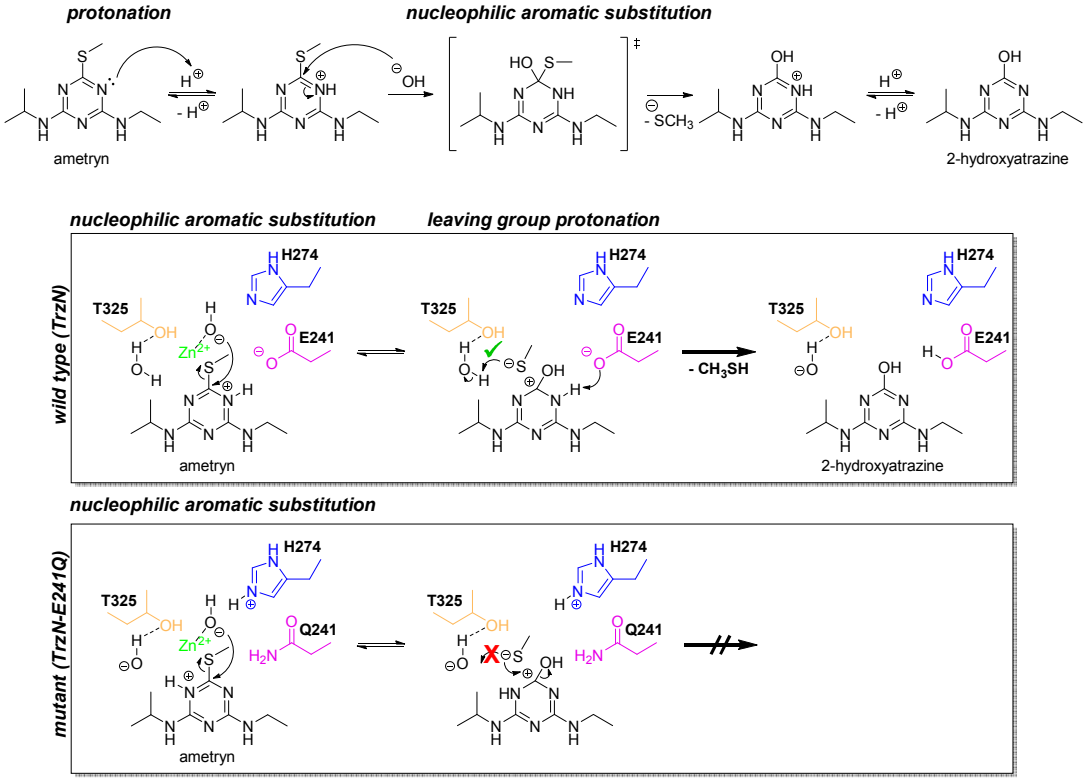

Figure 2.6: Proposed mechanism in ametryn degradation by wild type TrzN (middle panel) and TrzN-E241Q (lower panel). Reaction steps are illustrated starting from the nucleophilic aromatic substitution. The zinc ion has been omitted for clarity where necessary.

The fact that ametryn is degraded four times faster by TrzN than atrazine can also help to understand the degradation mechanism. Ametryn is a stronger base ($pK_a = 4.10$) and therefore easier to protonate than atrazine ($pK_a = 1.68$). In addition, the chlorine substituent deactivates the ring (*-I* effect, weak *+M* effect) while the thiomethyl moiety has the opposite effect (negligible *–I* effect, strong *+M* effect). Together, these explanations argue for a more rapid turnover of ametryn compared to atrazine in wild type TrzN, consistent with the observations by Seffernick *et al.*[43] This shift in relative reaction rates of the separate steps involved in enzymatic *N*-protonation may also be responsible for the difference between atrazine and ametryn in the two-dimensional isotope slopes. Figure 2.7 illustrates that although degradation of both compounds shows the characteristic inverse nitrogen isotope fractionation, the actual slope is different in the case of ametryn compared to reactions with atrazine.

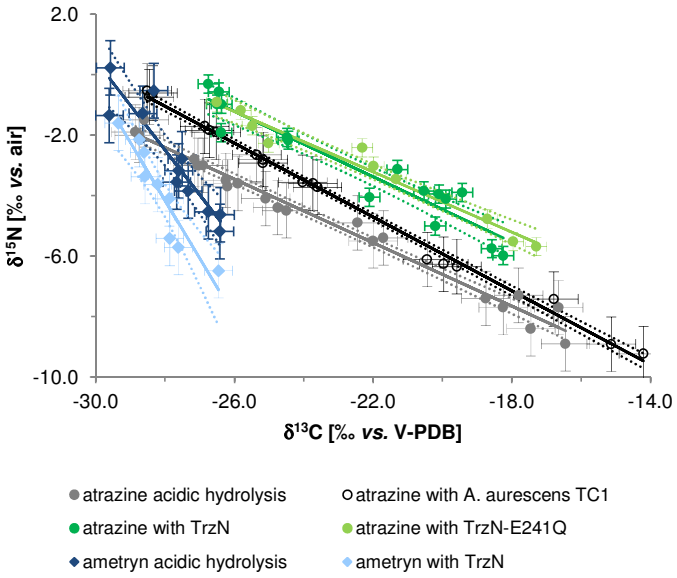

Figure 2.7: Two-dimensional isotope plot of carbon and nitrogen isotope ratios. Atrazine data of acidic hydrolysis and of degradation by *Arthrobacter aurescens* TC1 is taken from Meyer *et al.*[23] The slopes regressions are given as Δ (Table 2.1). Error bars represent total uncertainty of carbon (± 0.7‰ for atrazine acidic hydrolysis and *A. aurescens* TC1, ± 0.3‰ for atrazine with enzymes, ± 0.4‰ for ametryn) and nitrogen (± 0.9‰ for atrazine acidic hydrolysis and *A. aurescens* TC1, ± 0.3‰ for atrazine with enzymes, ± 0.9‰ for ametryn) isotope analysis. Dotted lines represent 95% confidence intervals of linear regression. Note that strictly spoken, slopes of atrazine and ametryn are not directly comparable because of the different number of carbon atoms (for atrazine $n_{carbon} = 8$; for ametryn $n_{carbon} = 9$).

2.4.4 Environmental Significance

Despite these differences in the numeric values of the slope, both substrates (ametryn and atrazine) display a characteristic pattern of inverse nitrogen and normal carbon isotope fractionation during TrzN enzymatic hydrolysis. This confirms the general trend observed in earlier studies.[23] The results of our study therefore imply that this pattern is caused by a remarkable ability of the TrzN enzyme for acid catalysis. Not only does this pattern extend from atrazine to ametryn, it also persists if one acidic group (E241) is replaced in the mutant indicating a remarkable functional redundancy for protonation of atrazine within the enzyme. This underlying mechanism is reflected in characteristic two-dimensional isotope slopes (Figure 2.7) that hold promise for the identification of biotic hydrolysis of *s*-triazines in natural systems. The present study provides a mechanistic understanding for the origin of these observable isotope effects.

3

Compound-specific Stable Isotope Fractionation of Pesticides and Pharmaceuticals in a Mesoscale Aquifer Model

Heide K. V. Schürner, Michael P. Maier, Dominik Eckert, Ramona Brejcha, Claudia-Constanze Neumann, Christine Stumpp, Olaf A. Cirpka, Martin Elsner, *Environ. Sci. Technol.*,
DOI: 10.1021/acs.est.5b03828

3.1 Introduction

Groundwater is widely used as drinking water resource, yet ubiquitously impacted by anthropogenic compounds. In addition to legacy chemicals known from point source contaminations at industrial sites (*e.g.*, petroleum or chlorinated hydrocarbons), increasing attention is directed at pesticides, pharmaceuticals, or consumer care products.[51] In contrast to most legacy chemicals – which typically occur in pure phase and, therefore, high concentrations (mg/L) at contaminated sites –, these substances are released ubiquitously in the urban water cycle or as a consequence of agricultural activities. They are frequently termed micropollutants,[2,3] because they are rapidly diluted to lower (ng/L to µg/L) concentrations, or "chemicals of emerging concern" (CECs), because their relevance has only recently been recognized.[51] These compounds tend to contain distinct functional groups and are often quite soluble in water so that they have a potential of reaching groundwater. Although typically low, their concentrations frequently exceed the permitted maximum drinking water concentrations in many countries[4] and some studies indicate negative impacts of pesticides and pharmaceuticals on human and ecosystem health.[52,53] While micropollutants are primarily released into rivers and lakes through wastewater treatment plant effluents[54,55] and agricultural runoff,[56,57] their fate is also of interest in aquifers,[4] which they may reach as a consequence of agricultural application, through artificial groundwater recharge,[58,59] or by riverbank filtration.[60,61] To the extent that water scarcity intensifies and water reuse increases, the importance of micropollutant degradation in aquifers, sediments, and associated engineered systems increases. Therefore, even though the term micropollutant implies the importance of low concentrations (ng/L to µg/L range), a process understanding of their degradation is equally important for scenarios involving higher concentrations such as in biopurification systems used on farms to treat contaminated water.[62] In the current study we will stick to "micropollutants", because pesticides and pharmaceuticals are commonly associated with this term, even when present in µg/L rather than ng/L concentrations. Also, while field studies often focus on long-term release in contaminant plumes,[63,64] a pulse release, *e.g.*, by artificial aquifer recharge[58,59] or agricultural applications, is a particularly relevant scenario for these compounds that warrants investigation. By deliberately following such pulses through natural systems, the intrinsic degradation capacities of filter units in both natural and technical systems can be assessed.

Despite their importance, studies which address transformation of micropollutants in groundwater or sediments are only recently emerging,[65-67] and tracing their degradation in the environment is often difficult.[4,68,69] Many metabolites, especially of pharmaceuticals, are still unknown or not even detectable, because they are further transformed.[30] Therefore, mass balances are not easily closed and metabolite/parent compound ratios may be inconclusive. For instance, if metabolite/parent compound ratios are applied to estimate the extent of parent compound breakdown, further degradation of metabolites would bias this estimate.

A complementary approach to investigating the environmental behavior of contaminants is Compound-specific Stable Isotope Analysis (CSIA). This method is based on the change in the naturally occurring isotopic composition of a substance during its chemical transformation. CSIA has become an established tool to evaluate degradation of organic priority pollutants at contaminated sites.[8,11,26,28,29] These legacy compounds (petroleum and chlorinated hydrocarbons) have in common that they are typically volatile, non-polar, and, therefore, easily analyzable by Gas Chromatography coupled to Isotope Ratio Mass Spectrometry (GC-IRMS). In comparison, isotope analysis of micropollutants is challenging, because they possess more polar chemical structures involving heteroatoms so that method development including derivatization is often required prior GC-IRMS analysis.[25] Until today, studies targeting isotope analysis of such typical micropollutant structures have therefore primarily focused on method development and validation,[30,41,70-72] and on laboratory batch experiments aiming to evaluate the principal feasibility of CSIA to detect their degradation.[31,36,73,74] In comparison, investigations of micropollutant degradation in environmental or near-natural systems by CSIA are still rare.[64,75-77] Such CSIA examinations in a relevant setting are challenging because of the compounds' complex structure, their high polarity, and the presence of heteroatoms. Compared to aromatic or chlorinated solvents, they are more difficult to separate from background interferences,[76] smaller observable carbon isotope fractionation is expected because of larger molecular size,[9,35] nitrogen isotope analysis requires larger sample amounts and is less precise compared to carbon,[78] the performance of combustion reactors is critical,[71,79] and additional uncertainty is introduced through derivatization.[30] Conversely, heteroatoms (*e.g.*, nitrogen) facilitate multi-element CSIA offering the opportunity of pathway identification[30,36,73,80] and may provide additional information if carbon isotope analysis alone is inconclusive.[19] Taken together, these aspects emphasize

the research need to investigate how confidently CSIA can be used to study degradation of typical micropollutants in a near-natural setting.

A physical aquifer model is particularly suited to this end because mass fluxes in the in- and outflow can be measured, and the flow field is reasonably well controlled so that mass balances can be established. By adding a conservative tracer as internal standard and comparing the breakthrough curve (BTC) of the latter with the BTCs of the contaminants, transformation rates and the sorption of the contaminants can be deduced. Further, the dimensions of an artificial aquifer filled with pristine aquifer material are large enough to mimic *in situ* conditions and to sample sufficiently large water volumes to obtain the necessary amount of substance for precise isotope analysis at relevant concentrations. This information allows revisiting biodegradation kinetics of micropollutant biodegradation and sorption properties. Finally, such aquifer models with dimensions of meters reflect already to some extent the complexity of field sampling. Even if packed as homogeneously as possible, such systems are prone to physical heterogeneity and similar to field applications, a fully resolved assessment of the internal heterogeneity would involve tremendous experimental effort. Thus, they provide a realistic case for the application of analytical methods to the experimental data that don't require a full three-dimensional representation of the system. On the one hand, the simplicity of such an approach is clearly advantageous; on the other hand, its validity must be justified by experimental evidence.

It is commonly assumed that isotope fractionation, *i.e.*, the change of the original isotopic composition, is mainly caused by bond breaking and formation of new bonds during degradation.[11] However, more and more field studies report isotope effects induced by physical processes for priority pollutants at contaminated sites. These include: sorption,[81,82] diffusion,[83] and transverse dispersion.[84] An experiment in a model aquifer allows investigating the importance of such isotope effects for micropollutants as more polar compounds for which less sorption is expected. The objectives of the present study were, therefore, (i) to demonstrate the feasibility of multi-element CSIA to monitor typical micropollutants in groundwater using isotope ratios of both carbon and nitrogen, and (ii) to examine CSIA of such compounds in an environmentally relevant setting. Towards this end, we introduced a pulse of important pesticides and pharmaceuticals consisting of the herbicide bentazone,[85,86] the herbicide-metabolite 2,6-dichlorobenzamide (BAM),[87,88] the anti-inflammatory drug diclofenac,[89,90] and the painkiller ibuprofen[53,91] together with D_2O as conservative tracer to a mesoscale aquifer

model. Batch degradation experiments had previously established the possibility of pronounced carbon and nitrogen isotope fractionation in BAM,[73] whereas pronounced nitrogen, but little carbon isotope fractionation was observed in diclofenac[30] and no data was available for the other two compounds. Subsequent to injection of the pulse, we analyzed BTCs of concentrations and isotope ratios downstream of the injection, and we fitted parsimonious reactive-transport models including isotope fractionation to the data.

3.2 Experimental Section

3.2.1 Chemicals

A complete list of chemicals used in this study is given in Appendix A.2.1.

3.2.2 Experimental Setup

The experiment was carried out in a mesoscale indoor aquifer (dimensions: $4.8 \times 0.8 \times 0.7$ m^3, Figure 3.1) filled with sieved sediment (grain size: 0-4 mm, total organic carbon (TOC) content: 0.25%) from a gravel pit in the Bavarian Alpine Foreland, Germany, and fed continuously with natural groundwater (rate: 240 L/d). The oxygen content was between 8.41 ± 0.27 mg/L (transect A) and 7.62 ± 0.17 mg/L (transect F). A detailed description of the system is given by Qui *et al.*[33] and Herzyk *et al.*[92] with the difference that since these studies, repetitive sediment-sampling campaigns may have increased the heterogeneity of the porous media. A pulse (total volume: 1 L) of contaminants (522.7 mg/L BAM, 271.3 mg/L bentazone, 64.2 mg/L diclofenac, and 53.7 mg/L ibuprofen) in 850 mL Milli-Q water and 150 mL D_2O (90 atom % D) was injected by a horizontal well (0.35 m from the bottom of the system, injection rate: 780 mL/d) over a period of 30 h.

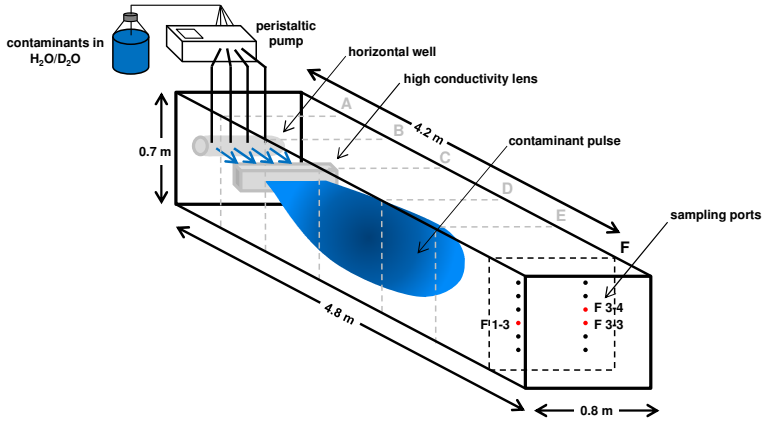

Figure 3.1: Schematic overview of the mesoscale aquifer (adapted with permission from Herzyk *et al.*[92] Copyright 2014 Springer). Samples were taken at transect F at the sampling ports 1-3, 3-3, and 3-4 (indicated in red and labeled).

3.2.3 Sampling

Samples were continuously taken at three ports 4.2 m downstream of the injection point with a peristaltic pump Minipuls Evolution (Gilson, Inc., Middleton, USA; rate: 1 mL/min) where sampling started 30 h after injection. Each sampling event took 4.5 h (total sample volume: ~270 mL). Three sampling ports (1-3, 3-3, and 3-4) were chosen where a bromide tracer test, performed two weeks prior to this study, had shown highest concentrations (data not shown). Therefore, these ports can be considered as representative for the main flow paths of the injected compounds through the aquifer. The corresponding sampling heights were 0.32 m (1-3, 3-3) and 0.41 m (3-4) from the bottom of the system. Additional samples (1 L) were taken at the outflow of the system to determine mass balances. Of each sample, 1 mL was taken for concentration analysis of the contaminants (LC-MS/MS) and of the conservative tracer D_2O (δ^2H isotope analysis). The remaining volume was adjusted to pH 10 using 1 M NaOH and stored at 4 °C until further use.

3.2.4 Quantification with LC-MS/MS

Concentrations of BAM, bentazone, diclofenac, 4'-hydroxydiclofenac, ibuprofen, and 2-hydroxyibuprofen were measured on a LC-MS/MS system consisting of an Agilent 1200 binary pump (Agilent Technologies, Böblingen, Germany) and an AB Sciex API 2000 Q-TRAP mass spectrometer (Applied Biosystems, Framingham, USA). A Luna

C18(2) column (5 µm, 100 × 2 mm) purchased from Phenomenex (Aschaffenburg, Germany) was used. Detailed method information is given in Appendix A.2.1.

3.2.5 Sample Enrichment with SPE

Based on the BTCs resulting from the concentration measurements, all samples between 48-102 h (sampling ports) as well as every second sample between 57-120 h (outflow) were used for further analysis. To enrich the samples, Solid Phase Extraction (SPE) was performed with a vacuum chamber (Macherey-Nagel, Düren, Germany) equipped with Oasis® HLB extraction cartridges (6 cm^3, 200 mg) purchased from Waters (Milford, USA). More information is given in Appendix A.2.1.

3.2.6 Preparative HPLC and Derivatization

While BAM was analyzed without further modification, isotope analysis of bentazone, diclofenac, and ibuprofen required online derivatization by trimethylsulfonium hydroxide (TMSH) in the case of bentazone[70] or offline derivatization by methanolic BF_3 in the case of diclofenac and ibuprofen.[30] To this end, the contaminants were separated after preconcentration by preparative HPLC using an LC-A10 series HPLC system (Shimadzu, Kyōto, Japan) equipped with a fraction collector. The column was an Allure C18 (5 µm, 150 × 4.6 mm) from Restek (Bad Homburg, Germany). Detailed information on the method is described in Appendix A.2.1.

3.2.7 Isotope Analysis

δ^2H of Tracer D_2O

Hydrogen isotope analysis was performed on a pyrolysis-IRMS system containing a reactor filled with "glassy carbon" granulate (2000-3150 µm) and Ni-coated carbon (IVA Analysentechnik, Meerbusch, Germany) at 1480 °C. After pyrolysis of H_2O, CO and H_2 were separated at 95 °C in a molecular sieve column and subsequently transferred to a Finnigan MAT 253 isotope ratio mass spectrometer *via* a ConFlow III system (both Thermo Fisher Scientific, Bremen, Germany) using a continuous He stream of 80 mL/min. The injected sample volume was 2 µL.

δ^2H values are reported in the delta notation (in per mil, ‰) relative to Vienna Standard Mean Ocean Water (V-SMOW):

$$\delta\,^{2}\mathrm{H} = \frac{\left[\left(\,^{2}\mathrm{H}/\,^{1}\mathrm{H}\right)_{\mathrm{sample}} - \left(\,^{2}\mathrm{H}/\,^{1}\mathrm{H}\right)_{\mathrm{standard}}\right]}{\left(\,^{2}\mathrm{H}/\,^{1}\mathrm{H}\right)_{\mathrm{standard}}} \qquad \text{eq. 3.1}$$

The deuterium concentration $c_{\,^{2}\mathrm{H}}$ was calculated from the measured δ^2H values according to the following equation

$$c_{\,^{2}\mathrm{H}} = \chi_{\,^{2}\mathrm{H}} \times \left(\frac{\rho_{\mathrm{H_2O}}}{MW_{\mathrm{H_2O}}} \times 2\right) \times MW_{\,^{2}\mathrm{H}} \qquad \text{eq. 3.2}$$

where $\rho_{\mathrm{H_2O}}$ is the density of water, whereas $MW_{\mathrm{H_2O}}$ and $MW_{\,^{2}\mathrm{H}}$ are the molecular weights of water and deuterium, respectively. The molar fraction $\chi_{\,^{2}\mathrm{H}}$ of deuterium can be expressed as

$$\chi_{\,^{2}\mathrm{H}} = \frac{^{2}\mathrm{H}}{^{2}\mathrm{H} + \,^{1}\mathrm{H}} \approx \frac{^{2}\mathrm{H}}{^{1}\mathrm{H}} = \left(\frac{^{2}\mathrm{H}}{^{1}\mathrm{H}}\right)_{\mathrm{standard}} \times \delta\,^{2}\mathrm{H} + \left(\frac{^{2}\mathrm{H}}{^{1}\mathrm{H}}\right)_{\mathrm{standard}} \qquad \text{eq. 3.3}$$

with $(^2\mathrm{H}/^1\mathrm{H})_{\mathrm{standard}}$ given as 155.76 ppm. Finally, all values were corrected for the background concentration of the groundwater (δ^2H = -73.3‰ or $^2\mathrm{H}/^1\mathrm{H}$ = 145 ppm) in order to consider just the artificial labeling.

δ^{13}C and δ^{15}N of BAM, Bentazone, and Diclofenac

Concentration breakthrough curves of BAM and ibuprofen were both in agreement with the BTC of D_2O suggesting that both substances behaved similarly and acted like conservative tracers (no sorption, no degradation, Appendix Figure A.2-1). Of the two, only BAM contains both carbon and nitrogen so that this compound was chosen for further analysis and discussion. Analysis of the contaminants was accomplished with established in-house methods.[30,70,73] Carbon and nitrogen isotope analysis of BAM, as well as of bentazone and diclofenac derivatives, was carried out on a GC-IRMS system consisting of a TRACE GC Ultra gas chromatograph (Thermo Fisher Scientific, Milan, Italy) equipped with a DB-5 analytical column (30 m, 0.25 mm ID, 1.0 µm film, Agilent Technologies, Böblingen, Germany). The GC was coupled to a Finnigan MAT 253 isotope ratio mass spectrometer *via* a Finnigan GC Combustion III interface (both

Thermo Fisher Scientific, Bremen, Germany). Liquid samples were injected with a GC Pal autosampler (CTC Analytics, Zwingen, Switzerland).

$\delta^{13}C$ and $\delta^{15}N$ values are expressed in per mil (‰) relative to Vienna PeeDee Belemnite (V-PDB) and air, respectively:

$$\delta^{13}\mathrm{C} = \frac{\left[\left({}^{13}\mathrm{C}/{}^{12}\mathrm{C}\right)_{\mathrm{sample}} - \left({}^{13}\mathrm{C}/{}^{12}\mathrm{C}\right)_{\mathrm{standard}}\right]}{\left({}^{13}\mathrm{C}/{}^{12}\mathrm{C}\right)_{\mathrm{standard}}} \qquad \text{eq. 3.4}$$

$$\delta^{15}\mathrm{N} = \frac{\left[\left({}^{15}\mathrm{N}/{}^{14}\mathrm{N}\right)_{\mathrm{sample}} - \left({}^{15}\mathrm{N}/{}^{14}\mathrm{N}\right)_{\mathrm{standard}}\right]}{\left({}^{15}\mathrm{N}/{}^{14}\mathrm{N}\right)_{\mathrm{standard}}} \qquad \text{eq. 3.5}$$

3.2.8 Reactive Transport Modeling

General Modeling Approach

As will be shown in the Results section (3.3), there was no experimental evidence of isotope fractionation by transverse dispersion for the micropollutants. We thus resigned from a model formulation that includes such effects.[34] In general, we followed a strictly parsimonious approach of finding the simplest identifiable model that can explain the data.

Model Description

Multi-dimensional reactive transport, including linear, one-site, kinetic sorption onto the sediment and first-order decay, can be described by:

$$\frac{\partial c}{\partial t} + (R-1)\frac{\partial c_*}{\partial t} + \mathbf{v}\cdot\nabla c - \nabla\cdot(\mathbf{D}\nabla c) = -\lambda_{reaction} c \qquad \text{eq. 3.6}$$

$$\frac{\partial c_*}{\partial t} = \lambda_{sorption}(c - c_*) \qquad \text{eq. 3.7}$$

Here, c [ML^{-3}] is the concentration of the micropollutant in the aqueous phase, c_* [ML^{-3}] is s/K_d, in which s [MM^{-1}] is the concentration of the compound kinetically sorbed to the sediment and K_d [L^3M^{-1}] denotes the linear partitioning coefficient between water and the sediment in equilibrium. $R = 1 + \frac{\rho_b}{n}K_d$ is the dimensionless retardation

factor, in which p_b [ML^{-3}] is the dry bulk density of the sediments and n [ ] is the effective porosity. **v** [LT^{-1}] denotes the linear average flow velocity, **D** [LT^{-2}] is the dispersion tensor, $\lambda_{sorption}$ [T^{-1}] is the first-order exchange coefficient between the aqueous phase and the sorbent, and $\lambda_{reaction}$ [T^{-1}] is the first-order biodegradation rate coefficient for the compound in solution. The given formulation of the transport equation including kinetic sorption is derived in Appendix A.2.1.

In the following analysis, we consider one compound, namely BAM, as conservative internal standard with physical transport properties assumed to be identical to those of the other micropollutants, since – in contrast to D_2O – it has a similar molecular mass so that a similar dispersion coefficient is expected. The justification of assuming that BAM is conservative is given below. This approach allows us to restrict the model to a 1-D formulation in which the effect of transverse dispersion on the simulated BTC of any micropollutant at an observation point is accounted for by multiplication with a dilution factor f_{dil} [ ], determined by fitting the BTC of the internal standard at that observation point. The underlying assumption is that transverse dispersion coefficients are similar among the different compounds, which is justified by the similarity in their molecular masses. While multi-dimensional simulations are in principle possible, they are affected by aquifer heterogeneity. Different concentrations at ports with identical vertical coordinate would require a 3-D model, but the small number of observation points does not justify calibrating such a model. By relying on an internal standard, we circumvent these problems. While we cannot explain the differences in physical transport among the ports with such an approach, we can explain the differences in reactive behavior among the various micropollutants, which is the focus of the present study.

Modeling of Isotope Fractionation Processes

Biodegradation of organic contaminants typically shows a normal kinetic isotope effect,[9] in which contaminant molecules containing the light carbon or nitrogen isotopes (*i.e.*, ^{12}C and ^{14}N) at the reactive position are transformed slightly faster than those containing ^{13}C or ^{15}N, respectively. In the reactive-transport model, carbon and nitrogen isotope fractionation is simulated separately and implementation of the isotopic fractionation due to biodegradation is realized by considering the three most abundant carbon and nitrogen isotopologues $^{12}c/^{14}n$ (only light carbon/nitrogen isotopes), $^{13}c/^{14}n$, and $^{12}c/^{15}n$ (one light carbon/nitrogen isotope is substituted by a heavy one) as separate species. For carbon

isotope fractionation, $^{12}c/^{14}n$ and $^{13}c/^{14}n$ were considered, for nitrogen isotope fractionation $^{12}c/^{14}n$ and $^{12}c/^{15}n$. Cases with two or more positions substituted by ^{13}C or ^{15}N within the same molecule are negligible, due to the low natural abundance of ^{13}C and ^{15}N. Reflecting the average behavior of the different $^{13}c/^{14}n$ isotopomers (*i.e.*, molecules with ^{13}C at different molecular positions), an operational "bulk" isotope fractionation factor can be defined.[19]

This kinetic isotope fractionation factor $\alpha_{reaction}^{kin}$ for first-order biodegradation is given by the ratio of the first-order degradation rate constants for heavy and light isotopologues, respectively:

$$\alpha_{reaction}^{kin} = 1 + \varepsilon_{reaction}^{kin} = \frac{^{h}\lambda_{reaction}}{^{l}\lambda_{reaction}} \qquad \text{eq. 3.8}$$

Sorption to sediment is slightly stronger for the light isotopologues (*i.e.*, $^{12}K_d > {}^{13}K_d$ and $^{14}K_d > {}^{15}K_d$, respectively),[32,93] which leads to a faster breakthrough of the heavy isotopologues. This effect on the observed isotope signal is accounted for in the reactive transport model by different retardation factors R for $^{12}c/^{14}n$, $^{13}c/^{14}n$, and $^{12}c/^{15}n$ ($^{h}R < {}^{l}R$). Isotope fractionation due to equilibrium sorption can be described by the sorption-related equilibrium isotope fractionation factor $\alpha_{sorption}^{eq}$:[32]

$$\alpha_{sorption}^{eq} = 1 + \varepsilon_{sorption}^{eq} = \frac{^{h}R - 1}{^{l}R - 1} = \frac{^{h}K_d}{^{l}K_d} \qquad \text{eq. 3.9}$$

In addition, a kinetic component to sorption isotope effects may arise from differences in the mass-transfer coefficient $\lambda_{sorption}$. The espectation would be that heavy isotopologues sorb more slowly than light isotopologues. However, as shown in Appendix A.2, this would lead to breakthrough curves of $\delta^{13}C$ and $\delta^{15}N$ with increasing values at late times, which was not observed. Isotope effects on $\lambda_{sorption}$ were, therefore, not included into the model ($\alpha_{sorption}^{kin} = 1$). Finally, because fractionation factors α are close to unity, we used enrichment factors $\varepsilon = \alpha - 1$ instead, and report their values in per mil (‰).

Model Setup and Parameter Estimation

The observed breakthrough of the conservative tracer D_2O as well as the breakthrough of BAM, bentazone, and diclofenac at the three sampling ports F 1-3, F 3-3, and F 3-4 were

simulated as one-dimensional systems. The apparent linear average velocity v and the longitudinal dispersion coefficient D were obtained for each port by fitting the D_2O data. For both D_2O and BAM, a dilution factor f_{dil} [ ], parameterizing the effects of transverse dispersion were also obtained for each port, by considering the ratio of the plateau concentration reached in that port to the injection concentration. The dilution factors significantly differed between D_2O and BAM due to their different molecular masses and are of about the same order of magnitude as observed for bromide in a previous tracer test (Appendix Figure A.2-4). First-order decay coefficients $\lambda_{reaction}$ of diclofenac and bentazone, as well as sorption parameters (R-1 and $\lambda_{sorption}$) of diclofenac were obtained by fitting concentration BTCs. These coefficients were assumed to be identical in the models of all ports. Fitting of concentrations was done using a genetic algorithm and analytical solutions of the governing equations. To simulate isotope ratios, the dominant isotopologues were considered as independent compounds, and $\delta^{13}C$- and $\delta^{15}N$-values were computed from the concentrations. Here, a Finite Volume discretization was chosen. The values of the various enrichment factors ε were chosen from literature (see below). Details are given in Appendix A.2.1.

Table 3.1: Model parameters obtained by fitting of concentration breakthrough curves.

Conservative Transport Parameters

sampling port	v [m/s]	D [m^2/s]	f_{dil} D_2O [ ]	f_{dil} BAM [ ]
F 1-3	2.10×10^{-5}	1.74×10^{-7}	0.0107	0.0120
F 3-3	2.02×10^{-5}	2.43×10^{-7}	0.0069	0.0069
F 3-4	2.02×10^{-5}	1.93×10^{-7}	0.0119	0.0124

Reactive Transport Parameters

compound	R-1 [ ]	λ_{sorb} [1/s]	λ_{reac} [1/s]
bentazone	*n.a.* (0.0)	*n.a.*	1.60×10^{-6}
diclofenac	0.092	6.16×10^{-5}	2.32×10^{-6}

3.3 Results and Discussion

3.3.1 Concentration Breakthrough Curves

Figure 3.2 (upper panel) shows concentration breakthrough curves (BTCs) of BAM, bentazone, and diclofenac relative to the respective input concentrations. Concentration BTCs that are nearly identical to those of the conservative tracer D_2O indicate that the substances are neither degraded nor sorbed. A concentration decrease, by contrast, either points to degradation or irreversible sorption, whereas a shift of the center of mass to higher retention times gives evidence of reversible sorption according to the model assumptions. Based on the comparison to D_2O, the BTCs of BAM (Figure 3.2, first column) and ibuprofen (see Appendix Figure A.2-1) showed that both substances did not sorb or degrade. This is consistent with several studies on the persistence of BAM[87,94] in the environment, whereas ibuprofen has been shown to be both persistent[95] as well as readily degradable in previous studies.[96,97] At sampling ports F 1-3 and F 3-4 (Figure 3.2, blue diamonds and green triangles) BAM concentrations, normalized by the inflow concentration, were even higher than D_2O concentrations, which we attribute to the higher molecular diffusion coefficient of D_2O resulting in stronger transverse dispersion and, consequently, lower concentrations at locations close to the center line of the pulse. According to this, BAM was considered as internal standard for bentazone and diclofenac concentration data (Figure 3.2, second and third column). Finally, we note that concentration profiles of sampling ports F 1-3 and F 3-4 show similarly high concentrations even though they were not located at exactly the same depth. This indicates a small "twisting" of the pulse – likely attributed to local heterogeneity – so that the vertical concentration profile was slightly shifted up from right to left across the vertical pulse transect. For the same reason, lower concentrations in port F 3-3 indicate a greater distance from the maximum of the vertical profile, even though the port was at the same depth as F 1-3.

Compared to BAM, the BTC of bentazone (Figure 3.2, second column) had a smaller amplitude, but did not show a shift to higher retention times. This indicates (i) significant transformation of bentazone (27.4% ± 2.5% in all sampling ports, see Appendix Table A.2-2) and (ii) the absence of significant reversible sorption. Irreversible sorption can be neglected, because of the high mobility of bentazone in the environment, which is reflected in its low sorption coefficient (K_{oc} < 50 mL/g) even in soil and sediments that have much higher organic content than our model aquifer (up to 4.3% compared to 0.25%

in our system).[98,99] Most insightful was the BTC of diclofenac (Figure 3.2, third column). Reduced amplitudes compared to BAM gave (i) evidence of diclofenac transformation (39.2% ± 1.7%, see Appendix Table A.2-2), whereas the asymmetric shape and slight offset indicated (ii) sorption with a kinetic component (in contrast to toluene, forth column of Figure 3.2, where the symmetric peak shape allowed for a sorption model without kinetic component). The conclusion of diclofenac transformation was confirmed by the detection of small concentrations of the putative transformation product 4'-hydroxydiclofenac by LC-MS/MS (Appendix Figure A.2-2). No additional transformation products were detected.

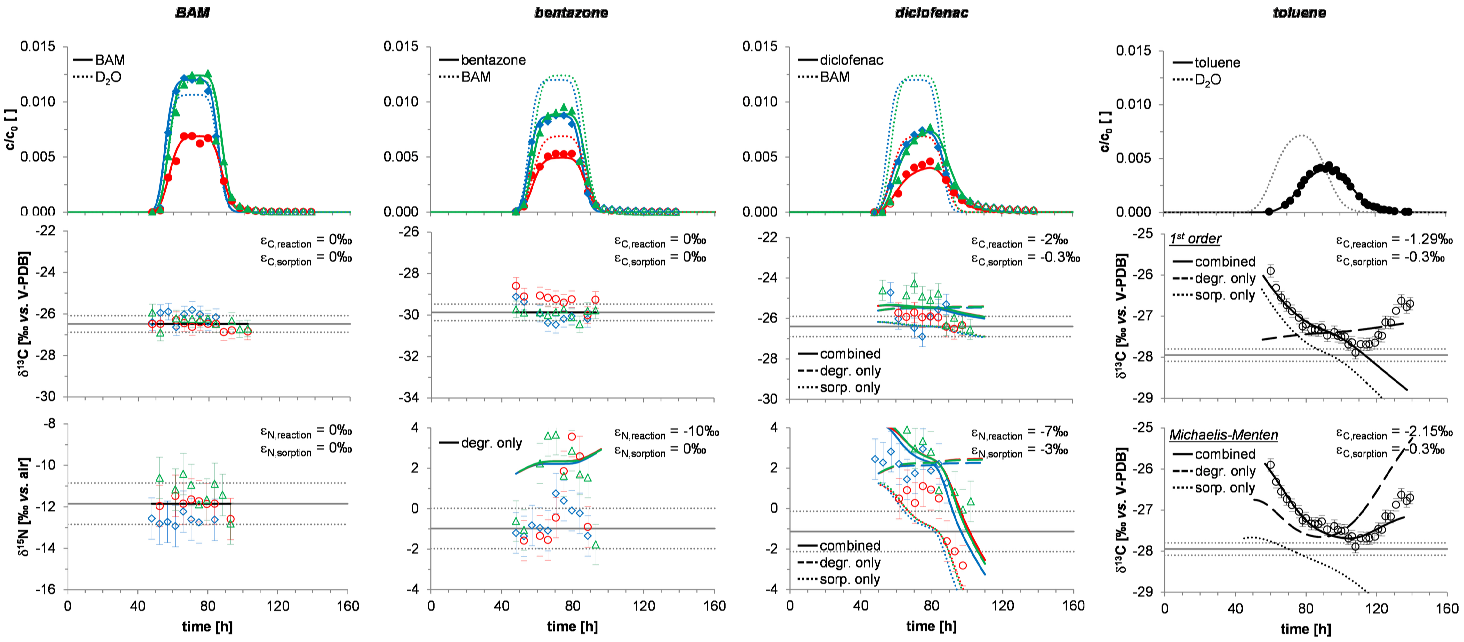

Figure 3.2: Measured relative concentrations (upper panel; filled symbols represent data points with corresponding isotope values) together with carbon isotope values of BAM, bentazone, diclofenac, and toluene (middle panel), and nitrogen isotope values of BAM, bentazone, and diclofenac (lower panel) in the sampling ports F 1-3 (blue diamonds), F 3-3 (red dots), and F 3-4 (green triangles). Ibuprofen data are not shown, because it demonstrated conservative behavior in the same way as BAM. Toluene data (sampling port F 2-8, black dots) are taken from Qiu *et al.*[32] and Eckert *et al.*[33] Solid and dotted lines (upper panel) represent modeled contaminant and D_2O data (in case of BAM and toluene) or modeled contaminant and BAM data (in case of bentazone and diclofenac), respectively. Gray solid lines (middle and lower panel) correspond to the carbon and nitrogen isotopic composition of the respective contaminant at the inflow determined by EA-IRMS. Gray dotted lines (middle and lower panel) represent the uncertainty of carbon (± 0.4‰ for BAM and bentazone, ± 0.5‰ for diclofenac, ± 0.15‰ for toluene) and nitrogen (± 1‰) isotope analysis. Black and colored dotted, broken, or solid lines (middle and lower panel) show the expected changes in isotope ratios considering only sorption, only biodegradation, or the combination of both. In all panels, 1st order degradation kinetics was assumed, except for the lowest panel at the right (toluene) where the model was based on Michaelis-Menten kinetics. ε-Values are set to zero where no significant degradation ($\varepsilon_{reaction} = 0‰$) or sorption ($\varepsilon_{sorption} = 0‰$) took place.

3.3.2 Carbon and Nitrogen Isotope Ratios

Isotope analysis was performed for concentrations down to 6 µg/L ($\delta^{13}C$ and $\delta^{15}N$ of BAM), 12 µg/L ($\delta^{13}C$ and $\delta^{15}N$ of bentazone), 2 µg/L ($\delta^{13}C$ of diclofenac), and 64 µg/L ($\delta^{15}N$ of diclofenac). Highest concentrations were 6.6 mg/L (BAM), 2.6 mg/L (bentazone), and 500 µg/L (diclofenac). These concentrations are in a similar range as those of typical groundwater pollutants that are routinely analyzed according to today's state-of-the-art in CSIA and correspond to those of toluene (28 µg/L to 2.1 mg/L; Figure 3.2, fourth column) in the previous study of Qiu *et al.*[33] This comparison shows that concentration-wise, a similarly sensitive isotope analysis of micropollutants is possible as for "traditional" pollutants and that it can be used to track the fate of micropollutants in these concentrations in (near-)environmental systems.

The second row of sub-plots in Figure 3.2 shows measured and simulated $\delta^{13}C$-BTCs, whereas in the third row $\delta^{15}N$-BTCs (of BAM, bentazone, and diclofenac) are presented. Regarding the precision, our data show that $\delta^{13}C$ and $\delta^{15}N$ analysis of typical micropollutant structures entails a greater standard deviation compared to $\delta^{13}C$ analysis of priority pollutants[100] such as toluene (Figure 3.2, fourth column). One reason for this larger error is the higher uncertainty of $\delta^{15}N$ compared to $\delta^{13}C$ analysis.[78] Additional reasons are the variable performance of combustion ovens[79] and bias from derivatization which both require correction by external standards introducing additional uncertainty.[72] While these factors are well-understood in theory, our data offers for the first time a realistic impression of the precision that can be obtained in routine analysis of micropollutants in groundwater samples and, therefore, allows a critical evaluation of the information that can be derived to assess their fate in the environment.

In the case of BAM, no carbon or nitrogen isotope fractionation was observed, confirming what has already been shown by concentration BTCs: that neither degradation nor sorption took place (Figure 3.2, first column). Also, the isotope ratios did not differ among the various ports in any consistent manner. If transverse dispersion had a significant effect on isotope fractionation, it would be identical for carbon and nitrogen, as fractionation by diffusion is a purely mass-related effect. We conclude that a relative difference in molecular mass between the heavy and light isotopologues by 0.5% is too small to result in noticeable fractionation by transverse dispersion. Corresponding to the observation that transverse dispersion did not lead to significant isotope fractionation, we therefore neglected its effect on the isotope signal in the model.

In contrast to BAM, carbon and nitrogen isotope ratios of diclofenac (Figure 3.2, third column) indicated an imprint of both degradation and sorption isotope effects. Despite larger uncertainties, the combined information of triplicate $\delta^{13}C$ and $\delta^{15}N$ values from the different ports clearly indicate (i) an overall enrichment of ^{13}C- and in particular of ^{15}N-containing isotopologues throughout the pulse compared to the input and (ii) a monotonous decrease of isotope values in the course of the pulse. The first observation implies selective elimination of ^{12}C- and ^{14}N-rich isotopologues, respectively, which is the typical imprint of a degradation-associated isotope effect. This overall enrichment was independently confirmed in an isotopic mass balance. For diclofenac, the concentration-weighted average of isotope values of all samples over time was more positive than that of the input, namely by $0.7‰ \pm 0.5‰$ (carbon) and $2.7‰ \pm 1.3‰$ (nitrogen), respectively.

The second observation may – in a similar way as previously for toluene[33,34] – be attributed to sorption: at the front of the pulse, preferential sorption of light isotopologues to sediment components is expected to enrich ^{13}C and ^{15}N; toward the end of the pulse, in contrast, more and more light isotopologues are detected as a result of their subsequent desorption. The observation that degradation-induced effects are more pronounced for nitrogen isotopes is consistent with the results of a study investigating aerobic biodegradation of diclofenac in batch experiments containing river sediment and water.[30] In turn, the observation that also sorption-induced effects are more strongly reflected in $^{15}N/^{14}N$ ratios may result from distinct isotope effects induced by hydrogen bonding of the diclofenac nitrogen atom.[101,102] The magnitude of this sorption-induced nitrogen isotope effect is in fact remarkable considering that the overall retardation of diclofenac was only minor (R-1 = 0.092, Table 3.1). As the basis for the model, enrichment factors from the literature for degradation ($\varepsilon_{C,reaction} = -2‰$, $\varepsilon_{N,reaction} = -7‰$)[30] and sorption ($\varepsilon_{C,sorption} = -0.3‰$)[34] were used; where data was not available, $\varepsilon_{N,sorption}$ was assumed to be -3‰. This resulted in good agreement of predicted values with the experimental data for both carbon and nitrogen (Figure 3.2, second and third row), further emphasizing that both sorption and degradation are processes that can be visualized by CSIA of micropollutants.

In the case of bentazone (Figure 3.2, second column), evidence of transformation was not obtained from $^{13}C/^{12}C$, but from $^{15}N/^{14}N$ data illustrating the advantage of investigating isotope changes in multiple elements. A small but significant overall enrichment of $^{15}N/^{14}N$ compared to the input value could be detected in the isotopic mass balance

(1.9‰ ± 1.4‰, see Appendix Table A.2-2). While this confirms the prospect of CSIA to assess degradation of micropollutants, it demonstrates the associated limitations imposed by the larger uncertainties compared to "traditional" groundwater contaminants. In this context, the negligible changes in carbon isotope ratios may be due to the fact that the kinetic isotope effect – which occurs at a specific carbon atom – is "diluted" in the observable fractionation when analyzing the whole molecule (total number n of carbon atoms in bentazone: $n = 10$) so that in the measured average no significant changes in $\delta^{13}C$ can be observed.

3.3.3 Concentration Dependency of Biotransformation

The possibility to perform CSIA on micropollutants also enables us to address an aspect for these compounds that was identified in a recent study on toluene in the same experimental system: a concentration dependency of biodegradation. In this study,[33] we previously obtained evidence of non-first-order degradation kinetics of toluene[34] meaning that the extent of biodegradation (in %) was higher at low (28 µg/L) than at high concentrations (2.2 mg/L) giving rise to the U-shaped profile of $\delta^{13}C$ values shown in Figure 3.2, fourth column. This could be described with a model of Michaelis-Menten kinetics where degradation is modelled to occur in the linear regime at low concentrations, but at saturation kinetics at high concentrations (see the last two panels in column 4 of Figure 3.2). Considering the comparable concentration range investigated in this study, we hypothesized that such Michaelis-Menten-like kinetics could also be expected for diclofenac. Contrary to our expectations, however, our data could be well described by a model assuming first-order kinetics within the concentration range of 2 µg/L to 500 µg/L. When considering again a Michaelis-Menten model,a possible interpretation could be that the enzymatic activity in diclofenac remained within the linear range of the Michaelis-Menten regime and was, thus, not yet used to its full extent.

In the case of bentazone, in contrast, shifts in nitrogen isotope values were smallest in the front and the tail of the pulse where concentrations are low (12 µg/L to 1.5 mg/L). Even though this observation seems to suggest that transformation only took place when a certain threshold concentration was exceeded, we assess that the bentazone data set needs to be interpreted with caution for the following reasons: The concentration and isotope breakthrough data (Figure 3.2), observed in the sampling ports of transect F (see Figure 3.1), gave confirmative, independent evidence that transformation of bentazone occurred

at sufficiently high concentrations. However, the BTC in the outflow of the model aquifer (*i.e.*, the mass balance over the whole system, see Appendix Figure A.2-1) did not show any deficit suggesting that bentazone was not degraded at all. Possible reasons to explain this contradiction could be that (i) transformation took place at a local hot spot which is not representative of the entire system, or that (ii) metabolite-to-parent-compound reversion occurred (which has been demonstrated in other cases, *e.g.*, for diclofenac and the antibiotic sulfamethoxazole,[103] or the anabolic steroid trenbolone[104]). As long as the underlying drivers (biotic / abiotic / metabolic / co-metabolic transformation) are not characterized, interpretations must, therefore, remain tentative.

3.3.4 Environmental Significance

In recent years, numerous lab studies on typical micropollutants have shown the promise of Compound-specific Stable Isotope Analysis to study their transformation mechanisms and related biodegradation pathways. As "proof of the pudding" this study investigated whether CSIA can also monitor degradation of such chemical structures in a model aquifer mimicking conditions in the saturated zone of sand filters or during artificial groundwater recharge. We found that - compared to CSIA of priority pollutants - similar concentration ranges are accessible to analysis. However, our study demonstrates that the analytical uncertainty of replicate measurements was somewhat higher. Despite this drawback, we could demonstrate that degradation of diclofenac may be reliably detected from observable changes in isotope values. Our results emphasize in particular the importance of nitrogen isotope analysis to obtain conclusive insight. These results provide an important proof of principle and lay an encouraging basis for further analytical efforts. Specifically, since environmentally relevant concentration ranges are often still lower than targeted here (ng/L instead of µg/L range), further analytical developments are necessary to enable CSIA of micropollutants at even lower concentrations in groundwater. For this development, our study may serve as a benchmark that better allows assessing prospects and limitations of CSIA of micropollutants in environmental systems. Also the design of this study may provide a blueprint for future assessments of micropollutants. Instead of investigating steady state contaminations (as for legacy chemicals at contaminated sites), capturing the dynamics of micropollutants may require chasing a pulse contamination through natural compartments.[66,105,106] Our study provides an illustration how the combined information from concentrations and isotope values can

provide direct *ad hoc* information about *in situ* degradation capacities of natural systems (see Figure 3.3). Finally, our contribution also illustrates the advantage of tailoring the modeling of micropollutant transport in natural systems to the available information from experimental data. Since such transport is inherently prone to spatial variability, we recommend following a data-driven approach, in which concentration and isotope data are first qualitatively analyzed to determine which processes are dominant, and then take the simplest adequate modeling approach. In contrast, we doubt that the full extent of spatial variability can be resolved at field sites with affordable effort, so that the practicability of models requiring such resolution must be considered critically. In our study, the data identified BAM as conservative compound and suggested that transverse dispersion did not significantly contribute to isotope fractionation. At other sites, other simplifications may be suitable.

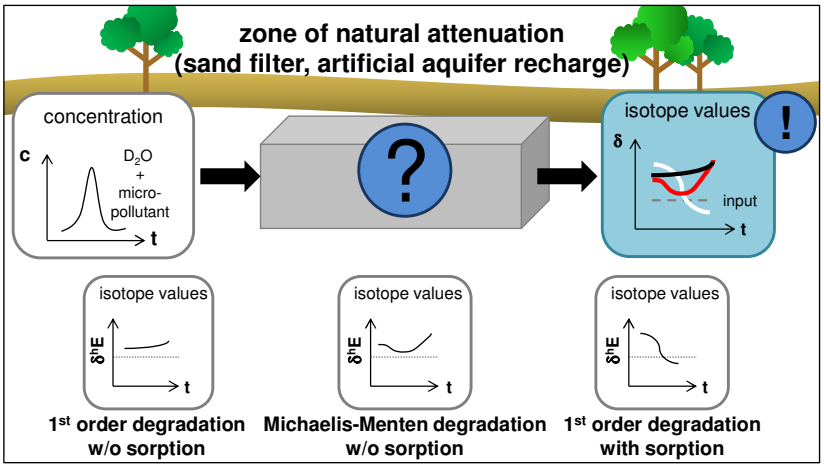

Figure 3.3: Ability of Compound-specific Stable Isotope Analysis to provide additional information about the *in situ* degradation capacity of natural systems.

4

Investigating the Drivers behind Sorption Isotope Effects of Organic Contaminants: Equilibrium Isotope Effects during Water-Air and Hexadecane-Air Partitioning

4.1 Introduction

In recent years, Compound-specific Stable Isotope Analysis (CSIA) at natural isotopic abundance has developed into a widely used method to assess the natural degradation of organic contaminants in the environment, to study underlying transformation mechanisms and to identify related biodegradation pathways.[11,35,107] In such assessments it is commonly assumed that physical processes such as sorption or vaporization have a negligible impact on the isotopic composition of groundwater contaminants.[13,14] However, significant isotopic fractionation was observed due to sorption of aromatic hydrocarbons to humic substances,[32] fluvisol and activated carbon,[93] and several organic solvents.[108] Likewise, measurable isotopic fractionation was traced in volatilization of trichloroethene,[109] methyl *tert*-butyl ether (MTBE), and benzene[110] demonstrating similar principles for isotope effects at natural abundance as known from isotopically labelled compounds.[111] The significance of this phenomenon could indeed be confirmed on a relevant scale in a mesoscale model aquifer by Qiu *et al.*,[33] Eckert *et al.*,[34] and in Chapter 3 of this thesis. Concentration and isotope breakthrough data of a contaminant pulse were measured at high temporal resolution. Modeling of the data allowed distinguishing the changes in isotope values that were attributable to sorption as opposed to biodegradation. These results showed that physical processes can affect a system significantly at transient conditions and, therefore, should ideally be considered when evaluating degradation of contaminants at non-steady state. This relevance contrasts, however, with our currently limited understanding of underlying drivers behind such sorption isotope effects. The following questions warrant investigation: (i) does the direction and magnitude of isotope effects correlate with the underlying types of molecular interactions (*i.e.*, hydrogen bonds and van-der-Waals forces)? (ii) How can these molecular interactions be resolved, if a compound partitions between two condensed phases (aqueous and organic phase) instead of between a condensed phase and the gas phase (as in volatilization)? (iii) Specifically, how can the isotope effect observed in a *solute* be correlated explicitly to properties of the *solvent*?

The studies mentioned above determined isotope effects either by stepwise vaporization of pure liquids,[13] or by partitioning of the respective substances between water and an organic solvent[108] or sorbent.[14,93] However, by studying isotope effects of partitioning between two condensed phases (*i.e.*, water and organic solvent/material) it is not possible to explore the effect of molecular interactions in each respective phase independently. Instead, it was therefore, the aim of this study to measure isotope effects between each

condensed phase and air – an ideal reference phase in which intermolecular interactions are absent. This allows separate investigations of the isotope effects imposed by the specific interactions of each phase. Subsequently, the results are put together according to a Bordwell thermodynamic cycle, as illustrated in Figure 4.1.

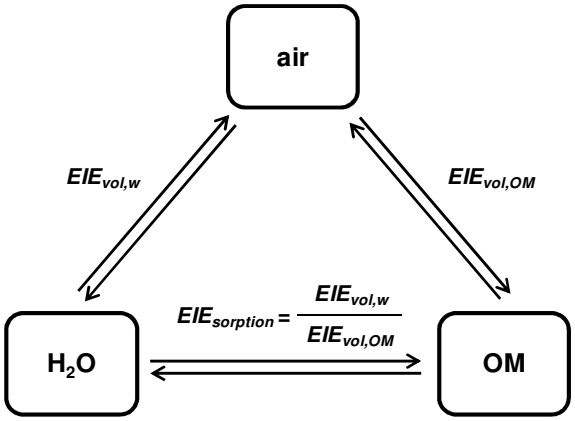

Figure 4.1: Bordwell thermodynamic cycle between the three phases water, organic material (OM; surrogated in this study by an organic solvent), and air expressed by the equilibrium isotope effects of volatilization EIE_{vol} and sorption $EIE_{sorption}$.

The equilibrium constant K_i for the partitioning of compound i between two phases is given as

$$K_i = \frac{c_{i,1}}{c_{i,2}} \qquad \text{eq. 4.1}$$

with c_i as the concentration in the respective phase. Considering the isotopic ratios, eq. 4.1 can be expressed according to

$$\text{EIE} = \frac{{}^{l}K_i}{{}^{h}K_i} = \frac{\left({}^{l}k_r / {}^{l}k_{-r}\right)}{\left({}^{h}k_r / {}^{h}k_{-r}\right)} = \frac{\left({}^{l}k / {}^{h}k\right)_r}{\left({}^{l}k / {}^{h}k\right)_{-r}} \qquad \text{eq. 4.2}$$

with EIE as the equilibrium isotope effect and k_r and k_{-r} as the rate constants of forward and backward reaction, respectively. If partitioning between water-air and organic solvent-air (the organic solvent serves as a substitute for organic material (OM)) is known, the sorption effect in the water-OM system can be calculated according to eq. 4.3[112]

$$K_{i,OM-w} = \frac{K_{i,a-w}}{K_{i,a-OM}} \qquad \text{eq. 4.3}$$

or, expressed as isotope effects, according to eq. 4.4 with the equilibrium isotope effect of volatilization from water ($EIE_{vol,w}$) or organic material ($EIE_{vol,OM}$), and $EIE_{sorption}$ as the sorption isotope effect between the two condensed phases.

$$\mathrm{EIE}_{sorption} = \frac{\mathrm{EIE}_{vol,w}}{\mathrm{EIE}_{vol,OM}} \qquad \text{eq. 4.4}$$

In addition, it is assumed that the two most important molecular interactions governing sorption processes are van-der-Waals forces and hydrogen bonds. Every substance is affected by van-der-Waals interactions when it condenses from gaseous to liquid phase, due to the dispersive interaction between polarizable molecules leading to weak attraction. In contrast, hydrogen bonds are additional attractive interactions which can only form between a hydrogen atom that is covalently bound to a highly electronegative atom (*e.g.*, oxygen, nitrogen, or fluorine) and a lone pair of the hydrogen bond acceptor. Isotope effects induced by these molecular interactions depend mainly on isotopic differences in the vibrational energies of heavy and light isotopes, respectively.[11] In the gas phase only *intra*molecular vibrations (*i.e.*, within covalent bonds) occur. Their contribution to vapor pressure equilibrium isotope effects is represented by term B of eq. 4.5 where P' and P are the vapor pressures of light and heavy isotopologues, respectively.

$$\ln\frac{P'}{P} \approx \frac{A}{T^2} - \frac{B}{T} \qquad \text{eq. 4.5}$$

eq. 4.5 can be linked to equilibrium isotope effects EIE by:[113]

$$\ln\frac{P'}{P} = -\ln\frac{P}{P'} = -\ln\alpha \approx -\alpha - 1 = -\varepsilon \qquad \text{eq. 4.6}$$

By condensation of a molecule from the gas phase to the liquid phase, these *intra*molecular vibrations (term B) are weakened, but at the same time, new additional vibrational modes are created that did not exist before (*i.e.*, *inter*molecular interactions, *e.g.*, induced by van-der-Waals forces or hydrogen bonds). The contribution of these *inter*molecular interactions is represented by term A in eq. 4.5. At low temperatures, term A dominates so that the isotope effect of volatilization is always normal. In contrast,

term *B* becomes more and more important with increasing temperatures leading to a temperature at which the isotope effect may change from normal to inverse. At very high temperatures, finally, both terms become zero and isotope effects are non-existent anymore. For more details on eq. 4.5 see the review of Jancso and Van Hook[101] on condensed phase isotope effects. Taking further into account that the vibration of hydrogen bonds are of higher energy than those of van-der-Waals forces, it can be expected that *inter*molecular vibrations of hydrogen bonding give greater contributions to term *A* than van-der-Waals interactions meaning that this term dominates a larger temperature range in the case of hydrogen bonds.

For our approach, these considerations imply that compounds interacting at room temperature *via* van-der-Waals interactions would show an inverse isotope effect when they partition from a condensed phase into the gas phase, because term *B* of eq. 4.5 is already dominating at this temperature. For compounds interacting at room temperature *via* hydrogen bonding, on the other hand, term *A* would still dominate and these substances are expected to show a normal isotope effect. Evidence for this is, *e.g.*, given by Zhang *et al.*[114] who conducted Rayleigh distillation of pure compounds including alcohols and observed normal hydrogen and oxygen isotope effects for the -OH groups (where hydrogen bonding was important), and inverse carbon and hydrogen isotope effects for the alkyl chains (where van-der-Waals interactions dominated). For our scenario of water-air and organic solvent-air partitioning (Figure 4.1) we would therefore hypothesize the following carbon and hydrogen isotope effects of benzene, triethylamine, and trichloromethane summarized in Table 4.1.

Table 4.1: Expected carbon isotope effects for benzene, triethylamine, and trichloromethane as well as expected hydrogen isotope effects for trichloromethane in water-air, organic material-air, and water-organic material partitioning, respectively. The isotope effect is normal if light isotopologues pass preferentially into the gas phase and inverse if volatilization of light isotopologues is preferred. Abbreviations used: HB – hydrogen bond; OM – organic material/solvent; vdW – van-der-Waals interactions.

	functionality	**isotope effect**		
		water-air	**OM-air**	**water-OM**
benzene, $\delta^{13}C$	vdW; HB acceptor (π electron system)	normal	inverse	?
NEt_3, $\delta^{13}C$	vdW at alkyl chains; HB acceptor (*N* atom)	inverse	inverse	inverse
$CHCl_3$, $\delta^{13}C$	vdW; HB donor (*H* atom)	normal	inverse	?
$CHCl_3$, $\delta^{2}H$		normal	inverse	?

Irrespective of these theoretical considerations, however, the actual experimental determination of equilibrium isotope effect between two phases is needed, and such investigations pose several challenges: (i) since observable isotope fractionation is expected to be small, a maximum of equilibration steps should be experimentally realized in order to obtain an isotopic shift that is significant compared to the uncertainty of GC-IRMS (Gas Chromatography coupled to Isotope Ratio Mass Spectrometry) measurements. (ii) To sample on the one hand a sufficiently large number of equilibration steps, and to have on the other hand enough substance left for the following equilibration steps, a distribution between liquid and gaseous phase of about 50% should be chosen. (iii) As another important aspect it should be possible to remove one of the phases completely. (iv) Additionally, it is important to work under equilibrium conditions, because isotope effects derived from continuous vaporization experiments are affected by a combination of vaporization and diffusion producing different values in comparison to stepwise (equilibrium) experiments, as shown by Jeannottat *et al.*[109]

The objectives of this study were, therefore, (a) to investigate sorption isotope effects in a simple model system using water-air and organic solvent-air partitioning wherein *n*-hexadecane was chosen as a reference medium that is only capable to interact *via* van-der-Waals forces; (b) to determine the equilibrium isotope effects of benzene, triethylamine, and trichloromethane by GC-IRMS as well as the hydrogen isotope effect of labelled trichloromethane by GC-MS; (c) to this end, to achieve 50:50 distribution of the compounds between liquid and headspace phase in an experimental system which allows selective sampling of the gas phase. For that purpose, special headspace vials (see Figure 4.2 and Experimental Section 4.2) were tested that allow easy sampling of the stepwise partitioning. In particular it was our objective to investigate whether the experimental results are consistent with the hypotheses given in Table 4.1. With this in mind, the following compounds were selected based on their chemical properties. Benzene was chosen as the simplest representative for aromatic hydrocarbons, which is in addition a member of the BTEX (benzene, toluene, ethylbenzene, *ortho*-, *meta*-, and *para*-xylene) contaminants, triethylamine represents tertiary amines as compounds with a hydrogen bond acceptor moiety at the nitrogen atom, and trichloromethane was chosen as an example for a hydrogen bond donor compound.[115]

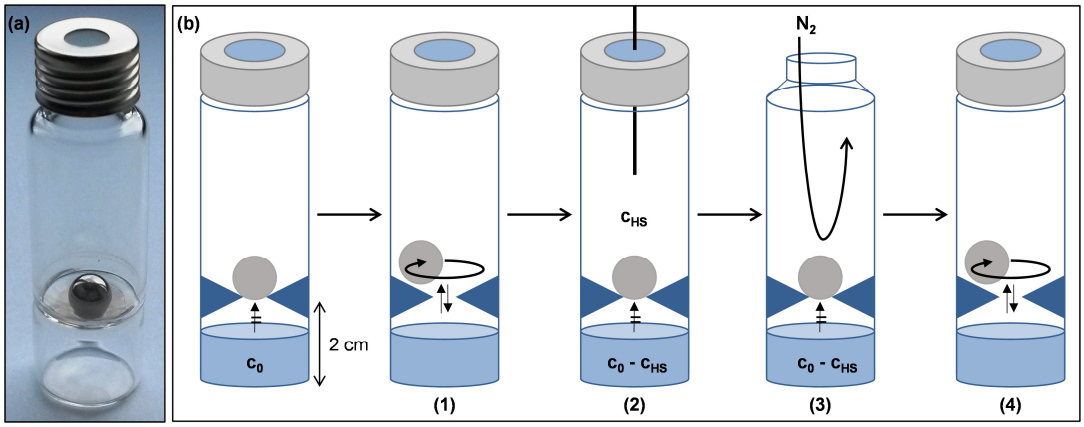

Figure 4.2: (a) Modified headspace vial. (b) Schematic illustration of the stepwise water-air and hexadecane-air partitioning, respectively: (1) equilibration in agitator; (2) automated headspace sampling; (3) exchange of headspace with gentle nitrogen stream; (4) repeat (1)-(3).

4.2 Experimental Section

4.2.1 Chemicals

Benzene was purchased from Merck (Darmstadt, Germany), triethylamine (NEt_3), trichloromethane ($CHCl_3$), deuterotrichloromethane ($CDCl_3$, 99.96 atom % D), and *n*-hexadecane were from Sigma-Aldrich (Steinheim, Germany). All organic substances were of LC-MS grade (purity > 99%). Milli-Q water was generated by a Milli-Q Advantage $A10_{system}$ from Millipore (Schwalbach, Germany).

4.2.2 Experimental Setup

Water stock solutions (~1 g/L benzene, ~6 g/L NEt_3, and ~5 g/L $CHCl_3$) were prepared in concentrations within the water solubility range of these compounds. For *n*-hexadecane stock solutions, the amount of substance was not exceeding 0.1% of total *n*-hexadecane phase (~266 mg/L benzene, ~33 µg/L NEt_3, ~28 µg/L $CHCl_3$). To avoid air bubbles, 250 mL glass bottles were filled completely with water and *n*-hexadecane, respectively, and closed with Mininert screw caps before the substances were injected by a syringe. Afterwards, the solutions were stirred rigorously for 48 h.

Water-air and hexadecane-air partitioning experiments were carried out in modified ND18 headspace vials (Figure 4.2). The vials were divided into two parts by a tapered grinding (2 cm from the bottom) resulting in a upper vial volume of ~14 mL and a lower

vial volume of ~4 mL, with a small hole to which a ball (stainless steel, diameter: 0.9 cm) was fitting. The lower part of the vial was filled with stock solution (Figure 4.2), the ball was added, and the system was closed with a screw cap (1.3 mm silicone/PTFE septum, 45°, Carl Roth, Karlsruhe, Germany). The amount of stock solution used was calculated to achieve 50:50 distribution by mass between headspace and condensed phase. The distribution (in %) between two equilibration steps *n* can be calculated according to:

$$\text{distribution} = \frac{\text{peak area}_n - \text{peak area}_{n+1}}{\text{peak area}_n} \qquad \text{eq. 4.7}$$

After equilibration in the autosampler agitator (speed: 500 rpm, incubation temperature: 33 °C, equilibration time: see Table 4.2) the ball closed the hole and headspace samples were taken automatically. Afterwards, the vial was opened manually, the gas phase was exchanged with a gentle nitrogen stream for 20 s and the vial was quickly closed with a new screw cap. The substance loss during the manual gas phase exchange was determined to be less than ~1.4% of the total amount after 30 s (see Appendix Figure A.3-1). Experiments were performed in duplicates. For quantification, standards prepared from stock solutions were added to unmodified ND18 headspace vials (with the same volume that was used for the experiments).

Table 4.2: Volume of stock solutions and different equilibration times of the substances benzene, triethylamine, and trichloromethane for water-air and hexadecane-air partitioning, respectively.

	volume of stock solution [mL]			**equilibration time [min]**		
	benzene	**NEt_3**	**$CHCl_3$**	**benzene**	**NEt_3**	**$CHCl_3$**
water-air	2.80	0.07	1.00	30	60	30
hexadecane-air	0.025	0.015	0.050	60	60	60

4.2.3 Compound-specific Stable Isotope Analysis (CSIA) of Water-Air Partitioning

Carbon isotope analysis of benzene, triethylamine, and trichloromethane was conducted on a GC-IRMS system using a TRACE GC Ultra gas chromatograph (Thermo Fisher Scientific, Milan, Italy) which was coupled to a Finnigan MAT 253 isotope ratio mass spectrometer *via* a Finnigan GC Combustion III interface (both Thermo Fisher Scientific, Bremen, Germany). For benzene, a Rxi-5Sil MS analytical column (30 m, 0.25 mm ID,

1.0 µm film) from Restek (Bad Homburg, Germany) was used. The initial GC oven temperature was 50 °C (hold 3 min), ramped 40 °C/min to 120 °C (hold 2 min), and ramped 55 °C/min to 280 °C (hold 5 min). The total uncertainty of benzene measurements was ± 0.2‰. Trimethylamine and trichloromethane were analyzed using a DB-624 analytical column (60 m, 0.25 mm ID, 1.4 µm film, Agilent Technologies, Böblingen, Germany). The GC oven program started at 120 °C (hold 12 min) and was ramped 100 °C/min to 280 °C (hold 2 min). The standard deviation of triethylamine and trichloromethane was ± 0.4‰ and ± 1‰, respectively. Detailed information on the method is described in Appendix A.3.

$\delta^{13}C$ values are expressed in per mil relative to Vienna PeeDee Belemnite (V-PDB):

$$\delta^{13}C = \frac{\left[\left({}^{13}C/{}^{12}C\right)_{sample} - \left({}^{13}C/{}^{12}C\right)_{standard}\right]}{\left({}^{13}C/{}^{12}C\right)_{standard}} \qquad \text{eq. 4.8}$$

Hydrogen isotope analysis of a trichloromethane and deuterotrichloromethane mixture (1:1, v/v) was performed on a GC-MS system in SIM mode. An Agilent 7890A GC system (Agilent Technologies, Santa Clara, USA) equipped with a DB-5 analytical column (30 m, 0.25 mm ID, 1.0 µm film, Agilent Technologies, Böblingen, Germany) was coupled to an Agilent 5975C mass selective triple-axis detector (Agilent Technologies, Santa Clara, USA). The initial GC oven temperature was 120 °C (hold 5 min), ramped 50 °C/min to 280 °C (hold 6 min). For detailed information on the method see Appendix A.3.

$^{2}H/^{1}H$ ratios are expressed in per mil using the following equation:

$$\frac{{}^{2}H}{{}^{1}H} = \frac{\left({}^{2}H/{}^{1}H\right)_{sample}}{\left({}^{2}H/{}^{1}H\right)_{initial}} - 1 \qquad \text{eq. 4.9}$$

Calculation of the enrichment factor ε for stepwise equilibrium exchange reactions is possible using (i) an approach considering consecutive equilibrium steps or (ii) the classical Rayleigh equation considering a continuous process. A comparison in the Appendix (Table A.3-2) gives essentially the same results for both evaluation methods so that – consistent with earlier findings by Jeannottat and Hunkeler[109] – the Rayleigh equation (eq. 4.10) was used in this study according to

$$\ln\left(\frac{\delta\,^{h}E_t + 1}{\delta\,^{h}E_0 + 1}\right) = \varepsilon \times \ln\left(\frac{c_t}{c_0}\right) \qquad \text{eq. 4.10}$$

where the isotopic signatures of element *E* are given as $\delta^h E_t$ (at time *t*) and $\delta^h E_0$ (at the beginning of the reaction) and c_t/c_0 is the fraction of the remaining substrate. Equilibrium isotope effects EIE can be correlated to the enrichment factor ε by the following equation:

$$\text{EIE} = \frac{1}{\varepsilon + 1} \qquad \text{eq. 4.11}$$

In the case of normal isotope effects (*i.e.*, molecules containing the light isotopologues escape preferentially into the gas phase), ε-values are negative, while positive ε-values indicate inverse isotope effects.

4.2.4 GC-FID Analysis for Hexadecane-Air Partitioning

Hexadecane-air partitioning of benzene, triethylamine, and trichloromethane was measured on a gas chromatograph equipped with a flame ionization detector (GC-FID, Hewlett Packard 5890 Series II, Wilmington, USA) using a VOCOL analytical column (30 m, 0.25 mm ID, 1.5 µm film) purchased from Supelco (Bellefonte, USA). Samples were injected manually (1 mL headspace for benzene, 2.5 mL headspace for triethylamine and trichloromethane) into an injector operating at 200 °C. The GC oven program was set to 120 °C (hold 60 min) with a constant N_2 carrier flow rate of 1.6 mL/min.

4.3 Results and Discussion

4.3.1 Water-Air Partitioning

As can be seen from Figure 4.3, the desired 50:50 distribution of the substances could approximately be achieved during water-air partitioning and in view of the data presented in Figure 4.4 it can be stated that the experimental setup used in this study (Figure 4.2) is generally suitable to determine isotope fractionation in partitioning experiments.

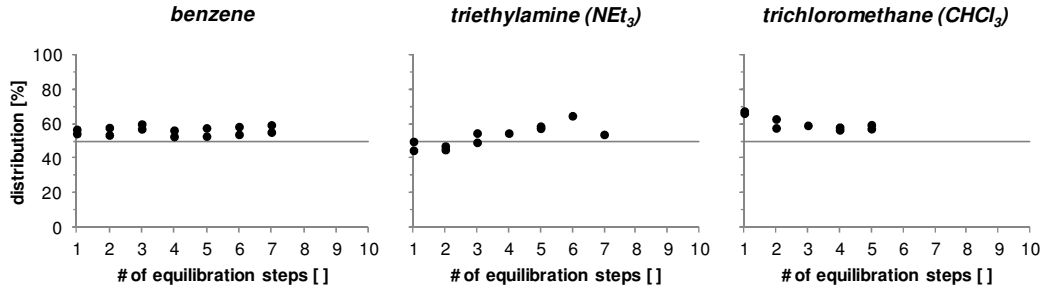

Figure 4.3: Distribution of benzene, triethylamine, and trichloromethane during water-air partitioning. Points that lie above the 50:50 distribution line indicate higher proportion of substance into the gas phase, while points that lie below that line show higher proportion in the liquid phase.

As shown in Figure 4.4, during stepwise water-air partitioning ^{13}C became enriched in the benzene of the aqueous phase corresponding to a normal isotope effect of volatilization (*i.e.*, light isotopologues escaped preferentially) with $\varepsilon = -0.12‰ \pm 0.03‰$. This result is in agreement with two studies reporting that the delocalized π electrons of the aromatic ring function as hydrogen bond acceptors[116,117] leading to strong *inter*molecular interactions in the condensed phase that are broken when the substance is evaporated into the gas phase. Carbon isotope fractionation during volatilization of pure benzene (Table 4.3), on the other hand, was observed to lead to an inverse isotope effect,[101] what, in turn, can be explained by the fact that benzene is not able to form hydrogen bonds with itself, but interacts *via* van-der-Waals forces. These observations clearly show that the properties of the *sorbent* in the condensed phase are a crucial factor in the sorption process and that this phenomenon can be investigated by our experimental approach (Figure 4.1).

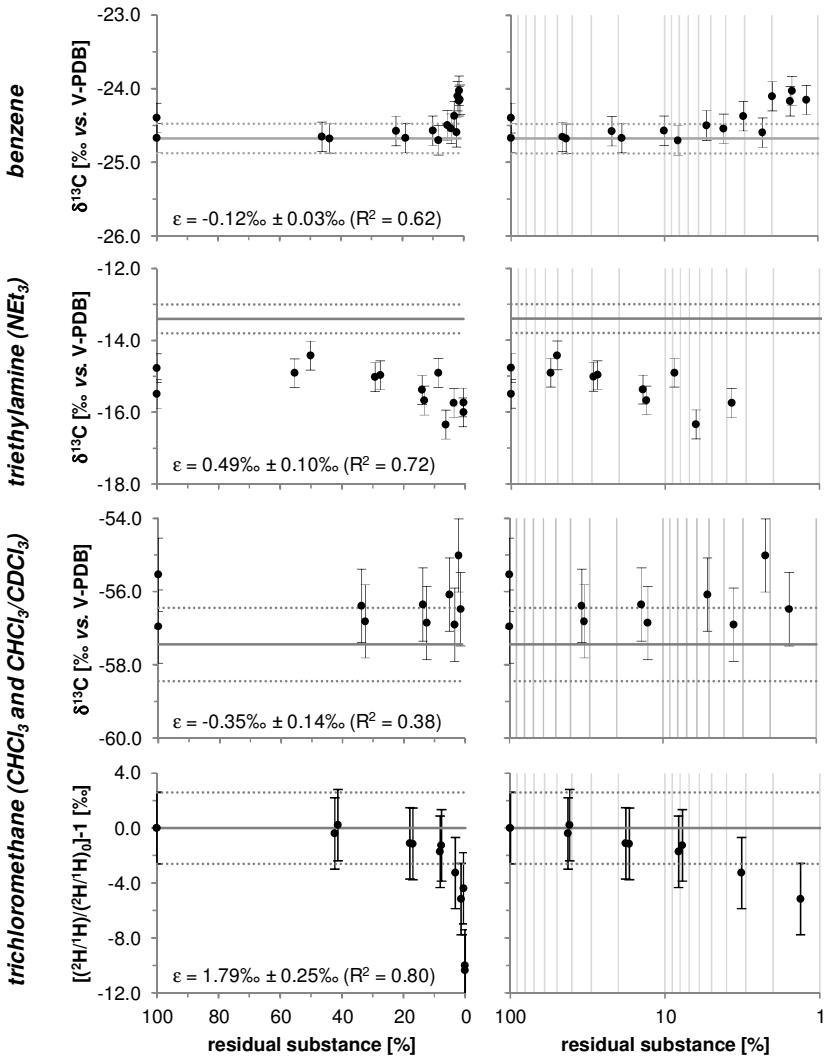

Figure 4.4: Carbon isotope data of benzene, triethylamine, and trichloromethane as well as hydrogen isotope data of trichloromethane determined from a $CHCl_3/CDCl_3$ mixture measured during water-air partitioning. For carbon isotope analysis, gray lines represent the isotopic composition of the standard determined by EA-IRMS. For hydrogen isotope analysis, the gray line denotes the measured initial average. Dotted lines and error bars represent the total uncertainty of carbon (± 0.2‰ for benzene, ± 0.4‰ for NEt_3, ± 1‰ for $CHCl_3$) and hydrogen (± 2.6‰) isotope analysis.

Table 4.3: Overview of vapor pressure ratios for light and heavy isotopologues and the corresponding equilibrium isotope effects of pure phase benzene, diethylamine, and trichloromethane determined at different temperatures. Values are taken from Jancso *et al.*[101]

substance	$ln\frac{P_l}{P}$ [ ] (temperature [°C])[a]	ε [‰]
benzene: $^{12}C_6H_6 - {}^{13}C^{12}C_5H_6$	-0.00023 (34.6)	0.23
	-0.00035 (78.0)	0.35
diethylamine:[b] $(CH_3)_2NH - (CD_3)_2NH$	-0.0793 (-50.0)	79.3
	-0.0478 (20.0)	47.8
trichloromethane: $^{12}CHCl_3 - {}^{13}CHCl_3$	-0.0008 (34.6)	0.80
$CHCl_3 - CDCl_3$	-0.0400 (-40.2)	40.0
	-0.0160 (9.85)	16.0

[a] $ln\frac{P_l}{P} > 0$, if substance interacts *via* hydrogen bonds (leading to a normal isotope effect); $ln\frac{P_l}{P} < 0$, if substance interacts *via* van-der-Waals interactions (leading to an inverse isotope effect). [b] data for triethylamine not available.

The tertiary amine triethylamine which provides a hydrogen bond acceptor moiety at the nitrogen atom showed a significant inverse carbon isotope effect of ε = 0.49‰ ± 0.10‰ (Figure 4.4). The inverse carbon isotope effect can on the one hand be explained by the fact that the ethyl side chains undergo only van-der-Waals interactions with the surrounding water molecules leading to additional *inter*molecular vibrations. Additionally, the hyperconjugation ($\sigma^*(C\text{-}H)_{CH_2} \rightarrow n_N$) which stabilizes the molecule in the gas phase is lost due to hydrogen bonding between water and the lone pair at the *N* atom of triethylamine leading to pronounced changes in *intra*molecular vibrations.[102,118] Hyperconjugation in the gas phase leads to loser *C-H* bonds (*i.e.*, *C-H* bond vibrations of lower energy) and stiffer *C-N* bonds (*i.e.*, *C-N* bond vibrations of higher energy), whereas the loss of hyperconjugation in water leads to stiffer *C-H* bonds (*i.e.*, *C-H* bond vibrations of higher energy) and loser *C-N* bonds (*i.e.*, *C-N* bond vibrations of lower energy).[102,118] The changes in *intra*molecular *C-H* bond vibrations (*i.e.*, stiff bonds → lose bonds on volatilization) contribute in the direction of a normal isotope effect, whereas the changes in *intra*molecular *C-N* bond vibrations (lose bonds → stiff bonds on volatilization) contribute to an inverse isotope effect. Vibrations of *C-N* bonds more strongly involve movement of the carbon atom than *C-H* bonds (as reflected in the reduced mass $\mu_{C\text{-}N}$ of the *C-N* bond vibration, which more strongly changes on substitution of ^{12}C by ^{13}C than

$\mu_{C\text{-}H}$). Hence, the inverse carbon isotope effect of the *C-N* bond vibrations is expected to dominate the contributions from *intra*molecular vibrations adding up to the inverse carbon isotope effect induced by the *inter*molecular van-der-Waals interactions. Unfortunately, no data is available for carbon vapor pressure ratios of pure triethylamine (Table 4.3). However, assuming that hydrogen and carbon atoms of the *C-H* bonds are – in terms of isotopic fractionation – behaving in a similar way,[114] if they are involved in van-der-Waals interactions, the data for deuterated ethyl groups in comparison to protonated ethyl groups provided in Table 4.3 indicate an inverse isotope effect for the alkyl side chains.

While the carbon isotope data of trichloromethane showed no clear isotopic trend, a significant inverse hydrogen isotope effect was observed for volatilization of the $CHCl_3/CDCl_3$ mixture from aqueous solution ($\varepsilon = 1.79‰ \pm 0.25‰$, Figure 4.4). This result is in contradiction to our hypothesis that trichloromethane is a weak hydrogen bond donor which interacts *via* hydrogen bonding in water so that a normal hydrogen isotope effect on volatilization is expected.[115] An explanation for this counterintuitive result is given by Rutkowski *et al.*[118] who showed that hydrogen bonding of trichloromethane elongates the *C-H* bond lowering the frequency of its stretching vibration. Therefore, the experimental results can again be explained by changes in *intra*- rather than *inter*molecular vibrations: the strong frequency shift in *intra*molecular vibrations leads to an inverse isotope effect that superimposes the predicted normal isotope effect expected from changes in *inter*molecular vibrations.

Therefore, most measured isotope effects agree with the predicted isotope effects for water-air partitioning (Table 4.1). However, it turned out that predictions of the prevailing isotope effect on the basis of *inter*molecular interactions expected from molecular structure may be wrong (*e.g.*, in case of trichloromethane), because *intra*molecular interactions can dominate the overall effect. In addition, the experiment showed clearly that the experimental determination of sorption isotope effects need to be accompanied by a careful interpretation of the molecular vibrations involved.

4.3.2 Hexadecane-Air Partitioning

Similar to the results of water-air partitioning, Figure 4.5 shows that the experimental setup (Figure 4.2) was also suitable to investigate hexadecane-air partitioning.

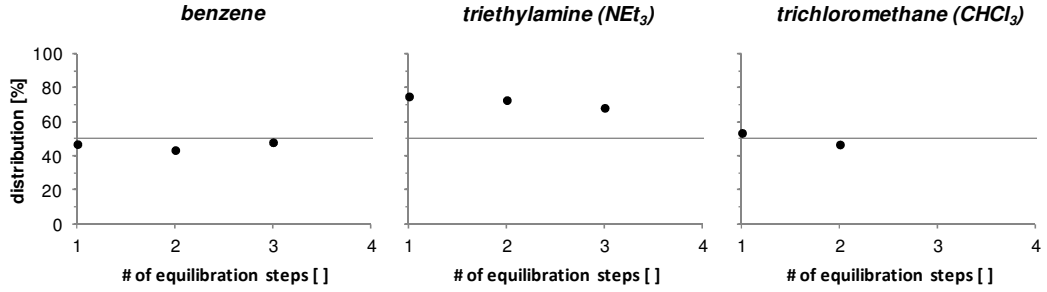

Figure 4.5: Distribution of benzene, triethylamine, and trichloromethane during hexadecane-air partitioning determined by GC-FID. Gray lines represent 50:50 distribution. For NEt_3, a 50:50 distribution was not realized so that a volume adjustment is needed. Due to the low concentration chosen, it was not possible to measure more than two equilibration steps for $CHCl_3$.

Hexadecane-air partitioning with the modified ND18 vials (Figure 4.2) turned out to be challenging, due to the following limitations of the isotope analysis by GC-IRMS. The amount of carbon that is at least required for precise carbon isotope measurement is 10 ng. Using stock solutions with 0.1% of the respective substance dissolved in *n*-hexadecane – this is the maximum possible amount to ensure that one substance molecule is surrounded just by *n*-hexadecane molecules excluding interactions of substance molecules with itself[112] –, Table 4.4 shows that GC-IRMS measurements are outside the reach of the experimental setup of the developed system (Figure 4.2). Only for benzene with a carbon content of 92.26%, up to five equilibration steps would be measurable.

Table 4.4: Calculation of the carbon mass on column for benzene, triethylamine, and trichloromethane in comparison to the minimum mass needed on column for precise isotope analysis.

	carbon content [%]	concentration of stock solution [mg/L]	volume of stock solution [µL]	mass on column[a] [ng]	mass needed on column[b] [ng]	possible number *n* of equilibration steps [ ]
benzene	92.26	266	25	170	10	5
NEt_3	71.22	345	15	100	10	4
$CHCl_3$	10.06	400	50	55.9	10	3

[a] mass on column after the 1st equilibration step calculated for a headspace sampling volume of 1 mL. [b] manufacturer specification (Thermo Fisher Scientific).

In order to obtain the amount of carbon needed on column for isotope analysis, other experimental approaches are necessary. By using a large bottle (up to 1 L) with two additional connections for fresh gas supply and an exit for the gas sampled, the mass problem could be circumvented (Figure 4.6).

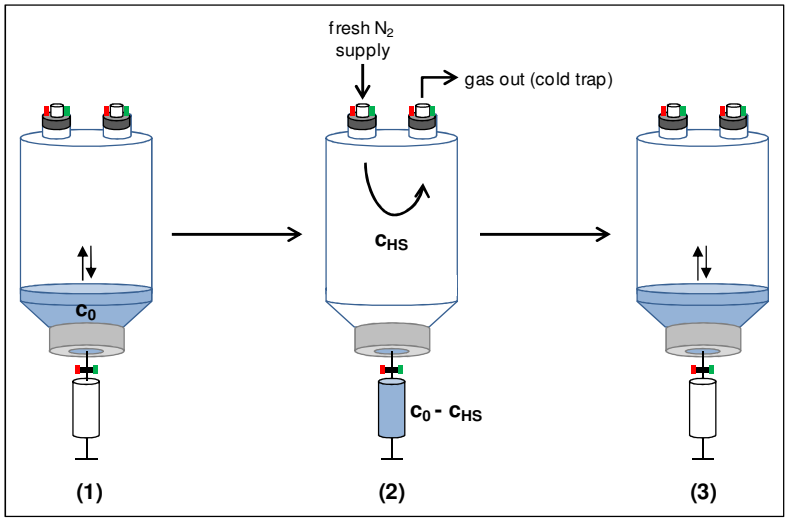

Figure 4.6: Schematic illustration of the alternative experimental setup for hexadecane-air partitioning: (1) equilibration on shaker; (2) exchange of the gas phase by a nitrogen stream while sampled headspace is collected on a cold trap; (3) repeat (1)-(2).

The sampled gas phase volume needs to be concentrated, *e.g.*, by a cooling trap containing liquid nitrogen. In addition, sampling and exchange of the gas phase

necessitates a possibility to prevent further distribution of the substances from the liquid to the gas phase. For this purpose, a syringe which can be closed, for instance, by a Mininert valve, would be the most suitable option, raising the syringe with the liquid phase, before the gas phase is exchanged. Also a setup similar to that investigated by Jeannottat *et al.*,[109] but with larger volumes, would be imaginable.

4.4 Outlook

Although the measurements have not been made for *n*-hexadecane so far, the behavior of the substances in the OM-air equilibrium can be approximated with the values given in Table 4.3 for pure phase volatilization. This calculation is feasible, because in pure phase none of the substances undergoes hydrogen bonding with itself (triethylamine provides just a hydrogen acceptor moiety, while trichloromethane functions as hydrogen bond donor) so that only van-der-Walls interactions are observed for pure phase volatilization. Together with the observations made for water-air partitioning (Figure 4.4), the following sorption isotope effects would be expected for molecules sorbing out of the water phase into an organic phase (Table 4.1):

(i) Prediction of the sorption isotope effect $\varepsilon_{water \rightarrow OM}$ *of benzene.* A slightly normal carbon isotope effect can be calculated for benzene when considering measured ($\varepsilon_{water \rightarrow air} = -0.12‰$) and vapor pressure isotope effects ($\varepsilon_{pure\ phase \rightarrow air} = 0.23‰$). According to eq. 4.4 (Bordwell thermodynamic cycle) and eq. 4.11 (correlation between EIE and ε) this results in a sorption isotope effect of $\varepsilon_{calculated} \approx -0.35‰$ that is in good agreement with the value for the sorption of benzene to humic substances obtained by Kopinke *et al.* ($\varepsilon = -0.44‰ \pm 0.10‰$).[32]

(ii) Prediction of the sorption isotope effect $\varepsilon_{water \rightarrow OM}$ *of trimethylamine.* The measured inverse isotope effect of water-air partitioning of triethylamine ($\varepsilon = 0.49‰ \pm 0.10‰$) is expected to be larger than that of OM-air partitioning (which has not been determined yet). Overall, it is therefore likely that the carbon sorption isotope effect of triethylamine is also inverse.

(iii) *Prediction of the sorption isotope effect* $\varepsilon_{water \rightarrow OM}$ *of trichloromethane.* Similar to benzene, a normal carbon sorption isotope effect can be calculated for trichloromethane ($\varepsilon_{calculated} \approx -1.15‰$) taking $\varepsilon_{water \rightarrow air} = -0.35‰$ and $\varepsilon_{pure\ phase \rightarrow air} = 0.80‰$ into account, while for hydrogen the isotope effect is expected to be normal ($\varepsilon_{water \rightarrow air} = 1.79‰$ and

$\varepsilon_{pure\ phase \rightarrow air}$ = 16.0‰ leading to $\varepsilon_{calculated} \approx$ -13.9‰). Both $EIE_{sorption}$ comprise mainly the contribution of trichloromethane's *intra*molecular interactions.

The results of the present study show that separate investigation of the sorption isotope effects *via* the Bordwell thermodynamic cycle (Table 4.1) allows a theoretical assessment of the involved molecular interactions. This is in particular evidenced by the good data consistency of the expected with the measured sorption isotope effect for benzene[32] providing a similar process understanding of sorption isotope effects also for other substances.

5

General Conclusion

In recent years, Compound-specific Stable Isotope Analysis (CSIA) has developed to a widely used method to evaluate degradation of organic contaminants in the environment, to study underlying transformation mechanisms, and to identify competing transformation pathways.[6,8,35] In order to enhance the understanding of natural attenuation processes, this thesis aimed to further develop CSIA particularly focusing on organic micropollutants.

Due to the large variety of competing (bio)chemical transformation pathways, investigation of underlying reaction mechanisms of micropollutants is important in order to track their behavior in the environment. Chapter 2, therefore, focused on the elucidation of the atrazine and ametryn degradation mechanism (both *s*-triazine herbicides). The enzymatic hydrolysis by TrzN was found to generate an enrichment of ^{13}C in the remaining substrate during the transformation process (normal carbon isotope effect), while ^{15}N was depleted (inverse nitrogen isotope effect). Together with crystal structure analysis and computational calculations these results give clear evidence that the degradation mechanism involves nitrogen atom protonation at the substrates' aromatic ring followed by nucleophilic aromatic substitution. Additionally, these results confirmed the trend observed in an earlier study on the degradation of atrazine with *Arthrobacter aurescens* TC1, a bacterial strain expressing enzyme TrzN.[23] Both members of the substance class showed characteristic $^{13}C/^{12}C$ and $^{15}N/^{14}N$ fractionation patterns and due to the different mechanism-specific slopes, the two-dimensional data evaluation ($\delta^{13}C$ *vs.* $\delta^{15}N$) demonstrates clearly that biotic hydrolysis can be distinguished from other degradation pathways, *e.g.*, biotic dealkylation.[42]

In the second part of this thesis (Chapter 3), CSIA was used to investigate isotope fractionation of organic contaminants (pesticides and pharmaceuticals) in a mesoscale aquifer model with emphasis to gain knowledge about the reliability of (multi-element) CSIA used to track the degradation of micropollutants in a near-natural setting. Isotope analysis confirmed the behavior evaluated from concentration breakthrough curves in comparison to the conservative tracer D_2O (BAM: no degradation, no sorption; bentazone: transformation, but no sorption; diclofenac: degradation and sorption). Both, carbon and nitrogen CSIA was carried out in similar concentrations as the isotope analysis of "traditional" priority pollutants (low µg/L range). However, CSIA of these compounds was limited in the method's precision showing uncertainties of ± 0.4-0.5‰ for carbon and ± 1‰ for nitrogen. These results can be considered as the fundamentals on the performance of CSIA to monitor the reactivity of pesticides and pharmaceuticals in

(near-)natural systems and may motivate future effort to accomplish CSIA at even lower concentrations (ng/L range) for the analysis of micropollutants in the environment.

Even though commonly neglected, several recent studies[32-34] and also Chapter 3 of this thesis demonstrated the influence of physical processes such as sorption on the fate of contaminants in the environment. Hence, Chapter 4 investigated the isotopic fractionation that occurs when a substance sorbs to soil components in correlation to the underlying type of molecular interaction (hydrogen bonding *vs.* van-der-Waals forces). In order to assign the $^{13}C/^{12}C$ and $^{2}H/^{1}H$ fractionation explicitly to van-der-Waals interactions (organic phase and water) or hydrogen bonds (water), both phases were considered separately using air as reference phase (no intermolecular interactions). The presented approach and the sorption in natural systems could be linked by a Bordwell thermodynamic cycle. Especially the result of benzene (calculated $\varepsilon_{sorption} \approx -0.35‰$) correlated well with that obtained by Kopinke *et al.* (measured $\varepsilon_{sorption} = -0.44‰$),[32] and for the first time this isotope effect could be explained by the underlying interactions between the solute and its surrounding solvent. Trichloromethane, on the other hand, was expected to act as hydrogen bond donor inducing a normal isotope effect. Instead, the measured inverse hydrogen isotope effect clearly demonstrated that intramolecular vibrations can superimpose the effect of intermolecular vibrations. A careful consideration of all molecular vibrations involved is therefore essential in the interpretation of sorption-induced isotope effects. The moiety-specific information about sorption isotope effects (*e.g.*, of the amine group in triethylamine) obtained from simple, volatile model compounds have the potential to be linked to more complex, nonvolatile molecules (*e.g.*, micropollutants containing an amine group such as diclofenac (see Chapter 3) or carbamate pesticides) where investigation *via* separate analysis (Bordwell thermodynamic cycle) is not possible. As a result, the contributions of sorption and (bio)transformation to the isotope effect can be better estimated in environmental systems and required remediation strategies can be adapted accordingly.

References

[1] Oki, T.; Kanae, S.; Global Hydrological Cycles and World Water Resources, *Science* **2006**, *313*, 1068-1072.

[2] Schwarzenbach, R. P.; Escher, B. I.; Fenner, K.; Hofstetter, T. B.; Johnson, C. A.; von Gunten, U.; Wehrli, B.; The Challenge of Micropollutants in Aquatic Systems, *Science* **2006**, *313*, 1072-1077.

[3] Schwarzenbach, R. P.; Egli, T.; Hofstetter, T. B.; von Gunten, U.; Wehrli, B.; Global Water Pollution and Human Health, *Annu. Rev. Environ. Resour.* **2010**, *35*, 109-136.

[4] Fenner, K.; Canonica, S.; Wackett, L. P.; Elsner, M.; Evaluating Pesticide Degradation in the Environment: Blind Spots and Emerging Opportunities, *Science* **2013**, *341*, 752-758.

[5] Lyman, W. J.; Reehl, W. F.; Rosenblatt, D. H.; *Handbook of chemical property estimation methods: Environmental behavior of organic compounds*, American Chemical Society, Washington, DC, USA, **1990**.

[6] Hofstetter, T. B.; Schwarzenbach, R. P.; Bernasconi, S. M.; Assessing Transformation Processes of Organic Compounds Using Stable Isotope Fractionation, *Environ. Sci. Technol.* **2008**, *42* (21), 7737-7743.

[7] Hunkeler, D.; Chollet, N.; Pittet, X.; Aravena, R.; Cherry, J. A.; Parker, B. L.; Effect of source variability and transport processes on carbon isotope ratios of TCE and PCE in two sandy aquifers, *J. Contam. Hydrol.* **2004**, *74*, 264-282.

[8] Schmidt, T. C.; Zwank, L.; Elsner, M.; Berg, M.; Meckenstock, R. U.; Haderlein, S. B.; Compound-specific stable isotope analysis of organic contaminants in natural environments: a critical review of the state of the art, prospects, and future challenges, *Anal. Bioanal. Chem.* **2004**, *378*, 283-300.

[9] Meckenstock, R. U.; Morasch, B.; Griebler, C.; Richnow, H. H.; Stable isotope fractionation analysis as a tool to monitor biodegradation in contaminated aquifers, *J. Contam. Hydrol.* **2004**, *75*, 215-255.

[10] Simon, H.; Palm, D.; Isotopeneffekte in der organischen Chemie und Biochemie, *Angew. Chem.* **1966**, *78* (22), 993-1028.

[11] Aelion, C. M.; Höhener, P.; Hunkeler, D.; Aravena, R.; *Environmental Isotopes in Biodegradation and Bioremediation*, 1st ed.; CRC Press - Taylor & Francis Group, Boca Raton, FL, USA, **2010**.

[12] Hoefs, J.; *Stable Isotope Geochemistry*, Springer-Verlag, Berlin, Germany, **2009**.

[13] Harrington, R. R.; Poulson, S. R.; Drever, J. I.; Colberg, P. J. S.; Kelly, E. F.; Carbon isotope systematics of monoaromatic hydrocarbons: vaporization and adsorption experiments, *Org. Geochem.* **1999**, *30*, 765-775.

[14] Slater, G. F.; Ahad, J. M. E.; Sherwood Lollar, B.; Allen-King, R.; Sleep, B.; Carbon Isotope Effects Resulting from Equilibrium Sorption of Dissolved VOCs, *Anal. Chem.* **2000**, *72* (22), 5669-5672.

[15] Bloom, Y.; Aravena, R.; Hunkeler, D.; Edwards, E.; Frape, S. K.; Carbon Isotope Fractionation during Microbial Dechlorination of Trichloroethene, *cis*-1,2-Dichloroethene, and Vinyl Chloride: Implications for Assessment of Natural Attenuation, *Environ. Sci. Technol.* **2000**, *34* (13), 2768-2772.

[16] Morasch, B.; Richnow, H. H.; Schink, B.; Meckenstock, R. U.; Stable Hydrogen and Carbon Isotope Fractionation during Microbial Toluene Degradation: Mechanistic and Environmental Aspects, *Appl. Environ. Microbiol.* **2001**, *67* (10), 4842-4849.

[17] Griebler, C.; Safinowski, M.; Vieth, A.; Richnow, H. H.; Meckenstock, R. U.; Combined Application of Stable Carbon Isotope Analysis and Specific Metabolites Determination for Assessing In Situ Degradation of Aromatic Hydrocarbons in a Tar Oil-Contaminated Aquifer, *Environ. Sci. Technol.* **2004**, *38* (2), 617-631.

[18] Rayleigh, J. W. S.; Theoretical Considerations respecting the Separation of Gases by Diffusion and similar Processes, *Phil. Mag. Series 5* **1896**, *42* (259), 493-498.

[19] Elsner, M.; Zwank, L.; Hunkeler, D.; Schwarzenbach, R. P.; A New Concept Linking Observable Stable Isotope Fractionation to Transformation Pathways of Organic Pollutants, *Environ. Sci. Technol.* **2005**, *39*, 6896-6916.

[20] Hirschorn, S. K.; Dinglasan, M. J.; Elsner, M.; Mancini, S. A.; Lacrampe-Couloume, G.; Edwards, E. A.; Sherwood Lollar, B.; Pathway Dependent Isotopic Fractionation during Aerobic Biodegradation of 1,2-Dichloroethane, *Environ. Sci. Technol.* **2004**, *38*, 4775-4781.

[21] Northrop, D. B.; The expression of isotope effects on enzyme-catalyzed reactions, *Annu. Rev. Biochem.* **1981**, *50*, 103-131.

[22] Zwank, L.; Berg, M.; Elsner, M.; Schmidt, T. C.; Schwarzenbach, R. P.; Haderlein, S. B.; New Evaluation Scheme for Two-Dimensional Isotope Analysis to Decipher Biodegradation Processes: Application to Groundwater Contamination by MTBE, *Environ. Sci. Technol.* **2005**, *39*, 1018-1029.

[23] Meyer, A. H.; Penning, H.; Elsner, M.; C and N Isotope Fractionation Suggests Similar Mechanisms of Microbial Atrazine Transformation Despite Involvement of Different Enzymes (AtzA and TrzN), *Environ. Sci. Technol.* **2009**, *43* (21), 8079-8085.

[24] Brand, W. A.; High Precision Isotope Ratio Monitoring Techniques in Mass Spectrometry, *J. Mass Spectrom.* **1996**, *31*, 225-235.

[25] Elsner, M.; Jochmann, M. A.; Hofstetter, T. B.; Hunkeler, D.; Bernstein, A.; Schmidt, T. C.; Schimmelmann, A.; Current challenges in compound-specific stable isotope analysis of environmental organic contaminants, *Anal. Bioanal. Chem.* **2012**, *403* (9), 2471-2491.

[26] Zwank, L.; Berg, M.; Schmidt, T. C.; Haderlein, S. B.; Compound-Specific Carbon Isotope Analysis of Volatile Organic Compounds in the Low-Microgram per Liter Range, *Anal. Chem.* **2003**, *75* (20), 5575-5583.

[27] Shouakar-Stash, O.; Frape, S. K.; Drimmie, R. J.; Stable hydrogen, carbon, and chlorine isotope measurements of selected chlorinated organic solvents, *J. Contam. Hydrol.* **2003**, *60*, 211-228.

[28] Hunkeler, D.; Aravena, R.; Berry-Spark, K.; Cox, E.; Assessment of Degradation Pathways in an Aquifer with Mixed Chlorinated Hydrocarbon Contamination Using Stable Isotope Analysis, *Environ. Sci. Technol.* **2005**, *39*, 5975-5981.

[29] Hunkeler, D.; Meckenstock, R. U.; Lollar, B.; Schmidt, T. C.; Wilson, J. T.; *A Guide for Assessing Biodegradation and Source Identification of Organic Groundwater Contaminants Using Compound Specific Isotope ANalysis (CSIA). EPA/600/R-08/148*, U.S. Environmental Protection Agency, Washington, DC, USA, **2009**.

[30] Maier, M. P.; De Corte, S.; Nitsche, S.; Spaett, T.; Boon, N.; Elsner, M.; C & N Isotope Analysis of Diclofenac to Distinguish Oxidative and Reductive Transformation and to Track Commercial Products, *Environ. Sci. Technol.* **2014**, *48*, 2312-2320.

[31] Meyer, A. H.; Dybala-Defratyka, A.; Alaimo, P. J.; Geronimo, I.; Sanchez, A. D.; Cramer, C. J.; Elsner, M.; Cytochrome P450-catalyzed dealkylation of atrazine by *Rhodococcus* sp. strain NI86/21 involves hydrogen atom transfer rather than single electron transfer, *Dalton Trans.* **2014**, *43* (32), 12175-12186.

[32] Kopinke, F.-D.; Georgi, A.; Voskamp, M.; Richnow, H. H.; Carbon Isotope Fractionation of Organic Contaminants Due to Retardation on Humic Substances: Implications for Natural Attenuation Studies in Aquifers, *Environ. Sci. Technol.* **2005**, *39*, 6052-6062.

[33] Qiu, S.; Eckert, D.; Cirpka, O. A.; Huenniger, M.; Knappett, P.; Maloszewski, P.; Meckenstock, R. U.; Griebler, C.; Elsner, M.; Direct Experimental Evidence of Non-first Order Degradation Kinetics and Sorption-Induced Isotopic Fractionation in a Mesoscale Aquifer: $^{13}C/^{12}C$ Analysis of a Transient Toluene Pulse, *Environ. Sci. Technol.* **2013**, *47*, 6892-6899.

[34] Eckert, D.; Qiu, S.; Elsner, M.; Cirpka, O. A.; Model Complexity Nedded for Quantitative Analysis of High Resolution Isotope and Concentration Data from a Toluene-Pulse Experiment, *Environ. Sci. Technol.* **2013**, *47*, 6900-6907.

[35] Elsner, M.; Stable isotope fractionation to investigate natural transformation mechanisms of organic contaminants: principles, prospects, and limitations, *J. Environ. Monit.* **2010**, *12* (11), 2005-2031.

[36] Penning, H.; Sørensen, S. R.; Meyer, A. H.; Aamand, J.; Elsner, M.; C, N, and H Isotope Fractionation of the Herbicide Isoproturon Reflects Different Microbial Transformation Pathways, *Environ. Sci. Technol.* **2010**, *44* (7), 2372-2378.

[37] Pinto, G. M. F.; Jardim, I. C. S. F.; Use of silid-phase extraction and high-performance liquid chromatography for the determination of triazine residues in water: validation of the method, *J. Chromatogr. A* **2000**, *869*, 463-469.

[38] Radosevich, M.; Traina, S. J.; Hao, Y.-L.; Tuovinen, O. H.; Degradation and Mineralization of Atrazine by a Soil Bacterial Isolate, *Appl. Environ. Microbiol.* **1995**, *61* (1), 297-302.

[39] Mandelbaum, R. T.; Allan, D. L.; Wackett, L. P.; Isolation and Characterization of a *Pseudomonas* sp. That Mineralizes the *s*-Triazine Herbicide Atrazine, *Appl. Environ. Microbiol.* **1995**, *61* (4), 1451-1457.

[40] Hartenbach, A. E.; Hofstetter, T. B.; Tentscher, P. R.; Canonica, S.; Berg, M.; Schwarzenbach, R. P.; Carbon, Hydrogen, and Nitrogen Isotope Fractionation During Light-Induced Transformation of Atrazine, *Environ. Sci. Technol.* **2008**, *42* (21), 7751-7756.

[41] Meyer, A. H.; Penning, H.; Lowag, H.; Elsner, M.; Precise and Accurate Compound Specific Carbon and Nitrogen Isotope Analysis of Atrazine: Critical Role of Combustion Oven Conditions, *Environ. Sci. Technol.* **2008**, *42* (21), 7757-7763.

[42] Meyer, A. H.; Elsner, M.; $^{13}C/^{12}C$ and $^{15}N/^{14}N$ Isotope Analysis To Characterize Degradation of Atrazine: Evidence from Parent and Daughter Compound Values, *Environ. Sci. Technol.* **2013**, *47* (13), 6884-6891.

[43] Seffernick, J. L.; Reynolds, E.; Fedorov, A. A.; Fedorov, E.; Almo, S. C.; Sadowsky, M. J.; Wackett, L. P.; X-ray Structure and Mutational Analysis of the Atrazine Chlorohydrolase TrzN, *J. Biol. Chem.* **2010**, *285* (40), 30606-30614.

[44] Grzybkowska, A.; Kaminski, R.; Dybala-Defratyka, A.; Theoretical predictions of isotope effects *versus* their experimental values for an example of uncatalyzed hydrolysis of atrazine, *Phys. Chem. Chem. Phys.* **2014**, *16*, 15164-15172.

[45] Lynch, B. J.; Patton, L. F.; Harris, M.; Truhlar, D. G.; Adiabatic Connection for Kinetics, *J. Phys. Chem. A* **2000**, *104* (21), 4811-4815.

[46] Zhao, Y.; Schultz, N. E.; Truhlar, D. G.; Design of Density Functionals by Combining the Method of Constraint Satisfaction with Parametrization for Thermochemistry, Thermochemical Kinetics, and Noncovalent Interactions, *J. Chem. Theory Comput.* **2006**, *2* (2), 364-382.

[47] Frisch, M. J.; Pople, J. A.; Binkley, J. S.; Self-consistent molecular orbital methods 25. Supplementary functions for Gaussian basis sets, *J. Chem. Phys.* **1984**, *80* (7), 3265-3269.

[48] Hay, P. J.; Wadt, W. R.; *Ab initio* effective core potentials for molecular calculations. Potentials for the transition metal atoms Sc to Hg, *J. Chem. Phys.* **1985**, *82* (1), 270-283.

[49] Frisch, M. J.; Trucks, G. W.; Schlegel, H. B.; Scuseria, G. E.; Robb, M. A.; Cheesman, J. R.; Scalmani, G.; Barone, V.; Mennucci, B.; Petersson, G. A.; Nakatsuji, H.; Caricato, M.; Li, X.; Hratchian, H. P.; Izmaylov, A. F.; Bloino, J.; Zheng, G.; Sonnenberg, J. L.; Hada, M.; Ehara, M.; Toyota, K.; Fukuda, R.; Hasegawa, J.; Ishida, M.; Nakajima, T.; Honda, Y.; Kitao, O.; Nakai, H.; Vreven, T.; Montgomery, J., J. A.; Peralta, J. E.; Ogliaro, F.; Bearpark, M.; Heyd, J. J.; Brothers, E.; Kudin, K. N.; Staroverov, V. N.; Kobayashi, R.; Normand, J.; Raghavachari, K.; Rendell, A.; Burant, J. C.; Iyengar, S. S.; Tomasi, J.; Cossi, M.; Rega, N.; Millam, J. M.; Klene, M.; Knox, J. E.; Cross, J. B.; Bakken, V.; Adamo, C.; Jaramillo, J.; Gomperts, R.; Stratmann, R. E.; Yazyev, O.; Austin, A. J.; Cammi, R.; Pomelli, C.; Ochterski, J. W.; Martin, J. W.; Morokuma, K.; Zakrzewski, V. G.; Voth, G. A.; Salvador, P.; Fox, D. J.; *Gaussian 09*, Revision A.1; Gaussian, Inc.: Wallingford, CT, **2009**.

[50] Buncel, E.; *Isotopes in Organic Chemistry Vol. 8, Heavy Atom Isotope Effects*, Elsevier Science Publisher B.V., Amsterdam, The Netherlands, **1992**, 303-306.

[51] Lapworth, D. J.; Baran, N.; Stuart, M. E.; Ward, R. S.; Emerging organic contaminants in groundwater: A review of sources, fate and occurence, *Environ. Pollut.* **2012**, *163*, 287-303.

[52] Oaks, J. L.; Gilbert, M.; Virani, M. Z.; Watson, R. T.; Meteyer, C. U.; Rideout, B. A.; Shivaprasad, H. L.; Ahmed, S.; Chaudhry, M. J. I.; Arshad, M.; Mahmood, S.; Ali, A.; Khan, A. A.; Diclofenac residues as the cause of vulture population decline in Pakistan, *Nature* **2004**, *427* (6975), 630-633.

[53] Ericson, H.; Thorsén, G.; Kumblad, L.; Physiological effects of diclofenac, ibuprofen, and propranolol on Baltic Sea blue mussels, *Aquat. Toxicol.* **2010**, *99*, 223-231.

[54] Kuster, M.; López de Alda, M. J.; Hernando, M. D.; Petrovic, M.; Martín-Alonso, J.; Barceló, D.; Analysis and occurrence of pharmaceuticals, estrogens, progestogens and polar pesticides in sewage treatment plant effluents, river water and drinking water in the Llobregat river basin (Barcelona, Spain), *J. Hydrol.* **2008**, *358* (1-2), 112-123.

[55] Bonvin, F.; Rutler, R.; Chèvre, N.; Halder, J.; Kohn, T.; Spatial and Temporal Presence of a Wastewater-Derived Micropollutant Plume in Lake Geneva, *Environ. Sci. Technol.* **2011**, *45* (11), 4702-4709.

[56] Wells, M. J. M.; Riemer, D. D.; Wells-Knecht, M. C.; Development and optimization of a solid-phase extraction scheme for determination of the pesticides metribuzin, atrazine, metolachlor and esfenvalerate in agricultural runoff water, *J. Chromatogr. A* **1994**, *659* (2), 337-348.

[57] Cooper, C.; Moore, M.; Bennett, E.; Smith Jr, S.; Farris, J.; Milam, C.; Shields Jr, F.; Innovative uses of vegetated drainage ditches for reducing agricultural runoff, *Water Sci. Technol.* **2004**, *49* (3), 117-123.

[58] Díaz-Cruz, M. S.; Barceló, D.; Trace organic chemicals contamination in ground water recharge, *Chemospere* **2008**, *72* (3), 333-342.

[59] Kuster, M.; Díaz-Cruz, M. S.; Rosell, M.; López de Alda, M.; Barceló, D.; Fate of selected pesticides, estrogens, progestogens and volatile organic compounds during artificial aquifer recharge using surface waters, *Chemospere* **2010**, *79* (8), 880-886.

[60] Verstraeten, I.; Heberer, T.; Scheytt, T.; Occurrence, Characteristics, Transport, and Fate of Pesticides, Pharmaceuticals, Industrial Products, and Personal Care Products at Riverbank Filtration Sites. In *Riverbank Filtration*, Ray, C.; Melin, G.; Linsky, R.; Eds. Springer Netherlands, **2003**, Vol. 43, 175-227.

[61] Heberer, T.; Mechlinski, A.; Fanck, B.; Knappe, A.; Massmann, G.; Pekdeger, A.; Fritz, B.; Field Studies on the Fate and Transport of Pharmaceutical Residues in Bank Filtration, *Ground Water Monit. R.* **2004**, *24* (2), 70-77.

[62] Sniegowksi, K.; Bers, K.; Ryckeboer, J.; Jaeken, P.; Spanoghe, P.; Springael, D.; Robust Linuron Degradation in On-Farm Biopurification Systems Exposed to Sequential Environmental Changes, *Appl. Environ. Microbiol.* **2011**, *77* (18), 6614-6621.

[63] Milosevic, N.; Qiu, S.; Elsner, M.; Einsiedl, F.; Maier, M. P.; Bensch, H. K. V.; Albrechtsen, H.-J.; Bjerg, P. L.; Combined isotope and enantiomer analysis to assess the fate of phenoxy acids in a heterogeneous geological setting at an old landfill, *Water Res.* **2013**, *47* (2), 637-649.

[64] Bashir, S.; Hitzfeld, K. L.; Gehre, M.; Richnow, H. H.; Fischer, A.; Evaluating degradation of hexachlorcyclohexane (HCH) isomers within a contaminated aquifer using compound-specific stable carbon isotope analysis (CSIA), *Water Res.* **2015**, *71*, 197-196.

[65] Huntscha, S.; Rodriguez Velosa, D. M.; Schroth, M. H.; Hollender, J.; Degradation of Polar Organic Micropollutants during Riverbank Filtration: Complementary Results from Spatiotemporal Sampling and Push–Pull Tests, *Environ. Sci. Technol.* **2013**, *47* (20), 11512-11521.

[66] Hillebrand, O.; Nödler, K.; Sauter, M.; Licha, T.; Multitracer experiment to evaluate the attenuation of selected organic micropollutants in a karst aquifer, *Sci. Total Environ.* **2015**, *506-507*, 338-343.

[67] Postigo, C.; Barceló, D.; Synthetic organic compounds and their transformation products in groundwater: Occurrence, fate and mitigation, *Sci. Total Environ.* **2015**, *503-504*, 32-47.

[68] Dębska, J.; Kot-Wasik, A.; Namieśnik, J.; Fate and Analysis of Pharmaceutical Residues in the Aquatic Environment, *Crit. Rev. Anal. Chem.* **2004**, *34* (1), 51-67.

[69] Bottoni, P.; Caroli, S.; Caracciolo, A. B.; Pharmaceuticals as priority water contaminants, *Toxicol. Environ. Chem.* **2010**, *92* (3), 549-565.

[70] Reinnicke, S.; Bernstein, A.; Elsner, M.; Small and Reproducible Isotope Effects during Methylation with Trimethylsulfonium Hydroxide (TMSH): A Convenient Derivatization Method for Isotope Analysis of Negative Charged Molecules, *Anal. Chem.* **2010**, *82*, 2013-2019.

[71] Spahr, S.; Huntscha, S.; Bolotin, J.; Maier, M. P.; Elsner, M.; Hollender, J.; Hofstetter, T. B.; Compound-specific isotope analysis of benzotriazole and its derivatives, *Anal. Bioanal. Chem.* **2013**, *405* (9), 2843-2856.

[72] Maier, M. P.; Qiu, S.; Elsner, M.; Enantioselective stable isotope analysis (ESIA) of polar herbicides, *Anal. Bioanal. Chem.* **2013**, *405*, 2825-2831.

[73] Reinnicke, S.; Simonsen, A.; Sørensen, S. R.; Aamand, J.; Elsner, M.; C and N Isotope Fractionation during Biodegradation of the Pesticide Metabolite 2,6-Dichlorobenzamide (BAM): Potential for Environmental Assessment, *Environ. Sci. Technol.* **2012**, *46*, 1447-1454.

[74] Birkigt, J.; Gilevska, T.; Ricken, B.; Richnow, H.-H.; Vione, D.; Corvini, P. F. X.; Nijenhuis, I.; Cichocka, D.; Carbon Stable Isotope Fractionation of Sulfamethoxazole during Biodegradation by *Microbacterium* sp. Strain BR1 and upon Direct Photolysis, *Environ. Sci. Technol.* **2015**, *49* (10), 6029-6036.

[75] Hijosa-Valsero, M.; Matamoros, V.; Sidrach-Cardona, R.; Martín-Villacorta, J.; Bécares, E.; Bayona, J. M.; Comprehensive assessment of the design configuration of constructed wetlands for the removal of pharmaceuticals and personal care products from urban wastewaters, *Water Res.* **2010**, *44*, 3669-3678.

[76] Schreglmann, K.; Hoeche, M.; Steinbeiss, S.; Reinnicke, S.; Elsner, M.; Carbon and nitrogen isotope analysis of atrazine and desethylatrazine at sub-microgram per liter concentrations in groundwater, *Anal. Bioanal. Chem.* **2013**, *405*, 2857-2867.

[77] Elsayed, O. F.; Maillard, E.; Vuilleumier, S.; Nijenhuis, I.; Richnow, H. H.; Imfeld, G.; Using compound-specific isotope analysis to assess the degradation of chloroacetnilide herbicides in lab-scale wetlands, *Chemospere* **2014**, *99*, 89-95.

[78] Sessions, A. L.; Isotope-ratio detection for gas chromatography, *J. Sept. Sci.* **2006**, *29*, 1946-1961.

[79] Reinnicke, S.; Juchelka, D.; Steinbeiss, S.; Meyer, A.; Hilkert, A.; Elsner, M.; Gas chromatography/isotope ratio mass spectrometry of recalcitrant target compounds: performance of different combustion reactors and strategies for standardization, *Rapid Commun. Mass Spectr.* **2012**, *26*, 1053-1060.

[80] Wijker, R. S.; Kurt, Z.; Spain, J. C.; Bolotin, J.; Zeyer, J.; Hofstetter, T. B.; Isotope Fractionation Associated with the Biodegradation of 2- and 4-Nitrophenols *via* Monooxygenation Pathways, *Environ. Sci. Technol.* **2013**, *47* (24), 14185-14193.

[81] van Breukelen, B. M.; Prommer, H.; Beyond the Rayleigh Equation: Reactive Transport Modeling of Isotope Fractionation Effects to Improve Quantification of Biodegradation, *Environ. Sci. Technol.* **2008**, *42* (7), 2457-2463.

[82] Blum, P.; Hunkeler, D.; Weede, M.; Beyer, C.; Grathwohl, P.; Morasch, B.; Quantification of biodegradation for o-xylene and naphthalene using first order decay models, Michaelis-Menten kinetics and stable carbon isotopes, *J. Contam. Hydrol.* **2009**, *105* (3-4), 118-130.

[83] Bouchard, D.; Hunkeler, D.; Gaganis, P.; Aravena, R.; Höhener, P.; Broholm, M. M.; Kjeldsen, P.; Carbon Isotope Fractionation during Diffusion and Biodegradation of Petroleum Hydrocarbons in the Unsaturated Zone: Field Experiment at Værløse Airbase, Denmark, and Modeling, *Environmental Science & Technology* **2008**, *42* (2), 596-601.

[84] Rolle, M.; Chiogna, G.; Bauer, R.; Griebler, C.; Grathwohl, P.; Isotopic Fractionation by Transverse Dispersion: Flow-through Microcosms and Reactive Transport Modeling Study, *Environ. Sci. Technol.* **2010**, *44* (6167-6173).

[85] Thorstensen, C. W.; Lode, O.; Laboratory degradation studies of bentazone, dichlorprop, MCPA, and propiconazole in Norwegian soils, *J. Environ. Qual.* **2001**, *30* (3), 947-953.

[86] Boivin, A.; Cherrier, R.; Perrin-Ganier, C.; Schiavon, M.; Time effect on bentazone sorption and degradation in soil, *Pest Manag. Sci.* **2004**, *60* (8), 809-814.

[87] Simonsen, A.; Holtze, M. S.; Sørensen, S. R.; Sørensen, S. J.; Aamand, J.; Mineralization of 2,6-dichlorobenzamide (BAM) in dichlobenil-exposed soils and isolation of a BAM-mineralising *Aminobacter* sp., *Environ. Pollut.* **2006**, *144*, 289-295.

[88] Sørensen, S. R.; Holtze, M. S.; Simonsen, A.; Aamand, J.; Degradation and Mineralization of Nanomolar Concentrations of the Herbicide Dichlobenil and Its Persistent Metabolite 2,6-Dichlorobenzamide by *Aminobacter* spp. Isolated from Dichlobenil-Treated Soils, *Appl. Environ. Microbiol.* **2007**, *73* (2), 399-406.

[89] Daughton, C. G.; Ternes, T. A.; Pharmaceuticals and personal care products in the environment: Agents of subtle change?, *Environ. Health Perspect.* **1999**, *107*, 907-938.

[90] Heberer, T.; Tracking persistent pharmaceutical residues from municipal sewage to drinking water, *J. Hydrol.* **2002**, *266* (3-4), 175-189.

[91] Winkler, M.; Lawrence, J. R.; Neu, T. R.; Selective degradation of ibuprofen and clofibric acid in two model river biofilm systems, *Water Res.* **2001**, *35* (13), 3197-3205.

[92] Herzyk, A.; Maloszewski, P.; Qiu, S.; Elsner, M.; Griebler, C.; Intrinsic potential for immediate biodegradation of toluene in a pristine, energy-limited aquifer, *Biodegradation* **2014**, *25* (3), 325-336.

[93] Höhener, P.; Yu, X.; Stable carbon and hydrogen isotope fractionation of dissolved organic groundwater pollutants by equilibrium sorption, *J. Contam. Hydrol.* **2012**, *129-130*, 54-61.

[94] Janniche, G. S.; Clausen, L.; Albrechtsen, H.-J.; Inherent mineralization of 2,6-dichlorobenzamide (BAM) in unsaturated zone and aquifers - Effect of initial concentrations and adaptation, *Environ. Pollut.* **2011**, *159*, 2801-2807.

[95] González-Naranjo, V.; Boltes, K.; Biel, M.; Mobility of ibuprofen, a persistent active drug, in soil irrigated with reclaimed water, *Plant Soil Environ.* **2013**, *59* (2), 68-73.

[96] Buser, H.-R.; Poiger, T.; Müller, M. D.; Occurrence and Fate of the Pharmaceutical Drug Diclofenac in Surface Waters: Rapid Photodegradation in a Lake, *Environ. Sci. Technol.* **1998**, *32* (22), 3449-3456.

[97] Packer, J. L.; Werner, J. J.; Latch, D. E.; McNeill, K.; Arnold, W. A.; Photochemical fate of pharmaceuticals in the environment: Naproxen, diclofenac, clofibric acid, and ibuprofen, *Aquat. Sci.* **2003**, *65* (4), 342-351.

[98] Li, K.; Liu, W.; Xu, D.; Lee, S.; Influence of Organic Matter and pH on Bentazone Sorption in Soils, *J. Agric. Food Chem.* **2003**, *51*, 5362-5366.

[99] Bergström, L. F.; Jarvis, N. J.; Leaching of dichlorprop, bentazone, and 36CL in undisturbed field lysimeters of different agricultural soils, *Weed Sci.* **1993**, *41*, 251-261.

[100] Sherwood Lollar, B.; Hirschorn, S. K.; Chartrand, M. M. G.; Lacrampe Couloume, G.; An Approach for Assessing Total Instrumental Uncertainty in Compound-Specific Carbon Isotope Analysis: Implications for Environmental Remediation Studies, *Anal. Chem.* **2007**, *79* (9), 3469-3475.

[101] Jancso, G.; Van Hook, W. A.; Condensed Phase Isotope Effects (Especially Vapor Pressure Isotope Effects), *Chem. Rev.* **1974**, *74* (6), 689-750.

[102] Chandra, A. K.; Parveen, S.; Zeegers-Huyskens, T.; Anomeric Effects in the Symmetrical and Asymmetrical Structures of Triethylamine. Blue-Shifts of the C-H Stretching Vibrations in Complexed and Protonated Triethylamine, *J. Phys. Chem. A* **2007**, *111*, 8884-8891.

[103] Barbieri, M.; Carrera, J.; Ayora, C.; Sanchez-Vila, X.; Licha, T.; Nödler, K.; Osorio, V.; Pérez, S.; Köck-Schulmeyer, M.; López de Alda, M.; Barceló, D.; Formation of diclofenac and sulfamethoxazole reversible transformation products in aquifer material under denitrifying conditions: Batch experiments, *Sci. Total Environ.* **2012**, *426*, 256-263.

[104] Qu, S.; Kolodziej, E. P.; Long, S. A.; Gloer, J. B.; Patterson, E. V.; Baltrusaitis, J.; Jones, G. D.; Benchetler, P. V.; Cole, E. A.; Kimbrough, K. C.; Tarnoff, M. D.; Cwiertny, D. M.; Product-to-Parent Revision of Trenbolone: Unrecognized Risks for Endocrine Disruption, *Science* **2013**, *342*, 347-351.

[105] Li, Z.; Maier, M. P.; Radke, M.; Screening for pharmaceutical transformation products formed in river sediment by combining ultrahigh performance liquid chromatography/high resolution mass spectrometry with a rapid data-processing method, *Analytica Chimica Acta* **2014**, *810*, 61-70.

[106] Acuña, V.; von Schiller, D.; García-Galán, M. J.; Rodríguez-Mozaz, S.; Corominas, L.; Petrovic, M.; Poch, M.; Barceló, D.; Sabater, S.; Occurrence and in-stream attenuation of wastewater-derived pharmaceuticals in Iberian rivers, *Science of The Total Environment* **2015**, *503–504*, 133-141.

[107] Jochmann, M. A.; Schmidt, T. C.; *Compound-specific Stable Isotope Analysis*, RSC Publishing, Cambridge, UK, **2012**.

[108] Imfeld, G.; Kopinke, F.-D.; Fischer, A.; Richnow, H. H.; Carbon and hydrogen isotope fractionation of benzene and toluene during hydrophobic sorption in multiple batch experiments, *Chemospere* **2014**, *107*, 454-461.

[109] Jeannottat, S.; Hunkeler, D.; Chlorine and Carbon Isotope Fractionation during Volatilization and Diffusive Transport of Trichloroethene in the Unsaturated Zone, *Environ. Sci. Technol.* **2012**, *46*, 3169-3176.

[110] Kuder, T.; Philp, P.; Allen, J.; Effects of Volatilization on Carbon and Hydrogen Isotope Ratios of MTBE, *Environ. Sci. Technol.* **2009**, *43*, 1763-1768.

[111] Van Hook, W. A.; Vapor Pressures of the Isotopic Waters and Ices, *J. Phys. Chem.* **1968**, *72* (4), 1234-1244.

[112] Schwarzenbach, R. P.; Gschwend, P. M.; Imboden, D. M.; *Environmental Organic Chemistry*, 2nd ed.; John Wiley & Sons, Inc., Hoboken, NJ, USA, **2003**.

[113] Narten, A.; Kuhn, W.; Genaue Bestimmung kleiner Dampfdruckunterschiede isotoper Verbindungen. Der $^{13}C/^{12}C$-Isotopeneffekt in Tetrachlorkohlenstoff und in Benzol, *Helv. Chim. Acta* **1961**, *44* (6), 1474-1479.

[114] Zhang, B.-L.; Jouitteau, C.; Pionnier, S.; Gentil, E.; Determination of Multiple Equilibrium Isotopic Fractionation Factors at Natural Abundance in Liquid-Vapor Transitions of Organic Molecules, *J. Phys. Chem. B* **2002**, *106*, 2983-2988.

[115] Paulson, S. L.; Barnes, A. J.; Trihalogenomethane-base complexes studied by vibrational spectroscopy in low-temperature matrices, *J. Mol. Struct.* **1982**, *80*, 151-158.

[116] Levitt, M.; Perutz, M. F.; Aromatic Rings Act as Hydrogen Bond Acceptors, *J. Mol. Biol.* **1988**, *201*, 751-754.

[117] Suzuki, S.; Green, P. G.; Bumgarner, R. E.; Dasgupta, S.; Goddard III, W. A.; Blake, G. A.; Benzene Forms Hydrogen Bonds with Water, *Science* **1992**, *257*, 942-945.

[118] Rutkowski, K. S.; Karpfen, A.; Melikova, S. M.; Herrebout, W. A.; Koll, A.; Wolschann, P.; van der Veken, B. J.; Cryospectroscopic and *ab initio* studies of haloform-trimethylamine H-bonded complexes, *Phys. Chem. Chem. Phys.* **2009**, *11*, 1551-1563.

Appendix

A.1 Supporting Information of Chapter 2

A.1.1 Experimental Section

Quantification with HPLC

Concentrations of atrazine, ametryn, and 2-hydroxyatrazine were measured using a LC-A10 series HPLC system and quantified with CLASS VP V6.10 software (both Shimadzu, Kyōto, Japan, http://www.shimadzu.com). The column used was an Allure C18 (5 µm, 150 × 4.6 mm, Restek, Bad Homburg, Germany, http://www.restek.com). Peak separation was conducted using gradient elution at a flow rate of 0.8 mL/min. Oven temperature was set to 45 °C. Initial eluent conditions were 15% acetonitrile and 85% KH_2PO_4 buffer (1 mM, pH 7) isocratic for 1 min followed by a linear gradient to 55% acetonitrile within 9 min, then increasing linearly to 75% acetonitrile within 3 min (hold 2 min). After that, initial conditions were reached within 2 min. The injected sample volume was 25 µL. Compounds were detected by UV absorbance at 220 nm. HPLC standards contained atrazine and 2-hydroxyatrazine, and ametryn and 2-hydroxyatrazine, respectively, dissolved in methanol with analyte concentrations of 1.25, 2.5, 5, and 10 mg/L.

Compound-specific Stable Isotope Analysis

Carbon and nitrogen isotope analysis of atrazine and ametryn was performed on a GC-IRMS system consisting of a TRACE GC Ultra gas chromatograph (Thermo Fisher Scientific, Milan, Italy, http://www.thermofisher.com) equipped with a DB-5 analytical column (30 m, 0.25 mm ID, 1.0 µm film, Agilent Technologies, Böblingen, Germany, http://www.agilent.com), which was coupled to a Finnigan MAT 253 isotope ratio mass spectrometer *via* a Finnigan GC Combustion III interface (both Thermo Fisher Scientific, Bremen, Germany). Liquid samples were injected with a GC Pal autosampler (CTC Analytics, Zwingen, Switzlerland, http://www.ctc.ch). The split/splitless injector (220 °C, He carrier flow rate: 1.4 mL/min) was operated in splitless mode for 2 min, then in split mode (split ratio 1:10). The initial GC oven temperature was 100 °C (hold 5 min), ramped 15 °C/min to 220°C, ramped 8 °C/min to 250 °C, and ramped 35 °C/min to

280 °C (hold 1 min). Before isotope analysis, the separated analytes were combusted online to CO_2 and N_2, respectively, with a NiO tube/CuO-NiO reactor (Thermo Fisher Scientific, Bremen, Germany) operating at 1000 °C. Herbicide standards of ~50 mg/L (atrazine) and ~100 mg/L (ametryn) were used. The carbon and nitrogen isotopic composition of these standards was determined by EA-IRMS consisting of an EuroEA elemental analyzer (EuroVector, Milan, Italy, http://www.eurovector.it) coupled to a Finnigan MAT 253 IRMS by a FinniganConFlow III interface (both Thermo Fisher Scientific, Bremen, Germany) and calibrated against organic reference materials (USGS 40, USGS 41, IAEA 600) provided by the International Atomic Energy Agency (IAEA, Vienna). During carbon and nitrogen analysis by GC-IRMS, analytes were measured against a laboratory standard gas (CO_2 and N_2, respectively) that was introduced at the beginning and the end of each run. Both standard gases were calibrated to V-PDB and air, respectively, by a Delta S isotope ratio mass spectrometer (Finnigan MAT) using reference materials (RM 8562, RM 8563, RM 8564, and N-SVEC) provided by the IAEA (Vienna). The total uncertainty of atrazine measurements was ± 0.3‰ for carbon as well as nitrogen, and ± 0.4‰ for carbon and ± 0.9‰ for nitrogen in ametryn measurements. Atrazine and ametryn standards were precisely analyzed (signal intensity of 500 mV (atrazine, carbon, 50 ppm), 1000 mV (atrazine, nitrogen, 100 ppm), 2000 mV (ametryn, carbon, 100 ppm), and 900 mV (ametryn, nitrogen, 100 ppm)). All samples were measured with intensities higher than the mentioned values, and were therefore higher than the limit of precise analysis. For measurement sequences in which the drift of carbon and nitrogen isotope values, respectively, was greater than the total uncertainty of carbon and nitrogen measurements, values were corrected with a drift correction based on the change in isotope values of the standards over time. Otherwise, the difference between the averaged measured standards and the standard value determined by EA-IRMS was used for correction.

Sulfur isotope analysis of ametryn was conducted on the EA-IRMS system already mentioned above. Dried ametryn samples and V_2O_5 (HEKAtech, Löbau, Germany, http://www.hekatech.com) were weighed in tin capsules (3.3 × 5 mm, IVA Analysentechnik, Meerbusch, Germany, http://www.iva-analysentechnik.de) and were combusted to SO_2 at 1027 °C in a reactor filled with reduced copper wires (0.7 mm) and WO_3/Al_2O_3 (HEKAtech, Löbau, Germany). Calibration was performed against inorganic reference materials (NBS 127, SO-5, SO-6) provided by the IAEA (Vienna).

Theoretical Predictions of Isotope Effects for Abiotic Hydrolysis of Ametryn

Taking into account two different protonation scenarios, two models containing ametryn, nucleophile (water) and two explicit water molecules were constructed. Either the N_3 atom of the *s*-triazine ring or the sulfur atom of the leaving group was protonated. All stationary points were optimized using the MPW1K[A1] functional which was combined with the split valence 6-31+G(d,p)[A2] basis set. All calculations were performed using the Gaussian 09 package.[A3] Tight convergence criteria and ultrafine grid were applied. To confirm the nature of the stationary points ($3n - 6$ real vibrations in the case of reactants and one imaginary frequency corresponding to the desired reaction coordinate in the case of transition states) and validate transition states, vibrational analysis and the Intrinsic Reaction Coordinate (IRC) calculations were performed, respectively. The bulk water solvation effect was taken into account by computing single point energies of optimized geometries using the SMD solvation model[A4] for aqueous solution along with the MPW1K functional and the 6-311+G(2df,2p) basis set. In order to calculate free energies in solution we computed zero-point energies and thermal contributions to the Gibbs free energy in gas phase using the 6-31+G(d,p) basis set and the single point electronic energies calculated using the SMD/MPW1K/6-311+G(2df,2p)//MPW1K/6-31+G(d,p) level of theory. Gibbs free energies of activation and reaction were calculated using the previously reported procedure.[A5] Position-specific sulfur (^{32}k/^{34}k), carbon (^{12}k/^{13}k), and nitrogen (^{14}k/^{15}k) kinetic isotope effects have been calculated using the Bigeleisen equations and ISOEFF07 program.[A6] We did not use scaling factors for frequencies as well as tunneling corrections as these effects have been found to cancel each other out in prediction of heavy atom isotope effects.[A7]

Truncated Models of TrzN Active Site with Ametryn Bound

The crystal structure of wild type TrzN (PDB ID: 3LS9) was used to construct a model of TrzN active site. Since this crystal structure does not contain the substrate molecule bound, we used the fact that non-significant changes in geometries of active site of wild type and mutant of TrzN were observed[A8] and utilized the position of a substrate bound to any of two E241Q mutant crystal structures (PDB ID: 3LSB and 3LSC) to place ametryn in the active site of the wild type enzyme. The final model consisted of the zinc ion, its first shell ligands histidine H63, H65, H238, and the nucleophile water, as well as glutamic acid E68 and E241, histidine H274, threonine T325, aspartic acid D300,

ametryn and the other crystal water molecule located within hydrogen bonding distance of E68 and the ametryn ring (see Figure A.1-5). Side chains of all mentioned amino acids were truncated at the C_β atoms and the hydrogen atoms were added manually. During the geometry optimization C_β atoms were fixed to their corresponding positions in the X-ray structure. A similar approach was described previously by Manta *et al.*[A9] and allowed to maintain the overall structure of the active site and prevent from artificial movements of various groups. The prepared model was used to optimize the enzyme-substrate (ES) and enzyme-intermediate (EI) complexes at the M05-2X level of theory and the 6-31+G(d,p) basis set. This particular combination of functional and basis set has been shown previously to perform very well for the zinc coordination chemistry.[A10,A11] EI turned out to be a stable Meisenheimer-like complex in which both the thiomethyl (leaving group) and the hydroxyl (nucleophile) group are attached to the nucleophilic attack center (carbon atom) of the ametryn ring. Then, the same procedure described above for abiotic hydrolysis of ametryn was applied – single point energies of optimized complexes using the SMD solvation model for chlorobenzene to mimic the environment of low dielectric constant – along with the MPW1K[A1] functional and the 6-311+G(2df,2p) basis set were computed and Gibbs free energies in solution were calculated.

A.1.2 Results and Discussion

Temporal Courses of Enzymatic Degradation of Atrazine and Ametryn, and Abiotic Hydrolysis of Ametryn

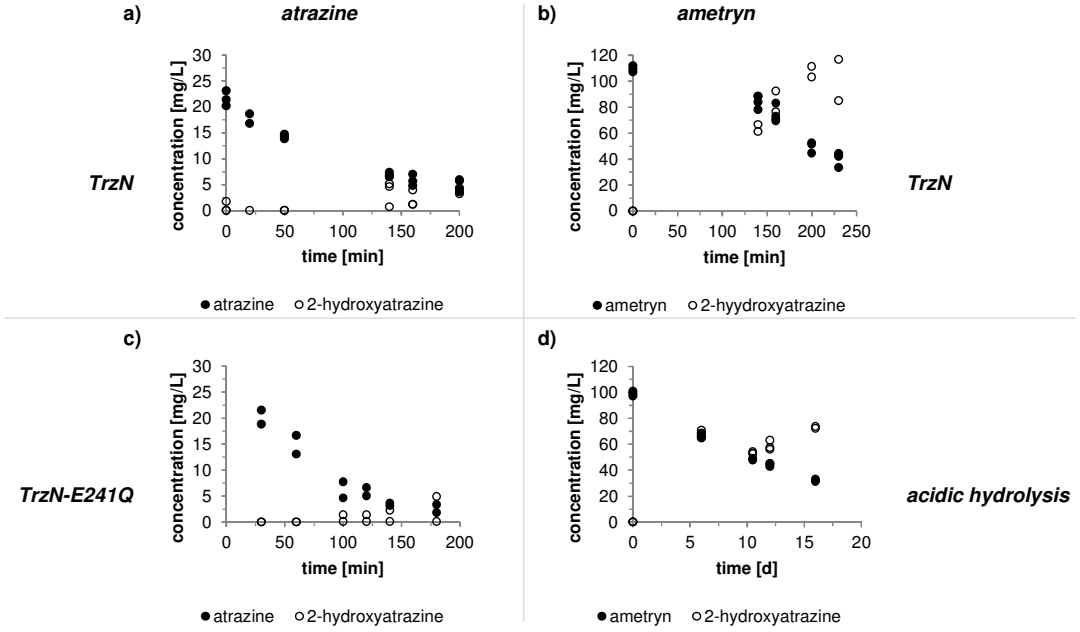

Figure A.1-1: Concentration of atrazine and ametryn, respectively, (filled dots) and the degradation product 2-hydroxyatrazine (open dots) over time for the experiments (a) atrazine with TrzN, (b) ametryn with TrzN, (c) atrazine with TrzN-E241Q, and (d) abiotic hydrolysis of ametryn. Total uncertainty of HPLC measurements are ± 0.2 mg/L for atrazine, ± 0.3 mg/L for ametryn, and ± 2.9 mg/L for 2-hydroxyatrazine.

Concentration Measurements and Isotope Analysis of Atrazine and Ametryn in Control Experiments

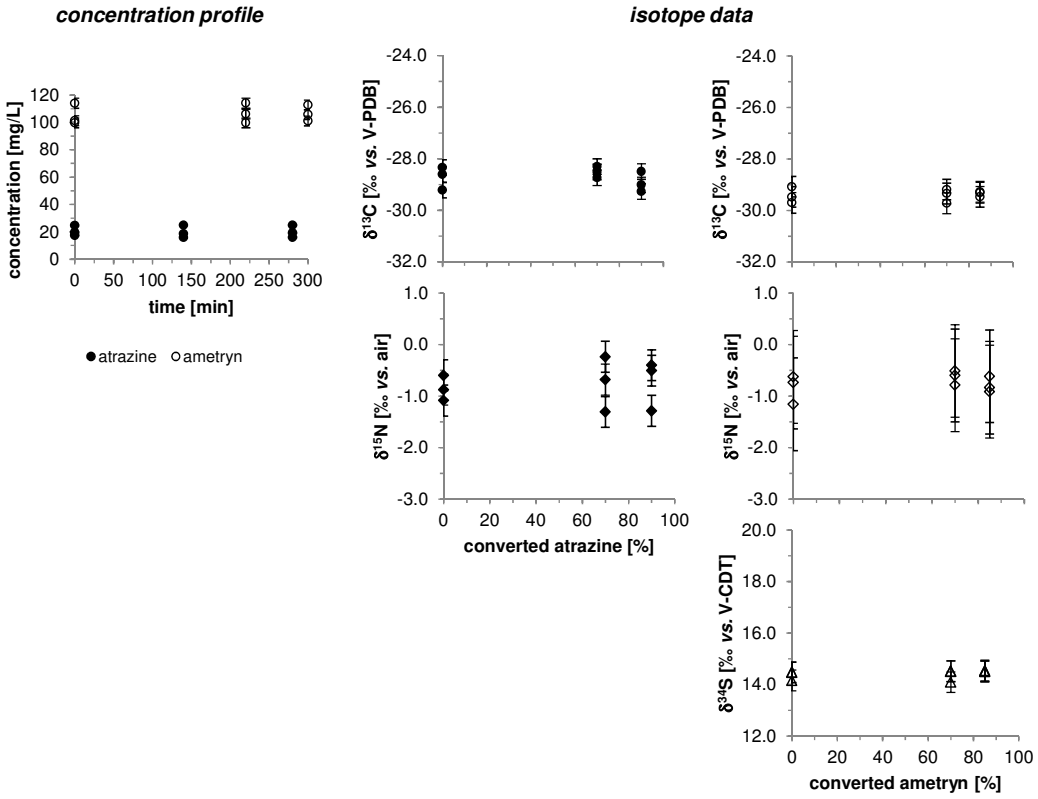

Figure A.1-2: Concentrations of atrazine (filled dots, left panel) and ametryn (open dots, left panel) over time. Error bars represent total uncertainty of atrazine (± 0.4 mg/L) and ametryn (± 3.6 mg/L) HPLC measurements. Isotope data of atrazine for carbon (filled dots, middle panel) and nitrogen (filled diamonds, middle panel) as well as isotope data of ametryn for carbon (open dots, right panel), nitrogen (open diamonds, right panel), and sulfur (open triangles, right panel). Error bars represent total uncertainty of carbon (± 0.3‰ for atrazine, ± 0.4‰ for ametryn), nitrogen (± 0.3‰ for atrazine, ± 0.9‰ for ametryn), and sulfur (± 0.4‰) isotope analysis.

Overview of all Determined Carbon, Nitrogen, and Sulfur Enrichment Factors ε

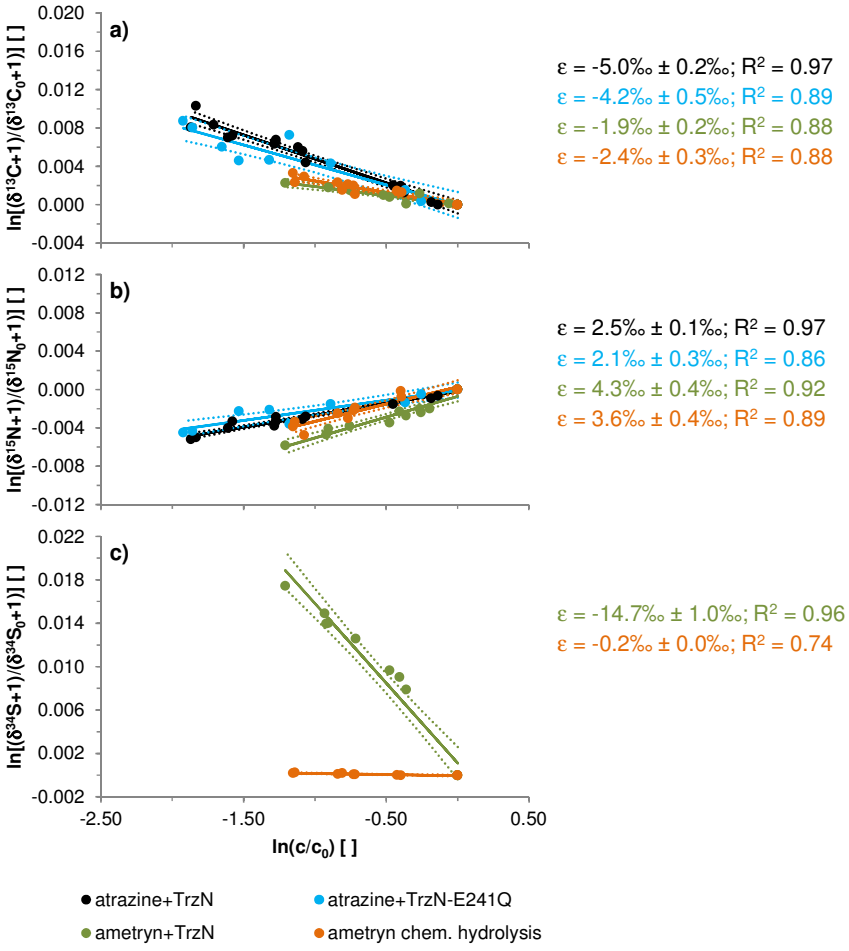

Figure A.1-3: (a) Carbon, (b) nitrogen, and (c) sulfur enrichment factors ε determined for reaction of atrazine with TrzN (black dots), reaction of atrazine with TrzN-E241Q (blue dots), reaction of ametryn with TrzN (green dots), and for chemical hydrolysis of ametryn (orange dots) using the Rayleigh equation. Dotted lines represent 95% confidence intervals of linear regression.

Theoretically Predicted Position-specific Carbon, Nitrogen, and Sulfur Kinetic Isotope Effects at 60 °C for two Mechanistic Scenarios for Acidic Abiotic Hydrolysis of Ametryn

Table A.1-1: Carbon, nitrogen, and sulfur position-specific kinetic isotope effects calculated at 60 °C for the studied pathways of acidic abiotic hydrolysis of ametryn.

N_3 protonation (Figure 2.4a)		**S protonation (Figure 2.4b)**
step I (RC → TS1)	**step II (ITN → TS2)**	**one step (RC → TS)**
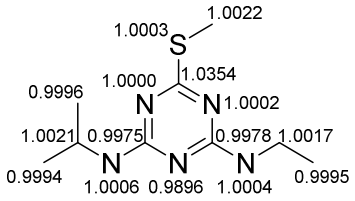	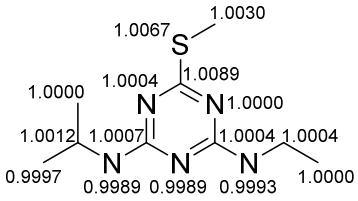	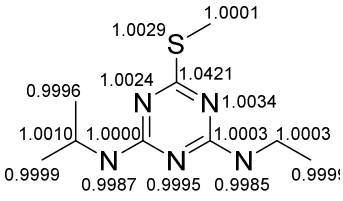

Energy Diagram for the First Intermediate (EI) Formation in the Active Site of TrzN

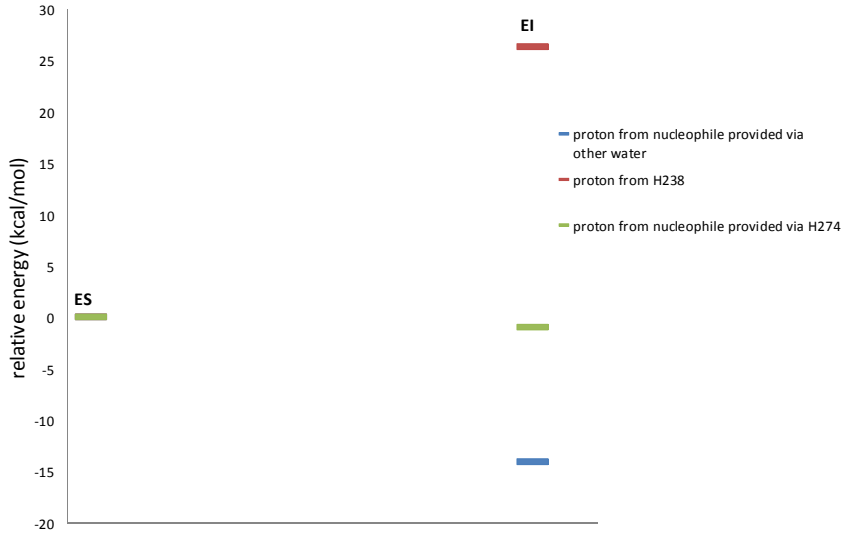

Figure A.1-4: Energy diagram for the first intermediate (EI) formation in the active site of wild type TrzN based on SMD/MPW1K/6-311+G(2df,2p)//M05-2X/LANL2DZ correction.

Comparison of Key Distances of Enzyme-Substrate (ES) Complexes and Elementary Charges e *Based on Truncated Model Optimization*

Table A.1-2: Key distances of enzyme-substrate (ES) complexes as well as elementary charges *e* of atrazine (atr-TrzN, atr-E241Q) and ametryn (amt-TrzN, amt-E241Q) based on truncated model optimization.

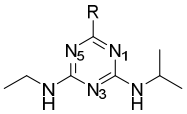

R = Cl, SCH_3

	key distance of ES complex [Å]			
	atr-TrzN	**atr-E241Q**	**amt-TrzN**	**amt-E241Q**
O of water (Nu) – C	2.91	3.13	3.12	3.28
O of water (Nu) – H	1.39	1.12	1.37	1.26
O of water (Nu) – $N_{\varepsilon 2}$ of H274	2.50	2.52	2.50	2.48
C – Cl	1.80	1.79	-	-
C – S	-	-	1.81	1.81
$N_{\delta 1}$ of H274 – H	1.13	1.14	1.19	1.16
N_1 – H of H_2O	2.22	1.86	1.72	1.86
	elementary charge *e*			
	atr-TrzN	**atr-E241Q**	**amt-TrzN**	**amt-E241Q**
Zn charge	1.50	1.52	1.53	1.52
C charge	0.54	0.53	0.37	0.38
Cl charge	-0.01	-0.03	-	-
S charge	-	-	0.22	0.22
O (Nu) charge	-1.27	-1.23	-1.27	-1.26
N_1 charge	-0.67	-0.71	-0.75	-0.73
N_5 charge	-0.71	-0.66	-0.63	-0.68

Optimized Geometry of the Truncated Model of TrzN

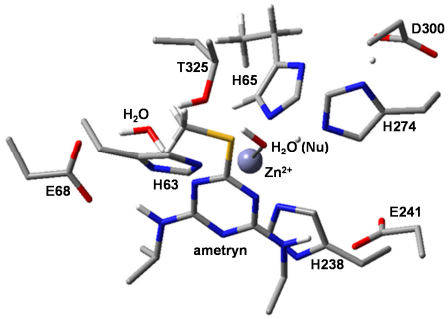

Figure A.1-5: Optimized geometry of the truncated model of wild type TrzN active site. Hydrogen atoms that are not transferred or do not participate in hydrogen bonding are omitted for clarity.

Overview of Key Distances in the X-ray Structure of TrzN Compared to Quantum Mechanical Calculations

Table A.1-3: Key distances (in angstroms) in wild type enzyme TrzN with bound ametryn obtained using QM/MM MD simulations and QM calculations on the truncated model compared to the X-ray structure of the enzyme (PDB ID: 3LS9).

	X-ray structure	**QM/MM MD simulation / QM truncated model**		
H274 – O of water (Nu)	2.67	3.05/2.50	H274 – H of water (Nu)	2.58/1.15
T325 – O of water	3.13	2.56/2.67		
H274 – E241	3.68	5.70/4.63		
H274 – S of ametryn	3.71	4.79/4.56		
E241 – O of water	5.41	5.11/6.31		
S of ametryn – O of water	2.96	4.01/3.98		
E68 – O of water	2.72	3.85/2.67		
E68 – ring N of ametryn	4.73	4.16/4.60		
E68 – side chain N of ametryn	3.26	3.20/2.85	E68 – H of side chain N	2.20/1.91
O of water (Nu) – O of water	4.39	4.54/4.46		
C of ametryn – O of water (Nu)	2.10	4.22/3.11		
			ring N of ametryn – H of water	3.45/1.72

A.2 Supporting Information of Chapter 3

A.2.1 Experimental Section

Chemicals

BAM (2,6-dichlorobenzamide, CAS: 2008-58-4, 99.9%), bentazone (3-*iso*-propyl-(1*H*)-2,1,3-benzothiadiazin-4(3*H*)-one 2,2-dioxide, CAS: 25057-89-0, 99.9%), diclofenac (2-[(2,6-dichlorophenyl)amino]benzeneacetic acid sodium salt, CAS: 15307-79-6), and ibuprofen ((*RS*)-2-[4-(2-methylpropyl)phenyl]propanoic acid, CAS: 15687-27-1, ≥ 98%) were purchased from Sigma-Aldrich (Steinheim, Germany). D_2O (90 atom % D) was from Berlin-Chemie (Berlin-Adlershof, Germany). BF_3 (10% in methanol) was purchased from Sigma-Aldrich (Steinheim, Germany), TMSH (trimethylsulfonium hydroxide, 0.25 M in methanol) was from Fluka, supplied by Sigma-Aldrich (Steinheim, Germany). HCl (32%) and KBr were from Merck (Darmstadt, Germany), H_3PO_4 (85%) and NaOH were from Sigma-Aldrich (Steinheim, Germany). Milli-Q water was generated by a Milli-Q Advantage $A10_{system}$ (Millipore, Schwalbach, Germany). Acetonitrile and ethyl acetate were from Fluka, supplied by Sigma-Aldrich (Taufkirchen, Germany), acetic acid (0.1% in water), *n*-hexane, and methanol were purchased from Carl Roth (Karlsruhe, Germany) and were of LC-MS grade (purity > 99%).

Quantification with LC-MS/MS

Concentrations of BAM, bentazone, diclofenac, 4'-hydroxydiclofenac, ibuprofen, and 2-hydroxyibuprofen were measured on an LC-MS/MS system consisting of an Agilent 1200 binary pump (Agilent Technologies, Böblingen, Germany) and an ABSciex API 2000 Q-TRAP mass spectrometer (Applied Biosystems, Framingham, USA). A Luna C18(2) column (5 µm, 100 × 2 mm) purchased from Phenomenex (Aschaffenburg, Germany) was used. Liquid samples (25 µL) were injected with a GC Pal autosampler (CTC Analytics, Zwingen, Switzerland). The peaks were separated by gradient elution starting with 4% acetonitrile and 96% acetic acid (0.1% in water) isocratic for 2 min at a constant flow rate of 0.3 mL/min. The gradient increased linearly within 28 min to 90% acetonitrile (hold 2 min), before initial conditions were reached within 8 min. Ionization was achieved with positive (0-12 min) and negative (12-40 min) electrospray ionization in multi reaction mode (MRM). The screened molecular and fragment masses are shown in Table A.2-1.

Table A.2-1: Overview of the LC-MS/MS settings used for quantification of 2,6-dichlorobenzamide (BAM), bentazone, diclofenac (Dic), 4'-hydroxydiclofenac (4'-OH-Dic), ibuprofen (Ibu), and 2-hydroxyibuprofen (2-OH-Ibu). $^{13}C_6$-diclofenac ($^{13}C_6$-Dic) and ibuprofen-d_3 (Ibu-d_3) were used as internal standards.

	BAM	**bentazone**	**Dic/ $^{13}C_6$-Dic**	**4'-OH-Dic**	**Ibu/ Ibu-d_3**	**2-OH-Ibu**
molecular mass $[M-H]^+$	190	-	-	-	-	-
fragment mass $[M-H]^+$	145	-	-	-	-	-
molecular mass $[M-H]^-$	-	239	294/300	310	205/208	221
fragment mass $[M-H]^-$	-	132	250/256	266	161/164	177
declustering potential	41	-26	-16	-16	-10	-10
extraction potential	8	-5.5	-6	-7.5	-6	-6
collision energy	35	-32	-12	-12	-12	-12
cell exit potential	4	0	-2	-4	-2	-2
ion spray voltage [V]	+5500	-4500	-4500	-4500	-4500	-4500
source temperature [°C]	350	350	350	350	350	350

Sample enrichment with SPE

To enrich the samples Solid Phase Extraction (SPE) was performed with a vacuum chamber from Macherey-Nagel (Düren, Germany) equipped with Oasis® HLB extraction cartridges (6 cm^3, 200 mg) purchased from Waters (Milford, USA). Stored samples were adjusted to pH 7 with 1 M HCl. First, the cartridges were conditioned (2 × 4 mL methanol, 2 × 4 mL Milli-Q water), then samples were loaded (flow: ~3 mL/min). Afterwards, the sorbent was washed with Milli-Q water (4 mL) and dried under vacuum. To elute the target compounds, methanol (2 × 4 mL) was used. The organic solvent was evaporated under the fume hood with a gentle nitrogen stream and the samples were redissolved in methanol (3 × 500 µL).

Preparative HPLC

Preparative HPLC was performed using an LC-A10 series HPLC system (Shimadzu, Kyōto, Japan) equipped with a fraction collector. The column was an Allure C18 (5 µm, 150 × 4.6 mm) from Restek (Bad Homburg, Germany). Peak separation was conducted using gradient elution with a flow rate of 0.8 mL/min. The oven temperature was set to 35 °C. Initial eluent conditions were 10% acetonitrile and 90% H_3PO_4 (5 mM, pH 2)

isocratic for 1 min, then increasing linearly to 30% acetonitrile within 5 min followed by a linear gradient to 50% acetonitrile within 5 min (hold 3 min). After another linear increase to 70% acetonitrile within 4 min (hold 2 min), initial conditions were reached within 3 min. The sample volume was ~330 µL (three measurements per sample) injected manually into a 500 µL loop. Compounds were detected by UV absorbance at 220 nm. Fractions with a volume of 1 mL each were collected between 5-26.5 min. Vials containing the same substance were combined and the solvent was evaporated under the fume hood with a gentle nitrogen stream.

Isotope Analysis – $\delta^{13}C$ and $\delta^{15}N$ Analysis of BAM, Bentazone, and Diclofenac

Carbon and nitrogen isotope analysis of BAM, bentazone, and diclofenac was carried out on a GC-IRMS system consisting of a TRACE GC Ultra gas chromatograph (Thermo Fisher Scientific, Milan, Italy) equipped with a DB-5 analytical column (30 m, 0.25 mm ID, 1.0 µm film, Agilent Technologies, Böblingen, Germany). The GC was coupled to a Finnigan MAT 253 isotope ratio mass spectrometer *via* a Finnigan GC Combustion III interface (both Thermo Fisher Scientific, Bremen, Germany). Liquid samples were injected with a GC Pal autosampler (CTC Analytics, Zwingen, Switzerland). Analysis of the contaminants was done with established in-house methods.[A12-A14] While BAM was analyzed without further modification, online derivatization by TMSH and offline derivatization by methanolic BF_3 was necessary prior to analysis of bentazone and diclofenac, respectively.

In short, the split/splitless injector (250 °C, He carrier flow rate: 1.4 mL/min) used for BAM analysis was operated in splitless mode for 2 min, then in split mode (split ratio 1:10). Initial GC oven temperature was 120 °C (hold 1 min), ramped 8 °C/min to 200 °C (hold 2 min), and ramped 15 °C/min to 280 °C (hold 2 min).

Bentazone was derivatized online with trimethylsulfonium hydroxide (TMSH) in a programmable GC injector (Optic 3-SG High Power Injection System, ATAS GL Sciences B.V., previously ATAS GL International B.V., Eindhoven, The Netherlands) equipped with a packed glassbead liner. Initial injector temperature was 40 °C and the column flow was set to 1.4 mL/min. After a vent time of 5 min with a split flow of 50 mL/min, the split flow was set to 0 mL/min for 3.5 min, while the injector was ramped 14 °C/min to 250 °C. The GC program began at 80 °C (hold 1 min), ramped 20 °C/min to 190 °C, and ramped 8 °C/min to 260 °C (hold 5 min).

Diclofenac was derivatized offline with BF_3/methanol prior to analysis and injected into the programmable GC injector already mentioned above. The injector was equipped with an on-column liner connected directly to a retention gap (FS-methyl-silyl, 3 m, 0.53 mm ID, Chromatographie Service GmbH, Langerwehe, Germany). Initial injector temperature was 40 °C (hold 4 min), ramped 17 °C/min to 200 °C, while the column flow was set to 0.3 mL/min (hold 2 min), ramped to 1.4 mL/min within 2 min. A constant split ratio of 1:10 was used. Initial GC oven temperature was 40 °C (hold 4 min), ramped 17 °C/min to 200 °C (hold 3 min), and ramped 15 °C/min to 260 °C (hold 20 min).

Derivatization (in this case methylation) is changing the bulk carbon isotope ratio by introduction of an additional carbon atom. To keep the resulting δ^{13}C-shift constant, the same batch of TMSH and BF_3/methanol, respectively, was used for all samples. To correct for the introduced methyl group, the following equation was used[A15]

$$\delta^{13}C_{\text{sample}} = \frac{(n+1) \times \delta^{13}C_{\text{analyte-Me}} - \delta^{13}C_{\text{Me}}}{n} \qquad \text{eq. A.2-1}$$

where n is the number of carbon atoms present in the analyte (bentazone: $n = 10$; diclofenac: $n = 14$), $\delta^{13}C_{\text{analyte-Me}}$ and $\delta^{13}C_{\text{Me}}$ are the isotope ratios of the derivatized analyte (measured) and the introduced methyl group, respectively, that, in turn, can be calculated according to:

$$\delta^{13}C_{\text{Me}} = (n+1) \times \delta^{13}C_{\text{analyte-Me}} - n \times \delta^{13}C_{\text{EA-IRMS}} \qquad \text{eq. A.2-2}$$

$\delta^{13}C_{\text{EA-IRMS}}$ is the carbon isotope ratio of the lab standard that was determined prior to derivatization on an EuroEA elemental analyzer (EuroVector, Milan, Italy) coupled to a Finnigan MAT253 IRMS by a FinniganConFlow III interface (both Thermo Fisher Scientific, Bremen, Germany) and calibrated against organic reference material (USGS 40, USGS 41, IAEA 600, IAEA CH6) provided by the International Atomic Energy Agency (IAEA, Vienna).

A.2.2 Results and Discussion

Breakthrough Curves of BAM, Bentazone, Diclofenac, Ibuprofen, and Conservative Tracer D_2O

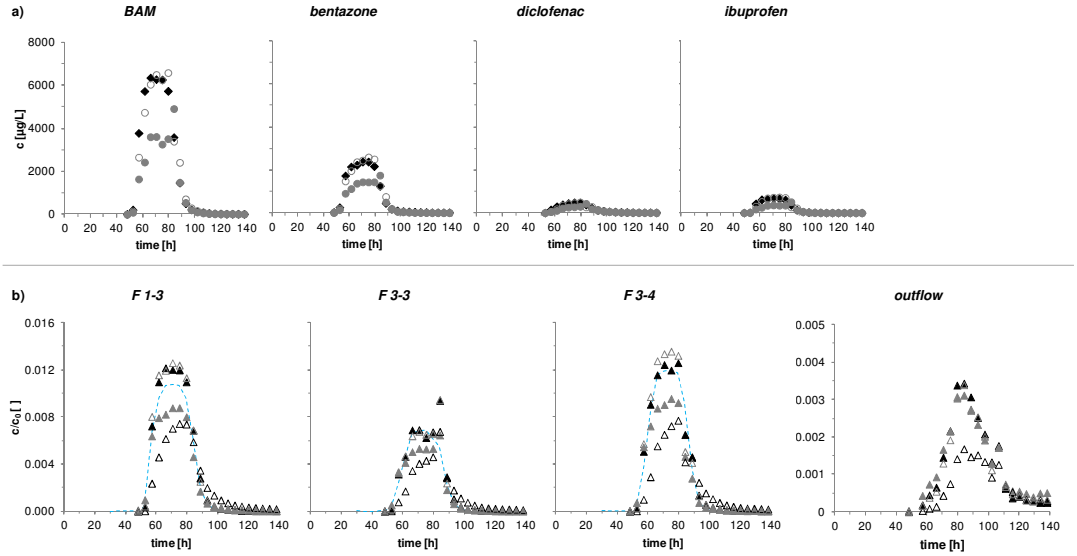

Figure A.2-1: Breakthrough curves of BAM, bentazone, diclofenac, and ibuprofen. (a) Absolute concentrations of contaminants measured in sampling ports F 1-3 (black diamonds), F 3-3 (gray dots), and F 3-4 (gray open dots). (b) Relative concentrations of BAM (black triangles), bentazone (gray triangles), diclofenac (black open triangles), and ibuprofen (gray open triangles) in each sampling port and the aquifer outflow compared to D_2O (blue broken line). Tracer data of the outflow was not analyzed. Note that the resolution of the outflow data is not as high as that of the sampling ports, because the various flow paths of the system are combined.

Recovery and Isotopic Mass Balance of Bentazone and Diclofenac

The isotopic mass balances were calculated according to the Rayleigh equation

$$ln\left(\frac{\overline{\delta\,^{h}E}+1}{\overline{\delta\,^{h}E_0}+1}\right)=\varepsilon\times lnf \qquad \text{eq. A.2-3}$$

with ε being the enrichment factor and f the fraction of the remaining substrate. The weighted average $\overline{\delta\,^{h}E}$ of the isotopic signature $\delta^{h}E_i$ (*i.e.*, $\delta^{13}C$ and $\delta^{15}N$, respectively) is given as

$$\overline{\delta\,^{h}E}=\frac{\sum_{i=1}^{n}\left(\delta\,^{h}E_i\times V_i\times c_i\right)}{\sum_{i=1}^{n}(V_i\times c_i)} \qquad \text{eq. A.2-4}$$

where V_i is the sample volume and c_i is the respective sample concentration at time i.

Table A.2-2: Recoveries and isotopic mass balances of bentazone and diclofenac in the sampling ports F 1-3, F 3-3, and F 3-4.

	bentazone				**diclofenac**			
	1-3	**3-3**	**3-4**	**average**	**1-3**	**3-3**	**3-4**	**average**
recovery [%]	69.7	74.0	74.1	72.6 ± 2.5	61.2	62.3	59	60.8 ± 1.7
degradation [%]	30.3	26.0	25.9	27.4 ± 2.5	38.8	37.7	41.0	39.2 ± 1.7
$\delta^{13}C$ mass balance [%]	-	-	-	-	83.5	80.6	52.2	72.1 ± 17.3
$\delta^{15}N$ mass balance [%]	93.5	84.8	70.7	83.0 ± 11.5	63.5	82.7	59.0	68.4 ± 12.6
$\delta^{13}C$ difference between weighted av and input [‰]	-	-	-	-	0.4	0.4	1.3	0.7 ± 0.5
$\delta^{15}N$ difference between weighted av and input [‰]	0.7	1.7	3.5	1.9 ± 1.4	3.2	1.3	3.7	2.7 ± 1.3

Breakthrough Curves of Diclofenac and its Metabolite 4'-Hydroxydiclofenac

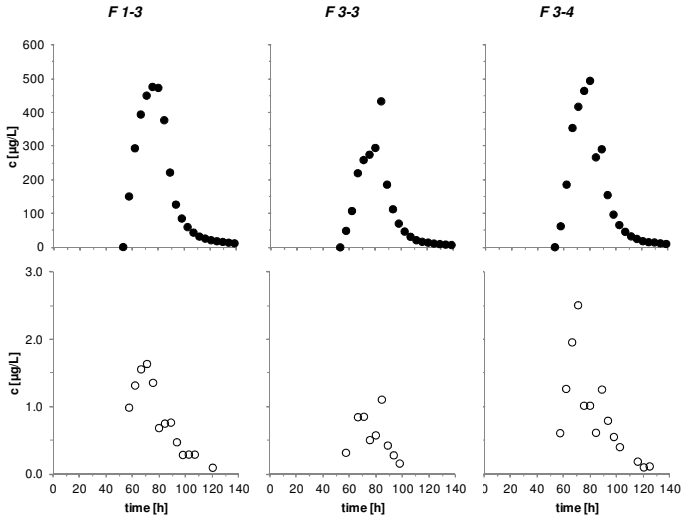

Figure A.2-2: Absolute concentrations of diclofenac (filled dots) and its metabolite 4'-hydroxydiclofenac (open dots).

A.2.3 Mathematical Model

Solute Transport Undergoing First-Order Degradation and Mass Exchange

The traditional notation of multi-dimensional advective-dispersive transport of a compound undergoing linear, one-site, kinetic sorption and first-order decay reads as

$$\frac{\partial c}{\partial t} + \frac{\rho_b}{n}\frac{\partial s}{\partial t} + \mathbf{v}\cdot\nabla \mathrm{c} - \nabla\cdot(\mathbf{D}\nabla c) = -\lambda_{reaction} c \qquad \text{eq. A.2-5}$$

$$\frac{ds}{dt} = \lambda_{sorption}(cK_d - s) \qquad \text{eq. A.2-6}$$

in which c [ML^{-3}] is the aqueous phase concentration, ρ_b [ML^{-3}] denotes the dry bulk density of the aquifer material, n [ ] is effective porosity, s [MM^{-1}] denotes the mass-related concentration of the sorbed compound (mass of the compound per mass of the solids), t [T] is time, $\mathbf{v}$ [LT^{-1}] is the average linear velocity of water, $\mathbf{D}$ [L^2T^{-1}] is the dispersion tensor, $\lambda_{reaction}$ [T^{-1}] expresses the rate coefficient of first-order degradation, $\lambda_{sorption}$ [T^{-1}] is the rate coefficient of first-order mass transfer between the sorbent and

the aqueous phases, and K_d [L^3M^{-1}] is the distribution coefficient of the compound between the sorbing and aqueous phases in equilibrium.

We express the sorbing phase concentration s by the equivalent aqueous-phase concentration c_* [ML^{-3}] if the two phases were in equilibrium:

$$c_* = \frac{s}{K_d} \qquad \text{eq. A.2-7}$$

Then, substitution into the preceding equations yields

$$\frac{\partial c}{\partial t} + \frac{\rho_b}{n} K_d \frac{\partial c_*}{\partial t} + \mathbf{v} \cdot \nabla c - \nabla \cdot (\mathbf{D} \nabla c) = -\lambda_{reaction} c \qquad \text{eq. A.2-8}$$

$$\frac{dc_*}{dt} = \lambda_{sorption}(c - c_*) \qquad \text{eq. A.2-9}$$

in which $\frac{\rho_b}{n} K_d$ can be replaced by (R-1), with R [ ] being the commonly known retardation factor, which is the mass stored in all phases divided by the mass stored in the aqueous phase if the sorbing and aqueous-phase concentrations are in equilibrium:

$$R = \frac{\rho_b}{n} K_d + 1 \qquad \text{eq. A.2-10}$$

This results in

$$\frac{\partial c}{\partial t} + (R - 1) \frac{\partial c_*}{\partial t} + \mathbf{v} \cdot \nabla c - \nabla \cdot (\mathbf{D} \nabla c) = -\lambda_{reaction} c \qquad \text{eq. A.2-11}$$

to be amended by eq. A.2-9. In case of instantaneous sorption (*i.e.*, in the limit of $\lambda_{sorption} \to \infty$), the concentrations c and c_* become identical, resulting in the standard retarded advection-dispersion-reaction equation.

As initial condition, we assume for all compounds a concentration of zero:

$$c(t = 0, \mathbf{x}) = 0 \ \forall \mathbf{x} \qquad \text{eq. A.2-12}$$

We may approximate the multi-dimensional domain as a rectangular box, where the inflow concentration is set to zero in the part of the inflow boundary representing ambient flow and to the time-dependent injected concentration c_{in} [ML^{-3}] at the part of the inflow boundary representing the injection tube. At all other boundaries, we may assume zero dispersive mass flux

$$\mathbf{n} \cdot (\mathbf{v}c - \mathbf{D}\nabla \mathrm{c})|_{x_1=0} = \begin{cases} \mathbf{n} \cdot \mathbf{v}c_{in}(t) & \text{if } -\frac{w}{2} \leq x_3 \leq \frac{w}{2} \\ 0 & \text{otherwise} \end{cases} \qquad \text{eq. A.2-13}$$

$$\mathbf{n} \cdot (\mathbf{D}\nabla \mathrm{c}) = 0 \text{ at all other boundaries} \qquad \text{eq. A.2-14}$$

in which w [L] is the effective injection height of the injection tube, x_1 is the longitudinal coordinate, and x_3 the vertical.

Approximation by One-Dimensional Transport Subjected to Dilution by Transverse Dispersion

The governing transport equation is linear with respect to the solute concentration. If we assume that the physical transport coefficients **v** and **D** are identical, we can approximate the simulated breakthrough curve at an observation point by a 1-D model, in which the effect of dilution by transverse dispersion is approximated from conservative steady-state transport of an internal tracer:

$$c_{reac}(t, \mathbf{x}_{obs}) = f_{dil}(\mathbf{x}_{obs}) \cdot c_{reac}^{1\mathrm{D}}(t, \mathbf{x}_{obs}) \qquad \text{eq. A.2-15}$$

$$\frac{\partial c_{reac}^{1\mathrm{D}}}{\partial t} + (R-1)\frac{\partial c_{reac,*}^{1\mathrm{D}}}{\partial t} + v\frac{\partial c_{reac}^{1\mathrm{D}}}{\partial x} - D\frac{\partial^2 c_{reac}^{1\mathrm{D}}}{\partial x^2} = -\lambda_{reaction} c_{reac}^{1\mathrm{D}} \qquad \text{eq. A.2-16}$$

$$\frac{dc_{reac,*}^{1\mathrm{D}}}{dt} = \lambda_{sorption}\left(c_{reac}^{1\mathrm{D}} - c_{reac,*}^{1\mathrm{D}}\right) \qquad \text{eq. A.2-17}$$

$$c_{reac}^{1\mathrm{D}}(t = 0, x) = 0 \qquad \text{eq. A.2-18}$$

$$vc_{reac}^{1\mathrm{D}} - D\frac{\partial c_{reac}^{1\mathrm{D}}}{\partial x} = vc_{in}(t) \text{ at } x = 0 \qquad \text{eq. A.2-19}$$

$$\mathbf{v} \cdot \nabla f_{dil} - \nabla \cdot (\mathbf{D}\nabla f_{dil}) = 0 \qquad \text{eq. A.2-20}$$

$$\mathbf{n} \cdot (\mathbf{v}f_{dil} - \mathbf{D}\nabla f_{dil})|_{x_1=0} = \begin{cases} \mathbf{n} \cdot \mathbf{v} & \text{if } -\frac{w}{2} \leq x_3 \leq \frac{w}{2} \\ 0 & \text{otherwise} \end{cases} \qquad \text{eq. A.2-21}$$

$$\mathbf{n} \cdot (\mathbf{D}\nabla f_{dil}) = 0 \text{ at all other boundaries} \qquad \text{eq. A.2-22}$$

This approximation introduces a small error because the dilution due to transverse dispersion is slightly smaller at the rising limb of a tracer breakthrough than at the falling limb, but these transient effects are negligible in practical applications.

Eqs. A.2-20 – A.2-22 contain the spatially variable transport coefficients **v** and **D**. Rather than solving these equations numerically, we obtain the dilution factor from the plateau concentration $c_{int.std.}^{plateau}$ [ML^{-3}] of the internal standard

$$f_{dil}(\mathbf{x}_{obs}) = \frac{c_{int.std.}^{plateau}(\mathbf{x}_{obs})}{c_{in,int.std.}} \qquad \text{eq. A.2-23}$$

which implies that we cannot make any statements about transverse dispersion coefficients or the spatial distribution of the velocity field.

Numerical Methods and Fitting Procedure

The 1-D transport eqs. A.2-16 – A.2-19 have an analytical solution in the Laplace domain

$$\tilde{c}_{reac}^{1D}(s) = \tilde{c}_{in}(s)\frac{v}{v + \alpha D}\exp(-\alpha x) \qquad \text{eq. A.2-24}$$

$$\alpha = \frac{-v + \sqrt{v^2 + 4Db}}{2D} \qquad \text{eq. A.2-25}$$

$$b = s + \frac{(R-1)s\lambda_{sorption}}{s + \lambda_{sorption}} + \lambda_{reaction} \qquad \text{eq. A.2-26}$$

in which s [T^{-1}] is the Laplace coordinate, and quantities with a tilde are the Laplace transform of the corresponding time function. We have programed these expressions in Matlab and use the numerical inverse Laplace transform of de Hoog *et al.*[A16] to obtain concentration BTC.

The numerical inverse Laplace transformation leads to spurious oscillations deeming the solution to inaccurate for the evaluation of isotope ratios. Thus, for the evaluation of isotope BTCs, we use another Matlab program relying on Finite Volume discretization in space using upstream differentiation for advective transport and a time stepwise to reach a Courant number of unity. Dispersion is solved implicitly. Subsequently, mass transfer and degradation is solved in a decoupled reaction step using explicit Euler integration. The grid spacing is 0.01 m. We consider each isotopologue as an independent species. Because of linearity they don't influence each other. After computing the concentrations of the isotopologues, we evaluate the corresponding isotope ratios using the δ notation.

The dilution factors f_{dil} for D_2O and BAM are obtained by scaling the second-largest concentration value in the corresponding breakthrough curve with the inflow concentration. The apparent velocity v and longitudinal dispersion coefficient D are obtained by fitting the model (without sorption and degradation) to the breakthrough curve of D_2O using the dilution factor already obtained. The degradation coefficients $\lambda_{reaction}$ of bentazone and diclofenac, as well as the sorption coefficients K_d and $\lambda_{sorption}$ of diclofenac are obtained by fitting the corresponding models to the concentration BTCs, using the dilution factor of BAM. These fits are done with the global-search genetic algorithm of the corresponding Matlab toolbox using standard parameters except for the population size, which was set to 1000. The isotope fractionation factors were manually adjusted.

Justification of $\alpha_{sorption}^{kin} = 1$ ($\varepsilon_{sorption}^{kin} = 0$)

Besides the equilibrium sorption isotope effect, also the rate constant of the sorption process may be subject to (kinetic) isotope effects. Heavy isotopologues would be expected to sorb and desorb more slowly because of their lower diffusion coefficient. The assumption of such a normal kinetic sorption isotope effect was evaluated for sorption of diclofenac with $\varepsilon_{sorption}^{kin}$ = -1.8‰ (both for carbon and nitrogen isotopologues). Figure A.2-3 shows, however, that the agreement of the model with experimental data got significantly worse. A kinetic isotope effect on sorption was, therefore, not integrated into the model, *i.e.*, $\varepsilon_{sorption}^{kin}$ = 0‰ was assumed.

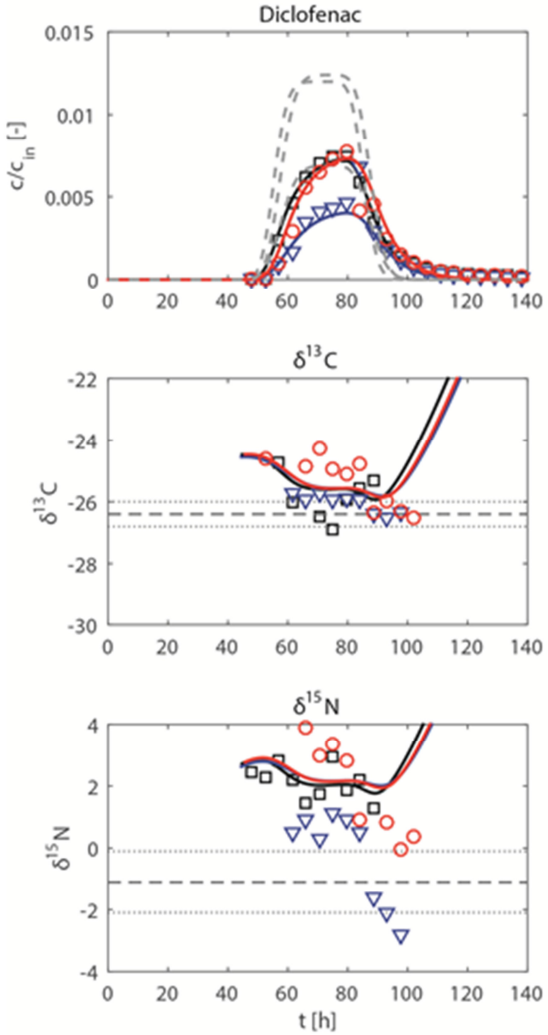

Figure A.2-3: Breakthrough curve of diclofenac assuming a kinetic isotope effect on sorption and desorption of $\varepsilon_{sorption}^{kin}$ = -1.8‰ (both for carbon and nitrogen isotopologues).

Plausibility of a Dilution Factor of BAM in the Order of 1% ($f_{dil} \approx 0.01$)

The dilution factor determined for BAM falls in the same order of magnitude as experimentally determined and modelled for bromide in our preceding study.[A17,A18]

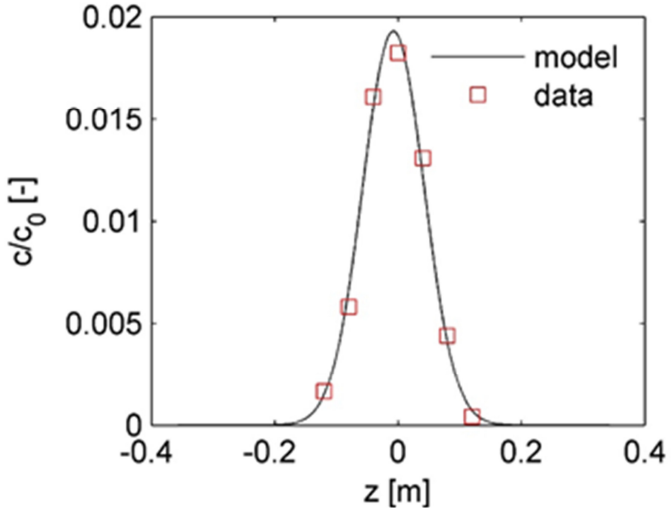

Figure A.2-4: Measured, steady-state bromide concentrations in the physical aquifer model at 4.2 m distance and the model fit used in the preceding toluene study.[A17,A18]

Model Quality

To determine the quality of the model, the normalized root mean square error (NRMSE) was calculated by dividing the root mean square error (RMSE) by the measurement uncertainty (± 0.4‰ (BAM, bentazone) and ± 0.5‰ (diclofenac) for carbon; ± 1‰ for nitrogen) of isotope analysis:

$$NRMSE = \frac{RMSE}{uncertainty} \qquad \text{eq. A.2-27}$$

with RMSE as

$$RMSE = \sqrt{\frac{\sum_{i=1}^{n}\left(\delta\,{}^{h}E_{obs,i} - \delta\,{}^{h}E_{mod,i}\right)^2}{n}} \qquad \text{eq. A.2-28}$$

$\delta^h E_{obs,i}$ and $\delta^h E_{mod,i}$ are the measured and modeled isotope values of carbon and nitrogen, respectively, and n is the number of data points.

Table A.2-3: (Normalized) root mean square errors ((N)RMSE) of BAM, bentazone, and diclofenac isotope analysis for the sampling ports F 1-3, F 3-3, and F 3-4.

		sampling ports		
		F 1-3	**F 3-3**	**F 3-4**
$RMSE_{carbon}$ [‰]	**BAM**	0.421	0.200	0.287
	bentazone	0.556	0.601	0.308
	diclofenac (combined)	0.901	0.646	0.577
	diclofenac (degr. only)	0.936	0.687	0.731
	diclofenac (sorp. only)	1.046	0.361	1.206
$NRMSE_{carbon}$ [ ]	**BAM**	1.052	0.501	0.718
	bentazone	1.390	1.503	0.771
	diclofenac (combined)	1.803	1.292	1.153
	diclofenac (degr. only)	1.871	1.375	1.463
	diclofenac (sorp. only)	2.091	0.722	2.412
$RMSE_{nitrogen}$ [‰]	**BAM**	0.754	0.375	0.985
	bentazone	2.761	2.261	2.413
	diclofenac (combined)	0.960	2.148	1.105
	diclofenac (degr. only)	0.664	2.591	1.587
	diclofenac (sorp. only)	2.954	1.378	3.991
$NRMSE_{nitrogen}$ [ ]	**BAM**	0.754	0.375	0.985
	bentazone	2.761	2.261	2.413
	diclofenac (combined)	0.960	2.148	1.105
	diclofenac (degr. only)	0.664	2.591	1.587
	diclofenac (sorp. only)	2.954	1.378	3.991

A.3 Supporting Information of Chapter 4

Experimental Section

Compound-specific Stable Isotope Analysis (CSIA)

Carbon isotope analysis of benzene, triethylamine, and trichloromethane was conducted on a GC-IRMS system using a TRACE GC Ultra gas chromatograph (Thermo Fisher Scientific, Milan, Italy) which was coupled to a Finnigan MAT 253 isotope ratio mass spectrometer *via* a Finnigan GC Combustion III interface (both Thermo Fisher Scientific, Bremen, Germany). Automated headspace injections were carried out using a GC Pal autosampler (CTC Analytics, Zwingen, Switzerland). The split/splitless injector (250 °C, He carrier flow rate: 1.4 mL/min) was operated in split mode (split ratios 1:10, 1:20, and 1:50 depending on the analyte concentration). For benzene, a Rxi-5Sil MS analytical column (30 m, 0.25 mm ID, 1.0 µm film) from Restek (Bad Homburg, Germany) was used. The initial GC oven temperature was 50 °C (hold 3 min), ramped 40 °C/min to 120 °C (hold 2 min), and ramped 55 °C/min to 280 °C (hold 5 min). Trimethylamine and trichloromethane were analyzed using a DB-624 analytical column (60 m, 0.25 mm ID, 1.4 µm film, Agilent Technologies, Böblingen, Germany). The GC oven program started at 120 °C (hold 12 min) and was ramped 100 °C/min to 280 °C (hold 2 min). Before isotope analysis, the analytes were combusted online to CO_2 with a reactor filled with a CuO/NiO/Pt-wire (Thermo Fisher Scientific, Bremen, Germany) operating at 940 °C. The carbon isotopic composition of benzene, triethylamine, and trichloromethane was determined by EA-IRMS consisting of an EuroEA elemental analyzer (Euro Vector, Milan, Italy) coupled to a Finnigan MAT 253 IRMS by a FinniganConFlow III interface (both Thermo Fisher Scientific, Bremen, Germany) and calibrated against organic reference materials (USGS 40, USGS 41) provided by the International Atomic Energy Agency (IAEA, Vienna). During carbon isotope analysis by GC-IRMS, analytes were measured against CO_2 (laboratory standard gas) that was introduced at the beginning and the end of each measurement. The standard gas was calibrated to V-PDB by a Delta S isotope ratio mass spectrometer (Finnigan MAT) using reference materials (RM 8562, RM 8563, and RM 8564) provided by the IAEA (Vienna). The total uncertainty of benzene measurements was ± 0.2‰, of triethylamine ± 0.4‰, and of trichloromethane ±1‰. The measurement sequences were corrected by linearity correction based on the change in isotope value of the standard gas CO_2 against the signal intensity. CO_2 linearity was determined before every sequence (Figure A.3-1).

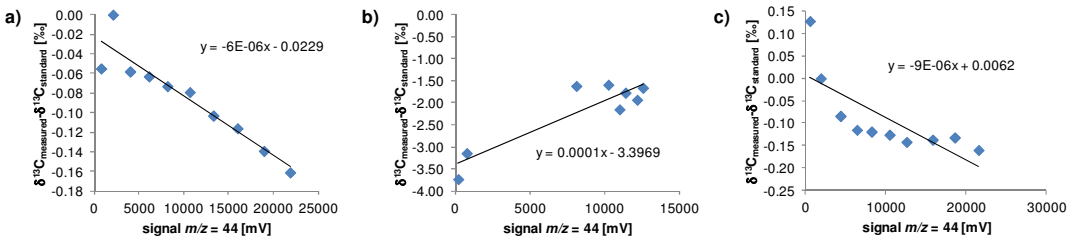

Figure A.3-1: Signal intensity of CO_2 standard gas plotted against the difference of measured and standard isotopic signature. The linear regressions were used to correct measured carbon isotope data of (a) benzene, (b) triethylamine, and (c) trichloromethane.

Hydrogen isotope analysis of a trichloromethane and deuterotrichloromethane mixture (1:1, v/v) was performed on a GC-MS system in SIM mode. An Agilent 7890A GC system (Agilent Technologies, Santa Clara, USA) equipped with a DB-5 analytical column (30 m, 0.25 mm ID, 1.0 µm film, Agilent Technologies, Böblingen, Germany) was coupled to an Agilent 5975C mass selective triple-axis detector (Agilent Technologies, Santa Clara, USA). Automated headspace injections were carried out using a Combi-xt PAL autosampler (CTC Analytics, Zwingen, Switzerland) at a split/splitless injector temperature of 250 °C, operating in split mode (split ratio 1:500). The GC system ran with a constant He carrier flow rate of 1.4 mL/min and the initial GC oven temperature was 120 °C (hold 5 min), ramped 50 °C/min to 280 °C (hold 6 min). The $CHCl_3$/$CDCl_3$ mixture was analyzed by the fragment ions $m/z = 83$ and $m/z = 84$, respectively, using a dwell time of 100 ms.

Determination of Substance Loss during Manual Gas Exchange (Tightness of the Ball)

To determine the tightness of the ball that was used to stop the liquid-gas equilibration, two modified ND18 vials (Figure 4.2) were used. The first one, without a ball serving as a reference, was filled with 3 mL benzene stock solution (100 mg/L) and closed with a screw cap. Afterwards, it was allowed to equilibrate for one hour. Then, the second vial was filled with 3 mL benzene stock solution (100 mg/L), the ball was immediately added, and the vial closed with a screw cap (start of experiment). Headspace samples (50 µL) were injected manually to the split/splitless injector (250 °C, He carrier gas flow rate: 1.4 mL/min) of the GC-IRMS system mentioned above using an isothermal GC oven method (120 °C (hold 70 min) with split ratio 1/10). The resulting retention times, peak

areas, and amplitudes are summarized in Table A.3-1, and the determined substance loss is illustrated in Figure A.3-2.

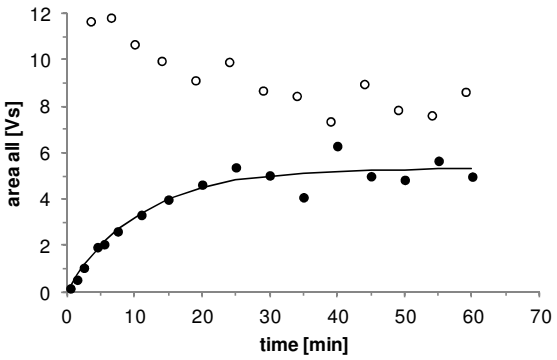

Figure A.3-2: Comparison of peak areas in the reference vial (without ball, open dots) to the test vial (with ball, filled dots) against time.

Table A.3-1: Overview of the retention times, peak areas, and amplitudes of the determination of the ball tightness using two modified ND18 vials where the vial without ball was used as reference.

with or w/o ball	injection time [min][a]	retention time [s]	area all [Vs]	amplitude *m/z* = 44 [V]
with	0.5	300.1	0.162	0.05
with	1.5	361.4	0.534	0.18
with	2.5	421.6	1.049	0.36
w/o	3.5	480.5	11.674	3.95
with	4.5	538.0	1.939	0.66
with	5.5	601.3	2.065	0.70
w/o	6.5	661.7	11.830	4.03
with	7.5	720.4	2.619	0.90
w/o	10	867.1	10.682	3.66
with	11	926.3	3.330	1.14
w/o	14	1112.9	9.968	3-47
with	15	1164.5	3.991	1.37
w/o	19	1402.2	9.129	3.23
with	20	1462.0	4.634	1.59
w/o	45	1703.6	9.922	3.42
with	25	1764.4	5.379	1.87
w/o	29	2005.6	8.689	3.10
with	30	2070.8	5.030	1.69
w/o	34	2296.1	8.458	3.04
with	35	2359.6	4.089	1.44
w/o	39	2598.1	7.359	2.64
with	40	2667.9	6.297	2.18
w/o	44	2898.6	8.971	3.19
with	45	2958.0	4.997	1.78
w/o	49	3195.0	7.854	2.76
with	50	3252.2	4.839	1.71
w/o	54	2486.7	7.621	2.70
with	55	3555.9	5.661	2.01
w/o	59	3789.6	8.634	3.04
with	60	3844.8	4.982	1.66

[a] refers to the time after start of the experiment (*i.e.*, after the vial with the ball was closed).

Data Evaluation of Stepwise Partitioning

Data evaluation was carried out using both, the classical Rayleigh approach (eq. 4.10), and the following equations for stepwise partitioning as described in detail by Jeannottat *et al.*[A19] In short, the following general equation applies for each equilibration step *n*

$$\delta\,{}^{h}E_{liquid,n+1} = \delta\,{}^{h}E_{liquid,n} \times f_{liquid} + \delta\,{}^{h}E_{HS,n} \times f_{HS} \qquad \text{eq. A.3-1}$$

where f_{HS} and f_{liquid}, respectively, are the fractions of compound in the respective phase and $\delta^{h}E_{n+1}$ and $\delta^{h}E_{n}$ are the isotopic signatures before and after equilibration, respectively. Substitution of $\delta^{h}E_{liquid}$ by

$$\varepsilon \approx \delta\,{}^{h}E_{HS} - \delta\,{}^{h}E_{liquid} \qquad \text{eq. A.3-2}$$

and rearrangement gives the isotopic shift after *n* equilibration steps (eq. A.3-3)

$$\Delta\delta\,{}^{h}E_{HS} = n \times \varepsilon \times f_{HS} \qquad \text{eq. A.3-3}$$

with

$$f_{HS} = \left(\frac{c_0 - c_{HS}}{c_0}\right)^{1/n} \qquad \text{eq. A.3-4}$$

Enrichment factor ε can be determined as the slope of the linear regression of eq. A.3-3.

Comparison of Rayleigh Data Evaluation with the Stepwise Partitioning Approach

Table A.3-2: Comparison of data evaluation, *i.e.*, determination of enrichment factor ε, for benzene, triethylamine (NEt_3), and trichloromethane ($CHCl_3$) using Rayleigh equation (eq. 4.10) and the stepwise partitioning equation (eq. A.3-3).

	ε [‰] Rayleigh equation	**ε [‰] stepwise partitioning**
benzene, ε_c	-0.12 ± 0.03 (R^2 = 0.62)	-0.11 ± 0.06 (R^2 = 0.25)
NEt_3, ε_c	0.49 ± 0.10 (R^2 = 0.72)	0.79 ± 0.18 (R^2 = 0.71)
$CHCl_3$, ε_c	-0.35 ± 0.14 (R^2 = 0.38)	-0.77 ± 0.61 (R^2 = 0.14)
$CHCl_3$, ε_H	1.79 ± 0.25 (R^2 = 0.80)	1.11 ± 0.56 (R^2 = 0.35)

Since the regression correlation is more reliable for Rayleigh data evaluation, this approach is used in Chapter 4.

A.4 References

[A1] Lynch, B. J.; Patton, L. F.; Harris, M.; Truhlar, D. G.; Adiabatic Connection for Kinetics, *J. Phys. Chem. A* **2000**, *104* (21), 4811-4815.

[A2] Frisch, M. J.; Pople, J. A.; Binkley, J. S.; Self-consistent molecular orbital methods 25. Supplementary functions for Gaussian basis sets, *J. Chem. Phys.* **1984**, *80* (7), 3265-3269.

[A3] Frisch, M. J.; Trucks, G. W.; Schlegel, H. B.; Scuseria, G. E.; Robb, M. A.; Cheesman, J. R.; Scalmani, G.; Barone, V.; Mennucci, B.; Petersson, G. A.; Nakatsuji, H.; Caricato, M.; Li, X.; Hratchian, H. P.; Izmaylov, A. F.; Bloino, J.; Zheng, G.; Sonnenberg, J. L.; Hada, M.; Ehara, M.; Toyota, K.; Fukuda, R.; Hasegawa, J.; Ishida, M.; Nakajima, T.; Honda, Y.; Kitao, O.; Nakai, H.; Vreven, T.; Montgomery, J., J. A.; Peralta, J. E.; Ogliaro, F.; Bearpark, M.; Heyd, J. J.; Brothers, E.; Kudin, K. N.; Staroverov, V. N.; Kobayashi, R.; Normand, J.; Raghavachari, K.; Rendell, A.; Burant, J. C.; Iyengar, S. S.; Tomasi, J.; Cossi, M.; Rega, N.; Millam, J. M.; Klene, M.; Knox, J. E.; Cross, J. B.; Bakken, V.; Adamo, C.; Jaramillo, J.; Gomperts, R.; Stratmann, R. E.; Yazyev, O.; Austin, A. J.; Cammi, R.; Pomelli, C.; Ochterski, J. W.; Martin, J. W.; Morokuma, K.; Zakrzewski, V. G.; Voth, G. A.; Salvador, P.; Fox, D. J.; *Gaussian 09*, Revision A.1; Gaussian, Inc.: Wallingford, CT, **2009**.

[A4] Marenich, A. V.; Cramer, C. J.; Truhlar, D. G.; Universal Solvation Model Based on Solute Electron Density and on a Continuum Model of the Solvent Defined by the Bulk Dielectric Constant and Atomic Suface Tensions, *J. Phys. Chem. B* **2009**, *113* (18), 6378-6396.

[A5] Grzybkowska, A.; Kaminski, R.; Dybala-Defratyka, A.; Theoretical predictions of isotope effects *versus* their experimental values for an example of uncatalyzed hydrolysis of atrazine, *Phys. Chem. Chem. Phys.* **2014**, *16*, 15164-15172.

[A6] Anisimov, V.; Paneth, P.; ISOEFF98. A program for studies of isotope effects using Hessian modifications, *J. Math. Chem.* **1999**, *26*, 75-86.

[A7] Adamczyk, P.; Dybala-Defratyka, A.; Paneth, P.; DFT Study of Trichloroethene Reaction with Permanganate in Aqueous Solution, *Environ. Sci. Technol.* **2011**, *45* (7), 3006-3011.

[A8] Seffernick, J. L.; Reynolds, E.; Fedorov, A. A.; Fedorov, E.; Almo, S. C.; Sadowsky, M. J.; Wackett, L. P.; X-ray Structure and Mutational Analysis of the Atrazine Chlorohydrolase TrzN, *J. Biol. Chem.* **2010**, *285* (40), 30606-30614.

[A9] Manta, B.; Raushel, F. M.; Himo, F.; Reaction Mechanism of Zinc-Dependent Cytosine Deaminase from *Escherichia coli*: A Quantum-Chemical Study, *J. Phys. Chem. B* **2014**, *118* (21), 5644-5652.

[A10] Amin, E. A.; Truhlar, D. G.; Zn Coordination Chemistry: Development of Benchmark Suites for Geometries, Dipole Moments, and Bond Dissociation Energies and Their Use To Test and Validate Density Functionals and Molecular Orbital Theory, *J. Chem. Theory Comput.* **2008**, *4* (1), 75-85.

[A11] López-Canut, V.; Martí, S.; Bertrán, J.; Moliner, V.; Tuñón, I.; Theoretical Modeling of the Reaction Mechanism of Phosphate Monoester Hydrolysis in Alkaline Phosphatase, *J. Phys. Chem. B* **2009**, *113* (22), 7816-7824.

[A12] Reinnicke, S.; Simonsen, A.; Sørensen, S. R.; Aamand, J.; Elsner, M.; C and N Isotope Fractionation during Biodegradation of the Pesticide Metabolite 2,6-Dichlorobenzamide (BAM): Potential for Environmental Assessments, *Environ. Sci. Technol.* **2012**, *46*, 1447-1454.

[A13] Reinnicke, S.; Bernstein, A.; Elsner, M.; Small and Reproducible Isotope Effects during Methylation with Trimethylsulfonium Hydroxide (TMSH): A Convenient Derivatization Method for Isotope Analysis of Negatively Charged Molecules, *Anal. Chem.* **2010**, *82*, 2013-2019.

[A14] Maier, M. P.; De Corte, S.; Nitsche, S.; Spaett, T.; Boon, N.; Elsner, M.; C & N Isotope Analysis of Diclofenac to Distinguish Oxidative and Reductive Transformation and to Track Commercial Products, *Environ. Sci. Technol.* **2014**, *48*, 2312-2320.

[A15] Maier, M. P.; Qiu, S.; Elsner, M.; Enantioselective stable isotope analysis (ESIA) of polar herbicides, *Anal. Bioanal. Chem.* **2013**, *405* (9), 2825-2831.

[A16] de Hoog, F. R.; Knight, J.H.; Stokes, A. N.; An improved method for numerical inversion of Laplace transforms, *S.I.A.M. J. Sci. Stat. Comput.* **1982**, *3*, 357-366.

[A17] Qiu, S.; Eckert, D.; Cirpka, O. A.; Huenniger, M.; Knappett, P.; Maloszewski, P.; Meckenstock, R. U.; Griebler, C.; Elsner, M.; Direct Experimental Evidence of Non-first Order Degradation Kinetics and Sorption-Induced Isotopic Fractionation in a Mesoscale Aquifer: $^{13}C/^{12}C$ Analysis of a Transient Toluene Pulse, *Environ. Sci. Technol.* **2013**, *47* (13), 6892-6899.

[A18] Eckert, D.; Qiu, S.; Elsner, M.; Cirpka, O. A.; Model Complexity Needed for Quantitative Analysis of High Resolution Isotope and Concentration Data from a Toluene-Pulse Experiment, *Environ. Sci. Technol.* **2013**, *47* (13), 6900-6907.

[A19] Jeannottat, S.; Hunkeler, D.; Chlorine and Carbon Isotope Fractionation during Volatilization and Diffusive Transport of Trichloroethene in the Unsaturated Zone, *Environ. Sci. Technol.* **2012**, *46*, 3169-3176.

Abbreviations

%..... *per centum* (Latin) – percent; parts per hundred; 1% = 1×10^{-2}

‰..... *pro mille* (Latin) – per mil; parts per thousand; 1‰ = 1×10^{-3}

°C..... degree Celsius; 0 °C = 273.15 K

µg..... microgram; 1 µg = 1×10^{-6} g

µL..... microliter; 1 µL = 1×10^{-6} L

µm..... micrometer; 1 µm = 1×10^{-6} m

µmol..... micromole; 1 µmol = 1×10^{-6} mol

1-D..... one-dimensional

2-OH-Ibu..... 2-hydroxyibuprofen

3-D..... three-dimensional

4'-OH-Dic..... 4'-hydroxydiclofenac

A..... ampere

Å..... angstrom; 1 Å = 1×10^{-10} m

A. aurescens..... *Arthrobacter aurescens*

AKIE..... apparent kinetic isotope effect

amt..... ametryn; 2-ethylamino-4-*iso*-propylamino-6-methylthio-1,3,5-triazine

atr..... atrazine; 2-chloro-4-ethylamino-6-*iso*-propylamino-1,3,5-triazine

av..... average

B.Sc. ..... Bachelor of Science

BAM..... 2,6-dichlorobenzamide

BTC..... breakthrough curve

BTEX..... benzene, toluene, ethylbenzene, *ortho*-, *meta*-, *para*-xylene

CAS..... Chemical Abstracts Service

CECs..... chemicals of emerging concern

cm..... centimeter; 1×10^{-2} m

CSIA..... Compound-specific Stable Isotope Analysis

d..... day; 1 d = 86,400 s

degr..... degradation

DFT..... density functional theory

Dic..... diclofenac; 2-[(2,6-dichlorophenyl)amiino]benzeneacetic acid sodium salt

DOI..... Digital Object Identifier

Dr. rer. nat..... *doctor rerum naturalium* (Latin) – Doctor of Natural Sciences

Dr..... Doktor (German) – Doctor; equivalent to PhD

e.g...... *exempli gratia* (Latin) – for example

EA..... Elemental Analysis

EI..... enzyme-intermediate complex

EIE..... equilibrium isotope effect

eq(s)..... equation(s)

ES..... enzyme-substrate complex

et al...... *et alii* (Latin) – and others

F..... sampling port at transect F

FID..... Flame Ionization Detector

g..... gram; 1 g = 1×10^{-3} kg

GC..... Gas Chromatography

geb..... geboren (German) – born

h..... hour; 1 h = 60 s

HB..... hydrogen bond

HLB..... hydrophilic lipophilic balanced

HPLC ..... High Performance Liquid Chromatography

I effect..... inductive effect

i.e. ..... *id est* (Latin) – that is; in other words

IAEA 600..... caffeine; $\delta^{13}C = -27.771‰ \pm 0.043‰$, $\delta^{15}N = 1.0‰ \pm 0.2‰$

IAEA CH6 ..... sucrose; $\delta^{13}C = -10.449‰ \pm 0.033‰$

IAEA..... International Atomic Energy Agency

Ibu..... ibuprofen; (*RS*)-2-[4-(2-methylpropyl)phenyl]propanoic acid

ID..... inner diameter; Identity Document

INT ..... intermediate

IRC ..... Intrinsic Reaction Coordination

IRMS ..... Isotope Ratio Mass Spectrometry

J ..... joule; 1 J = 1 kg m^2 s^{-2}

K..... Kelvin

kcal ..... kilocalorie; 1 kcal = 4.1868×10^3 J

kg..... kilogram

KIE ..... kinetic isotope effect

L ..... length (in model descriptions)

L ..... liter; 1 L = 1×10^{-3} m^3

LC..... Liquid Chromatography

M effect..... mesomeric or resonance effect

M ..... mass (in model descriptions)

m..... meter

M ..... molar; 1 M = 1 mol L^{-1} = 1×10^3 mol m^{-3}

M.Sc..... Master of Science

MD..... Molecular Dynamics

mg..... milligram; 1 mg = 1×10^{-6} kg

min..... minute; 1 min = 60 s

mL ..... milliliter; 1 mL = 1×10^{-3} L

mm ..... millimeter; 1 mm = 1×10^{-3} m

mM ..... millimolar; 1 mM = 1×10^{-3} M

mmol ..... millimole; 1 mmol = 1×10^{-3} mol

mol ..... mole

MRM ..... multi reaction mode

MS ..... Mass Spectrometry

ms ..... millisecond; 1 ms = 1×10^{-3} s

MTBE ..... methyl *tert*-butyl ether

mV ..... millivolt; 1 mV = 1×10^{-3} V

m/z ..... ratio of molecular (or atomic) mass to the charge number of the ion

n.a. ..... not available

n.d. ..... not determined

NBS 127 ..... barium sulfate; $\delta^{18}O = 9.3‰ \pm 0.4‰$, $\delta^{34}S = 20.3‰ \pm 0.4‰$

ng ..... nanogram; 1 ng = 1×10^{-9} g

nm ..... nanometer; 1 nm = 1×10^{-9} m

NRMSE ..... normalized root mean square error

N-SVEC ..... N_2; $\delta^{15}N = -2.8‰ \pm 0.2‰$

Nu ..... nucleophile

OM ..... organic material

P&T ..... Purge and Trap

PC ..... products complex

PD ..... Privatdozent (German) – academic title for PhDs denoting the ability to teach on university level

PDB ..... Protein Database

pH ..... *potentia Hydrogenii* (Latin) – decimal logarithm of the reciprocal of the hydrogen ion activity in solution

PhD ..... Doctor of Philosophy

pK_a ..... logarithmic form of the acid dissociation constant K_a; pK_a = -log$_{10}$ K_a

ppm ..... parts per million; 1 ppm = 1×10^{-6}

Prof. ..... Professor

PTFE ..... polytetrafluoroethylene

QM ..... Quantum Mechanics

QM/MM ..... hybrid Quantum Mechanics/Molecular Mechanics

RC ..... reactants complex

ref. ..... reference

RM 8562 ..... CO_2; $\delta^{13}C$ = -3.72‰ ± 0.04‰, $\delta^{18}O$ = -8.43‰ ± 0.22‰

RM 8563 ..... CO_2; $\delta^{13}C$ = -41.59‰ ± 0.06‰, $\delta^{18}O$ = -23.61‰ ± 0.24‰

RM 8564 ..... CO_2; $\delta^{13}C$ = -10.45‰ ± 0.04‰, $\delta^{18}O$ = 0.06‰ ± 0.20‰

RMSE ..... root mean square error

rpm ..... rounds per minute

Rs ..... reactants

s ..... second

SIM ..... selected ion monitoring

SMD ..... Solvation Model Density

SO-5 ..... barium sulfate; $\delta^{34}S$ = 0.5‰ ± 0.2‰

SO-6 ..... barium sulfate; $\delta^{34}S$ = -34.1‰ ± 0.2‰

sorp. ..... sorption

SPE ..... Solid Phase Extraction

T ..... time (in model descriptions)

TMSH ..... trimethylsulfonium hydroxide

TOC ..... total organic carbon

TrzN ..... *s*-triazine hydrolase

TS ..... transition state

USGS 40 ..... *L*-glutamic acid; $\delta^{13}C = -26.389‰ \pm 0.042‰$, $\delta^{15}N = -4.5‰ \pm 0.1‰$

USGS 41 ..... *L*-glutamic acid; $\delta^{13}C = 37.626‰ \pm 0.049‰$, $\delta^{15}N = 47.6‰ \pm 0.2‰$

UV ..... ultraviolet

V ..... volt; 1 V = 1 kg m^2 A^{-1} s^{-3}

V-CDT ..... Vienna Canyon Diablo Troilite

vdW ..... van-der-Waals interactions

V-PDB ..... Vienna PeeDee Belemnite

vs. ..... *versus* (Latin) – compared to; against

V-SMOW ..... Vienna Standard Mean Ocean Water

v/v ..... volume/volume

w/o ..... without

z.B. ..... zum Beispiel (German) – for example

ZPE ..... zero-point energy